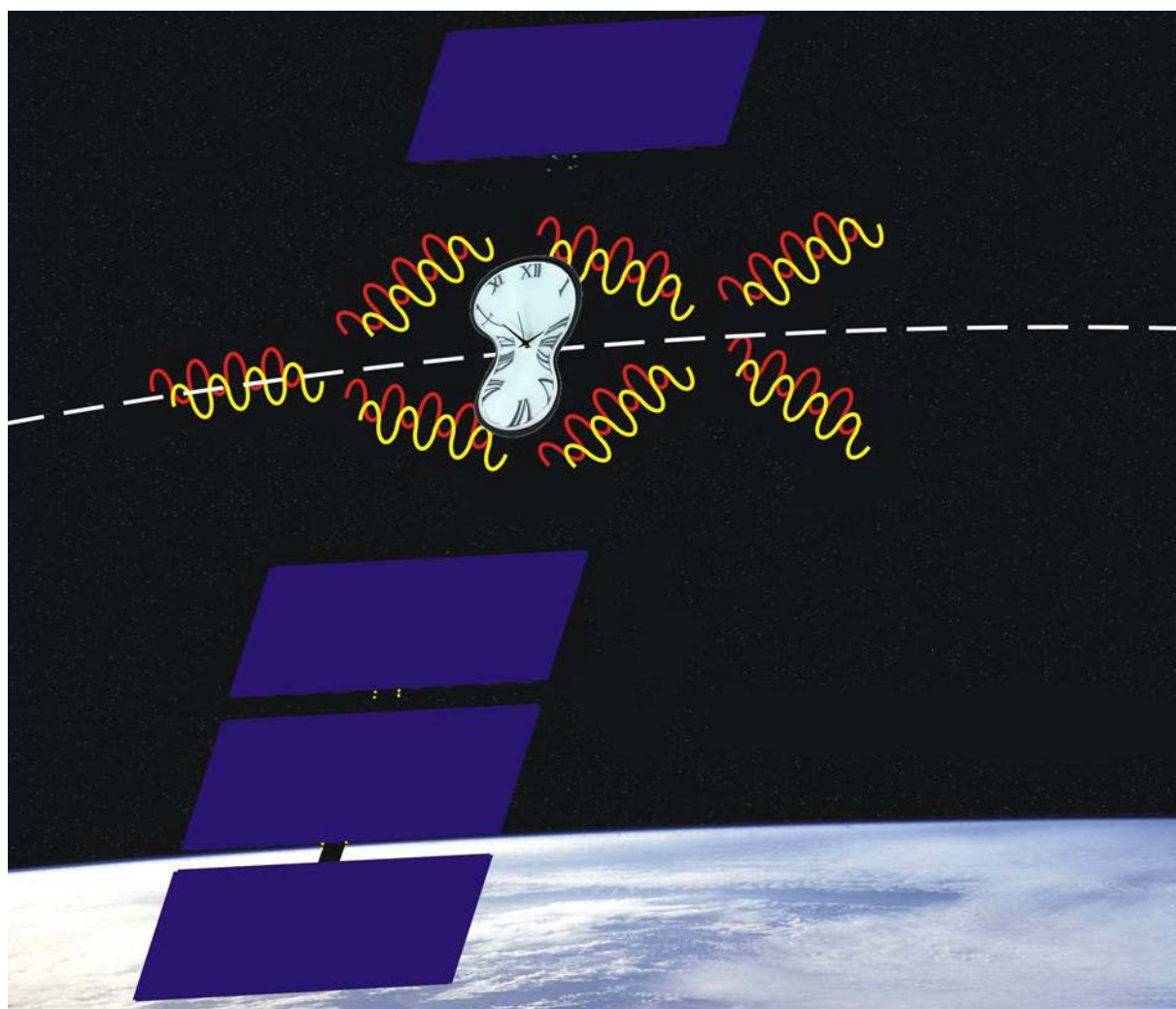


# STE-QUEST

## Space-Time Explorer and Quantum Equivalence Principle Space Test



Assessment Study Report

The front page shows an artist's impression of the STE-QUEST spacecraft in orbit around the Earth. The mission is designed to test the Einstein Equivalence Principle by tracking the free-fall motion of matter waves and by performing clock red-shift measurements.

# Mission Summary

SCIENTIFIC OBJECTIVES						
Test Einstein Equivalence Principle to high precision and search for new fundamental constituents and interactions in the Universe through:						
<b>Science</b>		<b>Measurement Requirement</b>				
<b>Weak Equivalence Principle Tests</b>						
<i>Free fall of matter-waves</i>		Test of the universality of free fall of matter waves to an uncertainty in the Eötvös ratio lower than $2 \cdot 10^{-15}$ .				
<b>Gravitational Red-shift Tests</b>						
<i>Sun field</i>		Sun gravitational red-shift measurement to a fractional uncertainty of $2 \cdot 10^{-6}$ , with an ultimate goal of $5 \cdot 10^{-7}$ .				
<i>Moon field</i>		Moon gravitational red-shift measurement to a fractional uncertainty of $4 \cdot 10^{-4}$ , with an ultimate goal of $9 \cdot 10^{-5}$ .				
<b>Local Lorentz Invariance and CPT Tests</b>						
<i>LLI and CPT</i>		Provide significant improvements on the determination of several parameters of the Lorentz and CPT symmetry violating Standard Model Extension.				
REFERENCE PAYLOAD						
<b>Instrument</b>		<b>Performance</b>				
		Instability ( Allan deviation )			Inaccuracy	
<i><sup>85</sup>Rb - <sup>87</sup>Rb atom interferometer</i>		$(13 \cdot 10^{-12} \text{ m/s}^2)/\sqrt{\tau}$ , for $20 \text{ s} \leq \tau \leq 3.5 \cdot 10^6 \text{ s}$			$< 2 \cdot 10^{-15}$	
<b>Payload Complement</b>		<b>Performance</b>				
<i>Microwave link 2-way, 3-frequency</i>		Ground-to-ground clock comparisons				
		Instability ( modified Allan deviation, $1 \text{ s} \leq \tau \leq 7 \cdot 10^5 \text{ s}$ ): $< \sqrt{(5.0 \cdot 10^{-13}/\tau^{3/2})^2 + (1.6 \cdot 10^{-13}/\tau)^2 + (5.9 \cdot 10^{-17}/\tau^{1/2})^2 + (5.0 \cdot 10^{-19})^2}$ Inaccuracy: $< 5 \cdot 10^{-19}$				
<i>GNSS receiver</i>		2 m level position error in post-processing		0.2 mm/s level velocity error in post-processing		
MISSION PROFILE						
<b>Launcher</b>		Soyuz Fregat from Kourou; launch window available all year.				
<b>Orbit</b>		Highly elliptical orbit around the Earth (~700 km perigee, ~51000 km apogee) with 16 h period; fixed ground track, optimized in terms of visibility at the selected ground terminals locations.				
<b>Mission duration</b>		5 years: 6 months of on-orbit commissioning and calibration; 4.5 years of routine science phase.				
<b>Communication</b>		ESTRACK network; 2 h per day during routine science phase; data rate: <5 Gb/orbit.				
SPACECRAFT						
<i>Spacecraft bus</i>		SVM/PLM architecture. Two design solutions proposed: 1- Custom hexagonal structure with central cylinder; 2- Telecom bus with custom box structure PLM				
<i>Propulsion</i>		Hydrazine propulsion system for orbit control				
<i>AOCS</i>		Cold gas / reaction wheel architecture for low acceleration and microvibration environment				
<i>Pointing</i>		Angular velocity averaged over the time interval $T$ between consecutive pulses in the atom interferometer sequence within $[-10^{-6}, +10^{-6}] \text{ rad/s}$				
	Payload module	Service module	Propellant	Adapter/Harness	Margin (20%)	Total
<i>Mass (kg)</i>	604÷516	780÷499	259÷95	86÷115	277÷203	2005÷1428
<i>Power (W)</i>	744÷817	247÷229	--	--	217÷209	1300÷1255
GROUND SEGMENT						
3 microwave terminals connected to atomic clocks; baseline locations: Boulder (US), Torino (IT), Tokyo (JP).						
<i>Ground clocks performance</i>		Instability (Allan deviation)		$< 2.5 \cdot 10^{-16}/\sqrt{\tau}$ , for $1 \text{ s} \leq \tau \leq 2.5 \cdot 10^5 \text{ s}$		
		Inaccuracy		$< 1 \cdot 10^{-18}$		

## Foreword

The genesis of the STE-QUEST science case dates back to the consultation process conducted in 2009 by the ESA-appointed “Fundamental Physics Roadmap Advisory Team” (FPR-AT). FPR-AT was convened to draw up recommendations on the scientific and technological roadmap necessary to lead Europe toward the realization of future fundamental physics missions in the framework of the Cosmic Vision 2015-2025 plan. FPR-AT activities were concluded in 2010 with the release of the document “A Roadmap for Fundamental Physics” [BINÈTRUY (2010)]. In the roadmap document, FPR-AT recommended the concept of a medium-class mission testing the Einstein Equivalence Principle (EEP) specifically addressing: clock red-shift tests, relying on the space-to-ground and ground-to-ground comparisons of state-of-the-art atomic clocks via high-performance links through the atmosphere; Weak Equivalence Principle (WEP) tests by tracking the propagation of matter waves in a differential atom interferometer thus addressing the quantum counterpart of classical tests based on macroscopic masses. As a result of the FPR-AT recommendation, ESA initiated a Concurrent Design Facility (CDF) study to investigate the feasibility of a clock mission testing Einstein Equivalence Principle through the gravitational red-shift effect. The study, denominated STE [SCHILLER (2009)], acronym for Space-Time Explorer, laid the foundations for the STE-QUEST mission concept, which complemented the STE clock experiments with a dual atom interferometer performing a WEP test on atoms. Submitted in reply to the 2010 Call for Medium-size Missions of the Cosmic Vision program, STE-QUEST was recommended by the ESA advisory structure and finally selected by the Agency for an assessment study. The assessment phase started in April 2011 and will be concluded with the presentation of the study results to the ESA advisory structure at the beginning of 2014.

In May 2011, an ESA internal study was conducted at the ESTEC CDF to identify the main mission drivers, the critical areas, and the key enabling technologies for the subsequent studies to be performed by industry on spacecraft and mission aspects, and by the STE-QUEST Consortia on the payload instruments. Following the Invitation to Tender for the STE-QUEST assessment study, two parallel contracts were then awarded to Thales Alenia Space – Italy (Torino) and Astrium GmbH (Friedrichshafen). Industrial studies started in January 2012. In parallel, the activities on the two STE-QUEST instruments, the atomic clock and the atom interferometer were also kicked off. Instrument Consortia were further consolidated after the ESA Announcement of Opportunity (AO) for the provision of scientific payload including science ground segment elements for STE-QUEST. As expected, two consortia replied to the AO, the first with a proposal covering the development of the differential atom interferometer, the second proposing a reuse of the PHARAO clock. PHARAO, presently under development in the ACES mission, is now approaching flight model maturity. The study of the STE-QUEST science links (microwave and optical) was kept under ESA responsibility. In May 2013, following the results of an ESA cost review, the STE-QUEST Study Science Team agreed in considering the STE-QUEST optical link as an optional payload element. The impact on the STE-QUEST science outcome was assessed and considered to be minor. During the assessment phase, the mission design went through a consolidation of the scientific requirements, of the orbit and mission architecture, of the spacecraft, payload and instruments design. In June 2013, the Mission Definition Review demonstrated the mission feasibility, showing a satisfactory degree of maturity of the industrial studies and of the STE-QUEST documentation. In parallel, instrument studies did progress in terms of design, interfaces and resources consolidation, performance budget analysis. To date, computational tools are available to verify traceability and compliance of the science requirements to mission objectives. Industry and Instrument Consortia activities concluded in the summer of 2013 with the delivery of the documentation due for the Preliminary Requirements Review (PRR). In September 2013, following the consolidation of the instruments development costs, a new configuration of the STE-QUEST payload had to be investigated to fit into the financial resources available at the National Space Agencies. At that time, the Study Science Team deliberated for considering the atomic clock as an optional payload element. In the new configuration, clock red-shift tests in the field of the Sun and of the Moon are possible to full performance, based on the common-view comparison of ground clocks via the on-board microwave link; space-to-ground clock comparisons are not any longer available for measuring the Earth red-shift effect. This solution significantly reduced payload costs and development risks, at the same time minimizing the impact on the STE-QUEST science outcome. This document presents the results of the mission assessment study as achieved at conclusion of PRR.

**The STE-QUEST Science Study Team, December 2013**

## Authorship

This report has been prepared by the STE-QUEST Team listed below:

<b>Science Study Team (SST)</b>		
<i>Name</i>	<i>Affiliation</i>	<i>City, Country</i>
Kai Bongs	Birmingham University	Birmingham, United Kingdom
Philippe Bouyer	Bordeaux University	Bordeaux, France
Luciano Iess	La Sapienza University	Roma, Italy
Philippe Jetzer	Zurich University	Zurich, Switzerland
Arnaud Landragin	LNE-SYRTE	Paris, France
Philip Tuckey	LNE-SYRTE	Paris, France
Ernst Rasel	LUH	Hannover, Germany
Stephan Schiller	HHUD	Düsseldorf, Germany
Uwe Sterr	PTB	Braunschweig, Germany
Guglielmo Tino	Firenze University	Firenze, Italy
Peter Wolf	LNE-SYRTE	Paris, France
<b>Instrument Principal Investigators</b>		
<i>Name</i>	<i>Affiliation</i>	<i>City, Country</i>
Ernst Rasel	LUH	Hannover, Germany
Philip Tuckey	LNE-SYRTE	Paris, France

The ESA Team supporting the study activities is composed of:

<b>ESA Study Team</b>		
Luigi Cacciapuoti ( <i>Study Scientist</i> )	ESA	Noordwijk, The Netherlands
Martin Gehler ( <i>Study Manager</i> )	ESA	Noordwijk, The Netherlands
Astrid Heske ( <i>Payload Manager</i> )	ESA	Noordwijk, The Netherlands
Peter Kretschmar ( <i>Science Operations Study Manager</i> )	ESA	Madrid, Spain
<b>ESA Coordinator</b>		
Arvind Parmar	ESA	Noordwijk, The Netherlands

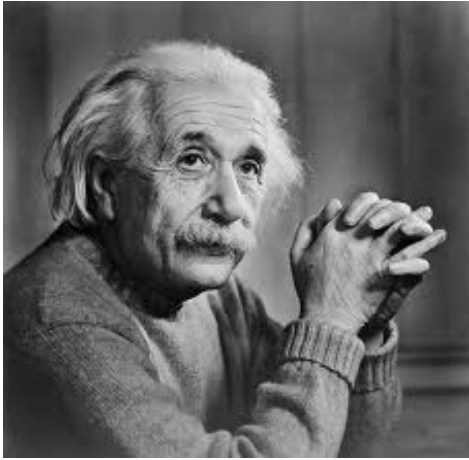
Significant support was provided by numerous scientists strongly involved in the elaboration of the science case, in the simulation activities, in the payload and instrument studies. A complete list of the scientists who have contributed to the STE-QUEST assessment study can be found in the acknowledgments.

# Table of contents

<b>1</b>	<b>EXECUTIVE SUMMARY</b> .....	<b>6</b>
<b>2</b>	<b>SCIENCE OBJECTIVES</b> .....	<b>9</b>
2.1	Introduction .....	9
2.1.1	The Einstein Equivalence Principle (EEP) .....	9
2.1.2	The Role of EEP in Theories of Gravitation.....	11
2.1.3	Why Would the EEP be Violated? .....	12
2.2	Einstein Equivalence Principle in the Context of Physics Today.....	13
2.2.1	Cosmology Context .....	13
2.2.2	Particle Physics Context .....	15
2.2.3	Quantum Mechanics and the Einstein Equivalence Principle .....	16
2.3	STE-QUEST Tests of the Einstein Equivalence Principle .....	19
2.3.1	Different Tests of the EEP .....	19
2.3.2	STE-QUEST Test of the Weak Equivalence Principle.....	21
2.3.3	STE-QUEST Test of Local Position Invariance.....	23
2.3.4	STE-QUEST Tests of Lorentz Invariance and CPT Symmetry .....	26
2.4	STE-QUEST Legacy Science.....	28
2.4.1	Time and Frequency Metrology .....	29
2.4.2	Terrestrial and Celestial Reference Frame of the Earth.....	31
2.4.3	Relativistic Geodesy: Reference Frames for Positioning, Timing, and Temporal Gravity .....	33
2.5	Need for Space .....	34
<b>3</b>	<b>SCIENTIFIC REQUIREMENTS</b> .....	<b>38</b>
3.1	Science Investigations vs. Measurement Requirements .....	38
3.2	STE-QUEST Orbit Characteristics.....	39
3.3	Performance Requirements and Measurement Modelling.....	40
3.3.1	Atom Interferometry Measurements.....	40
3.3.2	Clock Measurements .....	42
<b>4</b>	<b>PAYLOAD DESIGN</b> .....	<b>48</b>
4.1	Core Instruments .....	48
4.1.1	The Dual Species Atom Interferometer .....	48
4.1.2	Microwave Link .....	52
4.1.3	GNSS Receiver.....	56
4.2	Optional Payload Elements .....	56
4.2.1	The PHARAO Cold-atom Clock .....	56
4.2.2	Optical Link.....	60
<b>5</b>	<b>MISSION DESIGN</b> .....	<b>63</b>
5.1	Mission Profile .....	63
5.2	Mission Phases .....	63
5.2.1	Launch and Early Orbit Phase .....	64
5.2.2	System Commissioning Phase.....	64
5.2.3	Science Characterization Phase .....	65
5.2.4	Routine Science Phase.....	66
5.2.5	Extended Science Phase .....	66
5.2.6	Deorbiting.....	66
5.2.7	Post-operations Phase .....	66
5.3	Spacecraft Design.....	67
5.3.1	Mission Drivers and Design Consequences.....	67
5.3.2	Spacecraft Design: Solution A.....	70
5.3.3	Spacecraft Design: Solution B.....	73
5.4	Mass and Power Budget .....	75
5.5	Technical Risk Mitigation .....	76
5.6	Conclusion.....	76
<b>6</b>	<b>GROUND SEGMENT AND DATA HANDLING</b> .....	<b>77</b>

6.1	STE-QUEST Data and Data Products .....	77
6.1.1	Level 0 (L0): Raw Data .....	78
6.1.2	Level 1 (L1): Engineering Data .....	78
6.1.3	Level 2 (L2): Quick-look Performance Data .....	78
6.1.4	Level 3 (L3): Full Performance Clock Comparisons Results .....	78
6.1.5	Level 4 (L4): High-level Data .....	79
6.2	Mission Operations Elements .....	79
6.2.1	ESTRACK Network .....	79
6.2.2	Mission Operations Centre .....	79
6.2.3	Distributed Network of Ground Stations .....	80
6.3	Science Operations Elements .....	80
6.3.1	Science Operations Centre.....	81
6.3.2	Instrument Operations Centre.....	81
6.3.3	Orbitography Data Centre.....	82
6.3.4	Data Processing Centre.....	82
6.3.5	Data Archive.....	82
6.4	Data Handling .....	83
6.4.1	Data Flows .....	83
6.4.2	Data Processing .....	83
<b>7</b>	<b>MANAGEMENT .....</b>	<b>87</b>
7.1	Project Management .....	87
7.2	Procurement Philosophy.....	87
7.2.1	System Procurement .....	87
7.2.2	Payload Procurement .....	87
7.3	Schedule .....	87
7.4	Science Management.....	88
7.4.1	The ESA Project Scientist and the STE-QUEST Science Team .....	89
7.4.2	STE-QUEST Data Policy .....	89
<b>8</b>	<b>COMMUNICATIONS AND OUTREACH.....</b>	<b>91</b>
	<b>ACRONYMS .....</b>	<b>92</b>
	<b>REFERENCES.....</b>	<b>94</b>
	<b>ACKNOWLEDGMENTS .....</b>	<b>97</b>

# 1 Executive Summary



Einstein's theory of general relativity (GR) is a cornerstone of our current description of the physical world. It is used to understand the flow of time in presence of gravity, the motion of bodies from satellites to galaxy clusters, the propagation of electromagnetic waves in the presence of massive bodies, the evolution of stars, and the dynamics of the Universe as a whole. Although very successful so far, general relativity as well as numerous other alternative or more general theories of gravitation are classical theories. As such, they are fundamentally incomplete, because they do not include quantum effects. A theory solving this problem would represent a crucial step towards the unification of all fundamental forces of Nature. Several concepts have been proposed and are currently under investigation (e.g. string theory, quantum gravity, extra spatial dimensions) to bridge this gap and

most of them lead to tiny violations of the basic principles of GR. Therefore, a full understanding of gravity will require observations or experiments able to determine the relationship of gravity with the quantum world. This topic is a prominent field of activity with repercussions covering the complete range of physical phenomena, from particle and nuclear physics to galaxies and the Universe as a whole including dark matter and dark energy.

Precision measurements are at the heart of the scientific method that, since Galileo's time, is being used for unveiling Nature and understanding its fundamental laws. The assumptions and predictions of general relativity can be challenged by precision experiments on scales ranging from the laboratory to the solar system, in the latter case using spacecrafts or the orbiting Earth. The implementation of tests with significantly improved sensitivity obviously requires the use of state-of-the-art technology, at least as far as it is compatible with the boundary condition of the experiment, e.g. space-compatible systems in case of satellite-based experiments. Atomic clocks and high-performance time and frequency links, atom interferometers and classical accelerometers are today able to measure frequency, time, and distances, and furthermore to track the motion of massive bodies, quantum particles, and light to accuracy levels never reached before. These instruments achieve their ultimate performance in space, where the clean environment and the free-fall conditions become essential for identifying tiny deformations in space-time that might bring the signature of new physics or new fundamental constituents. From this point of view, it is not surprising that fundamental physics pervades all aspects of space science. Testing EEP and searching for its violation is therefore central to this field and STE-QUEST is specifically designed for that purpose.

**Primary Science Objectives:** STE-QUEST is a mission testing the different aspects of the Einstein Equivalence Principle with quantum sensors. The payload carries a differential atom interferometer comparing the free propagation of matter waves of different composition under the effect of gravity and a science link in the microwave domain for comparing atomic clocks on ground.

STE-QUEST performs a direct test of the Weak Equivalence Principle (WEP) by comparing the free fall of quantum objects of different composition. The Eötvös ratio between the matter waves of the two isotopes of rubidium atoms is measured in a differential atom interferometer down to the  $2 \cdot 10^{-15}$  uncertainty level. While present limits on WEP tests involving classical objects reach an uncertainty of a few parts in  $10^{13}$ , measurements performed on quantum objects (matter waves in states which have no classical counterpart, e.g. spatio-temporal quantum superpositions) are still at a few parts in  $10^7$ . From this point of view, STE-QUEST will explore the boundaries between gravitation and quantum mechanics significantly improving existing measurements and complementing experiments such as MICROSCOPE (MICRO-Satellite à traînée Compensée pour l'Observation du Principe d'Equivalence), designed for a classical WEP test in space to  $1 \cdot 10^{-15}$ .

STE-QUEST also tests another complementary aspect of the Einstein Equivalence Principle, one of the most fascinating effects predicted by general relativity and other metric theories of gravity: the gravitational red-shift or gravitational time dilation effect. As direct consequence of the Einstein Equivalence Principle, time

runs (or clocks tick) more slowly near a massive body. This effect can be detected when comparing the time intervals measured by identical clocks placed at different positions in a gravitational field. The science link in the microwave domain on-board the STE-QUEST satellite allows comparing ground clocks down to the  $1 \cdot 10^{-18}$  uncertainty level. Such measurements, far beyond the capabilities of existing long-distance time and frequency transfer systems, will perform clock red-shift tests in the field of the Sun and the Moon, respectively at the  $2 \cdot 10^{-6}$  and  $4 \cdot 10^{-4}$  uncertainty levels. For comparison, existing measurements of the Sun red-shift effect are at the few % uncertainty level while, to our knowledge, no such measurements have ever been performed in the field of the Moon. Clock red-shift measurements obtained in the field of the Sun and the Moon test the Local Position Invariance (LPI) principle and search for anomalous couplings depending on the composition of the source of the gravitational field. LPI is a constituent of EEP together with WEP and the Local Lorentz Invariance (LLI) principle.

In generic frameworks modelling a possible violation of EEP, WEP and clock red-shift tests are complementary and need to be pursued with equal vigor as, depending on the model used, either one of the tests can prove significantly more sensitive than the other. Improving the accuracy of these tests will bring significant progress in restricting the parameters space and discriminating between theories seeking to unify quantum mechanics with gravity. The eventual detection of an EEP violation would carry the signature of new fundamental constituents or interactions in the Universe (e.g. scalar fields for dark energy, particles for dark matter, fundamental strings, etc.). In this case, STE-QUEST tests would have a significant impact not only for fundamental physics research, but also for cosmology and particle physics.

**Legacy Science:** STE-QUEST has also important applications in domains other than fundamental physics, in particular in the fields of time and frequency metrology and for geodesy studies.

The STE-QUEST high-performance link provides the means for connecting atomic clocks on ground in a global network, enabling comparisons down to the  $1 \cdot 10^{-18}$  fractional frequency uncertainty level. Clock comparisons via STE-QUEST will contribute to the realization of international atomic time scales (UTC, TAI, etc.) and to the improvement of their stability and accuracy. Synchronization of clocks, space-to-ground and ground-to-ground, to better than 50 ps can be achieved through STE-QUEST for distributing time scales to unprecedented performance levels.

Common-view comparisons of ground clocks, primarily used for gravitational red-shift tests in the field of Sun or Moon, also provide direct information on the geopotential differences at the locations of the two ground clocks. STE-QUEST will therefore contribute to establishing a global reference frame for the Earth gravitational potential at the sub-cm level through local measurements. This method is complementary to current and future gravity space geodetic missions such as CHAMP, GRACE and GOCE as well as to altimetry missions like JASON and Envisat in defining the Global Geodetic Observing System (GGOS).

**On-board Instruments:** The satellite core payload consists of two instruments: an atom interferometer and a science link in the microwave domain of highest performance.

The atom interferometer (ATI) compares the free propagation of the coherent matter waves of the two rubidium isotopes  $^{85}\text{Rb}$  and  $^{87}\text{Rb}$  under the influence of the Earth's gravity. The use of ultra-cold matter close or down to quantum degeneracy (coherent atomic sources) and the long interrogation times possible in a freely falling laboratory will permit to go far beyond the current accuracy of tests. The atom interferometer is based on the strong European developments in this field, including the ESA pre-phase A studies in the ELIPS programme of "Space Atom Interferometer" (SAI) and "Quantum Gases in Microgravity: Space-BEC", the DLR project QUANTUS (QUANTengase Unter Schwerelosigkeit), and the CNES project ICE (Interferometrie Coherente pour l'Espace).

During the mission, atomic clocks on ground will be connected in a worldwide network and nearly continuously compared among themselves using precise microwave frequency transfer methods similar to those developed for the ACES mission (MWL). These comparisons will be carried out in common-view, without the need for a high performance on-board clock (an on-board quartz oscillator is sufficient). The highly elliptic orbit of the satellite provides long uninterrupted common-view durations from ground clocks located in different continents, maximizing the accuracy of clock red-shift measurements. At the same time, it allows for free fall tests in the vicinity of the Earth, where the signal of a possible WEP violation is maximized. A mission duration of up to 5 years is intended.

Pending refinement of resources estimates, two optional payload elements have been identified: a high-performance cold-atom clock and a time & frequency link in the optical domain.

The clock is derived from the well-developed microwave standard PHARAO, which is also the core instrument of the ACES mission. The performance of the clock will be improved compared to the current implementation for ACES by an optically derived ultra-pure microwave signal (MOLO).

The optical link is a coherent laser link based on the successful LCT technology in use by ESA. Its outstanding stability has the potential of drastically reducing the integration time needed to reach the specified frequency uncertainty in the comparison of ground clocks.

**Mission:** The spacecraft will be launched on a Soyuz Fregat from Kourou. The highly elliptic orbit of the satellite provides long common-view contacts to compare ground clocks from different continents and maximize the accuracy of the clock red-shift measurement. At the same time, it allows for WEP tests at perigee, in the vicinity of the Earth, where the signal of an eventual WEP violation is also maximized. The nominal mission duration is 5 years. After 6 months of calibration, the routine science phase will be started. During perigee passes ( $\leq 3000$  km altitude), the atom interferometer performs WEP tests by measuring the differential acceleration between freely falling  $^{85}\text{Rb}$  and  $^{87}\text{Rb}$  samples. The on-board science link compares clocks on the ground for a large fraction of the spacecraft orbit and in particular around apogee. A guidance system controls the spacecraft attitude and ensures the required environment in terms of accelerations and rotations at the instrument measurement head. The on-board GNSS receiver provides orbit information to perform clock red-shift tests. Data transfer from and to the spacecraft is ensured by the ESTRACK network; 2 h coverage per day during the routine science phase is sufficient to accommodate the  $< 5$  Gb/orbit data rate to be down-linked from the STE-QUEST spacecraft.

**Ground Segment:** STE-QUEST is a distributed system composed of a spacecraft carrying an ensemble of scientific instruments and a network of ground terminals equipped with high-performance time and frequency transfer links and connected to atomic clocks of ultimate stability and accuracy.

Mission operations are planned and executed at the Mission Operations Centre (MOC) located in ESOC. MOC is interfaced both to the STE-QUEST spacecraft (ESTRACK antennae) and to the distributed network of ground terminals (internet).

Science operations are performed in ESAC at the Science Operations Centre (SOC). SOC is responsible for coordinating all science operations activities and for optimizing the scientific exploitation of the mission. At SOC, the STE-QUEST Archive keeps a complete repository of all the raw and processed data generated by the mission. SOC activities are assisted by: the Data Processing Centres (DPCs), responsible for processing mission data and for generating higher level data products; the Instrument Operations Centre (IOC), responsible for near real-time monitoring and control of the STE-QUEST instrument; the Orbitography Data Centre (ODC), responsible for providing orbit determination and prediction products.

**Data Analysis:** Maximizing the scientific return of the mission imposes the development of a data analysis infrastructure commensurate with the challenges imposed by STE-QUEST in the comparison of distant clocks and in the measurement of differential accelerations.

The analysis of clock comparison data will be based on the approach and the algorithms already developed for the ACES mission. The evaluation of differential acceleration measurements and of the Eötvös parameter will benefit from the data analysis developed for ground-based experiments operated under microgravity conditions such as zero-g parabolic flights and drop tower.

The analysis of science data and the evaluation of systematic effects will be extremely important to achieve the STE-QUEST science goals, particularly in case a violation of the Einstein Equivalence Principle is found. The robustness of the final results strongly relies on the availability of several data centres able to work in parallel on the basis of independent data analysis codes and constantly running cross checks and comparisons among them.

The STE-QUEST data will be made publicly available 1 year after their validation (period of prior access) through the STE-QUEST Archive. During this period, the STE-QUEST data can only be accessed by the Science Team members and the different entities contributing to science operations (SOC, DPC, IOC, ODC). The 1-year proprietary data period is important to verify the quality of raw data, to extract the science products to the established accuracy levels, and finally validate them before release to the public. The STE-QUEST Archive will be continuously updated during the mission as the measurements accuracy and the evaluation of systematic effects will be constantly improving during the mission lifetime.

## 2 Science Objectives

### 2.1 Introduction

Our best knowledge of the physical Universe, at the deepest fundamental level, is based on two theories: Quantum Mechanics (more precisely Quantum Field Theory) and the classical theory of General Relativity (GR). Quantum Field Theory has been extremely successful in providing an understanding of the observed phenomena of atomic, particle, and high energy physics and has allowed a unified description of three of the conventionally four fundamental interactions that are known to us (electromagnetic, weak and strong interaction, the fourth one being gravitation). It has led to the Standard Model of particle physics that has been highly successful in interpreting all observed particle phenomena, and has been strongly confirmed with the recent discovery at the LHC of the Brout-Englers-Higgs (BEH) boson, which could in fact be viewed as the discovery of a new fundamental interaction. Although open questions remain within the Standard Model of particle physics (see e.g. Sec. 2.2.2), it is clearly the most compelling model for fundamental interactions at the microscopic level that we have at present.

Meanwhile general relativity brilliantly accounts for all observed phenomena related to gravitation, in particular all observations in the Earth's environment, the Solar system and, beyond that, on galactic and cosmological scales. The assumed validity of GR at large scales, and the fact that non gravitational interactions are described by the Standard Model of particle physics, together with a hypothesis of homogeneity and isotropy of cosmological solutions of these theories, have led to the "concordance model" of cosmology, generally referred to as the Lambda Cold Dark Matter model ( $\Lambda$ -CDM), which is in agreement with all present day observations at large scales, notably the most recent observations of the anisotropies of the cosmic microwave background by the Planck satellite [ADE (2013)]. However important difficulties remain, in particular the necessary introduction of dark energy, described by a cosmological constant  $\Lambda$ , and of dark matter, made of some unknown, yet to be discovered, stable particle.

There is a potential conflict on the problem of dark matter between the concordance model of cosmology and the Standard Model of particles. On the one hand, there is strong evidence [ADE (2013)] that 26.8 % of the mass-energy of the Universe is made of non-baryonic dark matter particles, which should certainly be predicted by some extension of the Standard Model of particles. On the other hand there is no indication of new physics beyond the Standard Model, which has been found at the LHC. For instance the search of supersymmetry at LHC has for the moment failed. We shall come back to this problem in Sec. 2.2.1.

Leaving aside the problem of dark matter (which shows up already at galactic scales), GR has clearly been, and still is, an extremely important theory for the understanding of gravitational phenomena and the structure of space-time. Nonetheless, most physicists believe that GR and the Standard Model of particles are only low energy approximations of a more fundamental theory that remains to be discovered (see also Sec. 2.1.3). One of the most desirable attributes of that theory is the unification of the fundamental interactions of nature, i.e. a unified description of gravity and the conventionally three other fundamental interactions. There are several attempts at formulating such a theory, but none of them are widely accepted and considered successful. Furthermore, they make very few precise quantitative predictions that could be verified experimentally. One of them is the Hawking radiation of black holes, which is however far from being testable experimentally for stellar size black holes we observe in astrophysics. Fortunately, most unification theories have in common a violation at some (a priori unknown) level of one of the basic postulates of general relativity, which *can* be tested experimentally: the Einstein Equivalence Principle (EEP). Let us emphasize that the Equivalence Principle is not a fundamental symmetry of physics, contrary to say the principle of local gauge invariance in particle physics. It is therefore an important challenge to test with the best possible accuracy one or several aspects of the EEP. This is then the main motivation of many experiments, and in particular space experiments like MICROSCOPE, ACES and STE-QUEST, in fundamental physics.

#### 2.1.1 The Einstein Equivalence Principle (EEP)

The foundations of gravitational theories and the equivalence principle have been clarified by many authors, including SCHIFF (1960), DICKE (1964), THORNE (1973), and others. Following the book of WILL (1993) the EEP is generally divided into three sub-principles: the Weak Equivalence Principle (WEP) also known as the Universality of Free Fall (UFF), the Local Lorentz Invariance (LLI), and the Local Position Invariance (LPI).

The EEP is satisfied if and only if all three sub-principles are satisfied. Below we describe these three sub-principles:

- WEP/UFF states that *if any uncharged test body is placed at an initial event in space-time and given an initial velocity there, then its subsequent trajectory will be independent of its internal structure and composition*. The most common test of WEP consists in measuring the relative acceleration of two test bodies<sup>1</sup> of different internal structure and composition freely falling in the same gravitational field. If WEP is satisfied, that relative acceleration is zero.
- LLI states that *the outcome of any local non-gravitational test experiment is independent of the velocity of the (freely falling) apparatus*. Tests of LLI usually involve a local experiment (e.g. the comparison of the frequency of two different types of clocks) whose velocity and/or orientation is varied in space-time. LLI is verified if the result of the experiment is unaltered by that variation.
- LPI states that *the outcome of any local non-gravitational test experiment is independent of where and when in the universe it is performed*. Tests of LPI usually involve a local experiment (e.g. the measurement of a fundamental constant, or the comparison of two clocks based on different physical processes) at different locations and/or times. In particular, varying the local gravitational potential allows for searches of some anomalous coupling between gravity and the fields involved in the local experiment. A particular version of such tests, known as test of the gravitational red-shift, uses the same type of clock, but at two different locations (different local gravitational potentials) and compares them via an electromagnetic signal. Then it can be shown (see WILL (1993), Sec. 2.4(c)) that the measured relative frequency difference is equal to  $\Delta U/c^2$  (where  $\Delta U$  is the difference in gravitational potential) if and only if LPI is satisfied.

One of the unique strengths of STE-QUEST is that it will test all three aspects of the EEP, using a combination of measurements in space and on the ground (relative acceleration of different atomic isotopes, comparison of distant clocks). Additionally, the explored domain of the possible violation of the LLI and LPI is maximized by the large variation of velocity and gravitational potential using a highly elliptic orbit of the spacecraft.

Since the three sub-principles described above are very different in their empirical consequences, it is tempting to regard them as independent. However, it was realized quite early that any self-consistent gravitational theory is very likely to contain connections between the three sub-principles. This has become known as *Schiff's conjecture*, formulated around 1960. Loosely stated, the Schiff conjecture implies that *if one of the three sub-principles is violated, then so are the other two*. This conjecture can be understood heuristically by the following example. Suppose that WEP/UFF is violated; then two different clocks (with different internal compositions) will acquire different accelerations in a gravitational field. In the freely falling frame of one of the clocks, the other one will be accelerated (though being located at the same position), and there will be an abnormal red-shift between the two clocks depending on their difference of internal composition, hence a violation of LPI. The Schiff conjecture has been *proved* within very general theoretical frameworks such as the formalism we shall review in Sec. 2.3.1. Alternative theories which do not satisfy the conjecture suffer from serious pathologies and are non-viable.

Schiff's conjecture has given rise to much debate, in particular concerning its empirical consequences and the relative merit of tests of the different sub-principles. Whilst it is true that any theory respecting energy conservation (i.e. based on an invariant action principle) must satisfy Schiff's conjecture, the actual quantitative relationship between violation of the sub-principles is model dependent and varies as a function of the mechanism used for the violation (see e.g. Sec. 2.3.1 for a phenomenological example). As a consequence, it is not known a priori which test (WEP/UFF, LLI, or LPI) is more likely to first detect a violation and the most reasonable approach is to pursue tests of the three sub-principles with equal vigor. This is the baseline of STE-QUEST.

For completeness, and to avoid possible confusion, we will say a few words about the Strong Equivalence Principle (SEP), although it is not directly related to, and will not be tested by STE-QUEST. The SEP is a generalization of EEP to include "test" bodies with non-negligible self-gravitation, together with experiments

---

<sup>1</sup> By test body is meant an electrically neutral body whose size is small enough that the coupling to inhomogeneities in the gravitational field can be neglected.

involving gravitational forces (e.g. Cavendish type experiments). Obviously, SEP includes EEP as a special case in which gravitational forces can be ignored. Typical tests of SEP involve moons, planets, stars or local gravitational experiments, the best known example being lunar laser ranging that tests the universality of free fall, with the two test bodies being the Moon and the Earth falling in the field of the Sun. Clearly the two test bodies have non-negligible self-gravitation and thus provide a test of SEP. The empirical consequences of SEP and EEP are quite different; in general a violation of SEP does not necessarily imply a violation of EEP. Similarly the theoretical consequences are very different: A violation of EEP excludes not only GR as a possible theory of gravitation, but also all other metric theories (eg. all PPN theories, Brans-Dicke theory, etc.). A violation of SEP on the other hand excludes GR, but allows for a host of other metric theories (e.g. PPN theories that satisfy a particular combination of parameters). In that sense, SEP and EEP tests are complementary and should be carried out in parallel within experimental and observational possibilities. STE-QUEST focuses on EEP, but this does not preclude the interest of SEP tests like continued and improved lunar laser ranging.

### 2.1.2 The Role of EEP in Theories of Gravitation

The EEP is the foundation of all curved space-time or “metric” theories of gravitation, including of course general relativity. It divides gravitational theories in two classes: metric theories, those that embody EEP and non-metric theories, those that do not. This distinction is fundamental, as metric theories describe gravitation as a geometric phenomenon, namely an effect of curvature of space-time itself rather than a field over space-time, quite unlike any of the other known interactions. It might thus appear unnatural to use a metric theory for gravitation, so different from the formalisms of the other interactions, and indeed most unification attempts cast doubt on precisely this hypothesis and thus on the validity of the EEP. Only experimental tests can settle the question and, in the light of the above, experimentally testing the EEP becomes truly fundamental.

To be more precise (see e.g. DICKE (1964), THORNE (1973), WILL (1993)), a metric theory of gravitation is one that satisfies the following postulates:

1. Space-time is endowed with a metric tensor  $g_{\nu\mu}$ , central to the metric equation that defines the infinitesimal line element i.e. the space-time separation between two events
 
$$ds^2 = g_{\nu\mu}(x^\alpha)dx^\nu dx^\mu \quad (2-1)$$
 in some 4-dimensional space-time coordinate system  $x^\alpha$ .
2. The trajectories of freely falling test bodies are geodesics of that metric of extremal length  $\delta \int ds = 0$ , i.e. they depend only on the geometry of space-time, but are independent of the test body composition.
3. Clocks measure proper time  $\tau$  along their trajectory, given by  $c^2 d\tau^2 = -ds^2$ , independent of the type of clock used.
4. In local freely falling reference frames, the non-gravitational laws of physics (i.e. the other three fundamental interactions) reduce to those of special relativity.

Obviously the above postulates are a direct consequence of the EEP, for example LLI and LPI are the foundations of points 3 and 4 and WEP is the basis of 2. It is important to note that GR is not the only possible metric theory that satisfies the above postulates. Indeed, there exist a large number of such theories like the scalar-tensor Jordan-Brans-Dicke theories and their generalizations. These theories differ from GR in the way that the metric tensor is related to the distribution of mass-energy through the existence of other fields associated with gravity (scalar field, vector field, etc.).

Theories in which varying non-gravitational coupling constants are associated with dynamical fields that couple to matter directly are not metric theories. In such theories, the fine structure constant  $\alpha$  for instance would vary with space and time. Neither, in this narrow sense, are theories in which one introduces additional fields (dilaton, moduli) that couple differently to different types of mass-energy, e.g. some versions of superstring theory. The fundamental ingredient of all such non-metric theories is non-universal coupling to gravity of all non-gravitational fields, i.e. the fields of the Standard Model of particle physics. In metric theories, coupling to the gravitational field is universal, and as a consequence the metric of space-time can be studied by a variety of devices made up of different non-gravitational fields and particles, and, because of universality, the results will be independent of the device. For instance, the proper time between two events is a characteristic of space-time and of the location of the events, not of the clocks used to measure it [WILL (1993)].

Thus experimental tests of the EEP are often viewed as tests of the universal coupling of gravity (through the metric of space-time  $g_{\nu\mu}$ ) to all non-gravitational fields of the Standard Model of particle physics [DAMOUR (2010)]. Violations occur when the coupling is dependent on some attribute of the non-gravitational fields at hand that may be different for different test bodies, e.g. electromagnetic charge, nuclear charge, total spin, nuclear spin, quark flavor, lepton number, etc... Exploring all possibilities of such anomalous couplings is the fundamental aim of experimental tests of the EEP. Note also that in any particular experimental situation, symmetry requires that such anomalous couplings be not only a function of the composition of the test body, but also of the mass which is the source of the gravitational field. As a consequence, the widest possible range of source and test body configuration needs to be explored when testing the different aspects of EEP, and this is one of the aims of STE-QUEST, which will test for EEP violation in the gravitational fields of the Sun and the Moon. Furthermore, although not discussed further here, the STE-QUEST data can also be analyzed to search for violation of EEP in other source fields, e.g. that of galactic dark matter as in [SCHLAMMINGER (2008)]. Such future searches will be part of the legacy of STE-QUEST.

### 2.1.3 Why Would the EEP be Violated?

It has already been pointed out that the EEP is in fact rather “unnatural” in the sense that it renders gravity so different from other interactions, because the corresponding universal coupling implies that gravitation is a geometrical attribute of space-time itself rather than a field over space-time like all other known interactions. Einstein himself initially called it the “hypothesis of equivalence” before elevating it to a “principle” once it became clear how central it was in the generalization of special relativity to include gravitation. This shows how surprising it is in fact that such a hypothesis should be satisfied at all, let alone down to the uncertainties of present day tests. Therefore, rather than asking why the EEP should be violated, the more natural question to ask is why no violation has been observed yet. Indeed most attempts at quantum gravity and unification theories lead to a violation of the EEP [TAYLOR (1988), DAMOUR (1994), DIMOPOULOS (1996), ANTONIADIS (1998), RUBAKOV (2001), MAARTENS (2010)], which in general have to be handled by some tuning mechanism in order to make the theory compatible with existing limits on EEP violation. For example, in string theory moduli fields need to be rendered massive (short range) [TAYLOR (1988)] or stabilized by e.g. cosmological considerations [DAMOUR (1994)] in order to avoid the stringent limits already imposed by EEP tests. Similarly M-theory and Brane-world scenarios using large or compactified extra dimensions need some mechanism to avoid existing experimental limits from EEP tests or tests of the inverse square law [ANTONIADIS (1998), MAARTENS (2010), RUBAKOV (2001), ADELBERGER (2009), ANTONIADIS (2011)]. The latter consider a modification of the gravitational inverse square law (e.g. in the form of a Yukawa potential) and are in many respects complementary to EEP tests. However, violations of the inverse square law will also be detected by certain EEP tests (e.g. red-shift tests), allowing for a much richer phenomenology with different distance dependences and anomalous couplings. Therefore, not only do we expect a violation of EEP at some level, but the non-observation of such a violation with improving uncertainty is already one of the major experimental constraints for the development of new theories in the quest for quantum gravity and unification (see Figure 2-1). This makes experimental tests of EEP in all its aspects one of the most essential enterprises of fundamental physics today.

It is interesting to note that experimental constraints for EEP violations at low energy are rather closely related to present day physics at the very small scale (particle physics) and the very large scale (cosmology). These connections are discussed in more detail in Sec. 2.2.1 and 2.2.2. Here we provide only a brief insight into those relations.

In particle physics the Standard Model requires a number of dimensionless coupling constants to be “put in” by hand, which seems somewhat arbitrary and is not very satisfactory [DAMOUR (2012)]. One of the aims of theoretical developments is then to replace these constants by some dynamical field that provides the coupling constants (e.g. moduli fields in string theory, dilaton, etc.), similarly to the Higgs field giving rise to the mass of fundamental particles. As a consequence the coupling constants become dynamical quantities that vary in space-time (e.g. space-time variation of the fine structure constant  $\alpha$ ), which necessarily leads to violations of the EEP (violation of LPI, but also of WEP/UFF, and LLI). However, the resulting phenomenological consequences are such, that in most approaches one requires some mechanism to stabilize these fields in order to be compatible with present day constraints from EEP tests [TAYLOR (1988), DAMOUR (1994)]. Although no firm predictions exist, this makes the discovery of the effect of such fields (e.g. EEP violation) a distinct possibility [DAMOUR (2012)]. Most such additional fields are scalar fields, and the recent experimental confirmation of the Higgs boson has thus lent strong credibility to their existence, as the Higgs

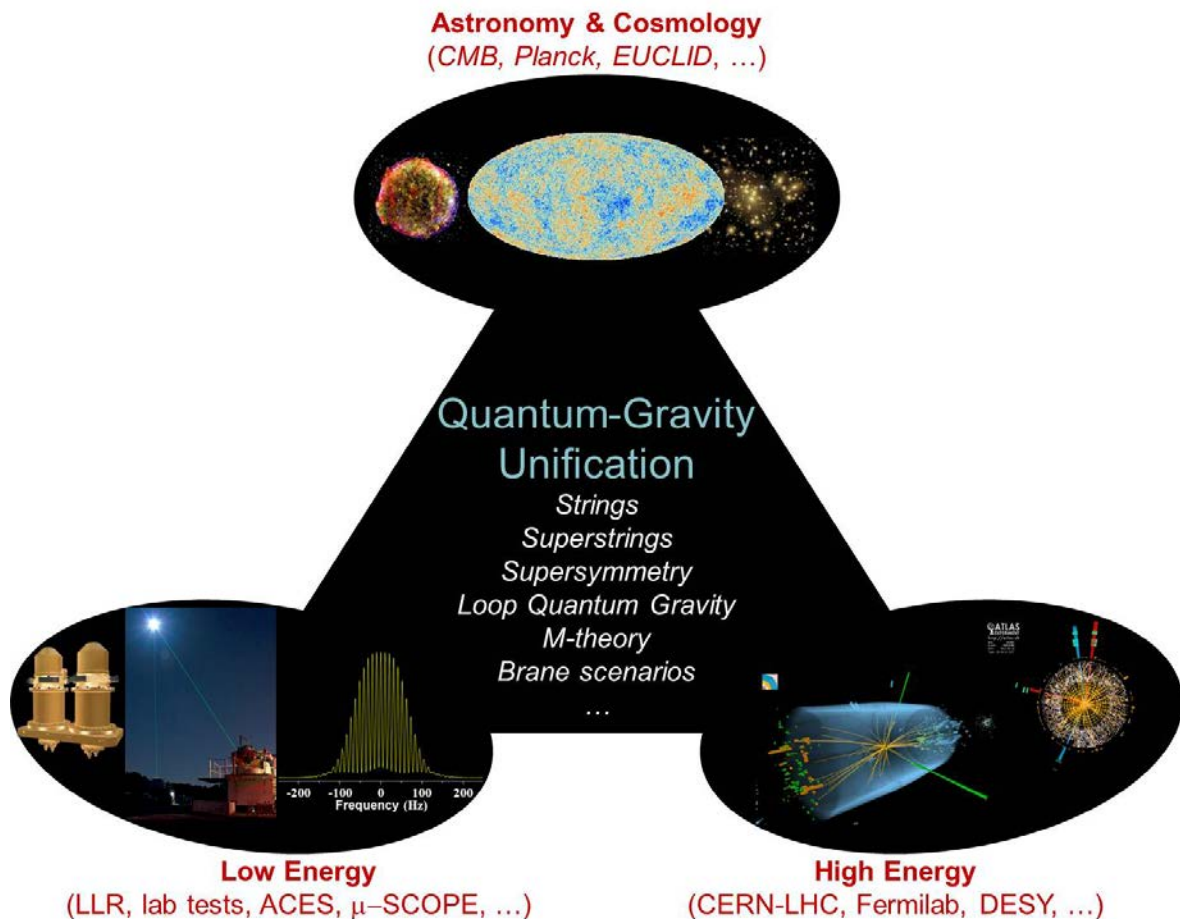


**Figure 2-1:** Experimental support for quantum gravity and unification theories. The relation to cosmology and high energy physics is discussed in Sec. 2.2.1 and 2.2.2. STE-QUEST will contribute to the low energy data by improving on several aspects of Einstein Equivalence Principle (EEP) tests.

is the first fundamental scalar field observed in nature. It is thus likely that additional long and/or short range scalar fields exist, as postulated by many unification theories, and EEP tests are one of the most promising experimental means for their observation.

At the other extreme, in cosmology, most models for Dark Energy (DE) are also based on long range scalar fields that, when considered in the context of particle physics, are non-universally coupled to the fields of the Standard Model [KHOURY (2004)]. As a consequence, one would expect EEP violations from such fields at some level, which might be detectable by experiments like STE-QUEST thus shedding light on the dark energy content of the universe from a completely different angle. Similarly, long range scalar fields coupled to Dark Matter (DM) have been investigated as a possible source of EEP violations [CARROLL (2009)], which again provides a very appealing route towards independent confirmation of DM, making it more tangible than only a hypothesis for otherwise unexplained astronomical observations.

## 2.2 Einstein Equivalence Principle in the Context of Physics Today

### 2.2.1 Cosmology Context

One of the most important discoveries of the past decade has been that the present Universe is not only expanding, but it is also accelerating [PERLMUTTER (1999), RIESS (1998), ADE (2013)]. Such a scenario is problematic within the standard cosmological model, based on General Relativity, and the Standard Model of particle physics. Together, these two models provide a set of predictions well in agreement with observations: the formation of light elements in the early Universe (the big bang nucleosynthesis (BBN)), the existence of the cosmic microwave background (CMB), and the expansion of the Universe. However, now the big challenge of modern cosmology and particle physics is to understand the observed acceleration of the Universe. Observations indicate that the content of matter and energy in our Universe is about 68.3% dark energy (DE), 26.8% dark matter (DM), and 4.9% baryonic matter [ADE (2013)]. These values are obtained

assuming the  $\Lambda$ -CDM model. There are independent confirmations of the DE component of the Universe from observations of high red-shift Type Ia Supernovae [PERLMUTTER (1999), RIESS (1998), GARNAVICH (1998), KNOP (2003)]. The evidence for DM comes essentially from the analysis of galactic rotation curves [FABER (1979)], acoustic oscillations in the CMB [HU (1995), JUNGMAN (1996), ZALDARRIAGA (1997)], large scale structure formation [EISENSTEIN (1998) and (2005)], and gravitational lensing [CLOWE (2006), ZHANG (2007)]. Nevertheless, although there is such a strong evidence for the existence of DE and DM, almost nothing is known about their nature and properties.

The simplest explanation of DE is the existence of a small, but nonzero, cosmological constant  $\Lambda$ . The latter does not undergo a dynamical evolution, and is conventionally associated to the energy of the vacuum in a quantum field theory (in other words, the cosmological constant is a constant energy density filling space homogeneously and isotropically, and physically is equivalent to vacuum energy). As a consequence, it should store the energy density of the present day Universe and its value should be of the order of the critical density. In fact, from the observations it follows that  $\Lambda \approx H_0^2$ , where  $H_0 = 2 \cdot 10^{-42}$  GeV is the present value of the Hubble parameter and is related to the dimension of the Universe. The vacuum energy density associated to the cosmological constant is therefore  $\rho_\Lambda = \Lambda/8\pi G \approx 10^{-47}$  GeV<sup>4</sup> ( $\approx \rho_{\text{critical}}$ ). On the other hand, arguments from quantum field theory imply that the vacuum energy density is the sum of zero point energy of quantum fields with a cutoff determined by the Planck scale ( $m_P = 1.22 \cdot 10^{19}$  GeV) giving  $\rho_{\text{vacuum}} \approx 10^{74}$  GeV<sup>4</sup>, which is about 121 orders of magnitude larger than the observed value  $\rho_\Lambda = 10^{-47}$  GeV<sup>4</sup>. A lower scale, fixed for example at the QCD scale, would give  $\rho_{\text{vacuum}} \approx 10^{-3}$  GeV<sup>4</sup> which is still too large with respect to  $\rho_\Lambda = 10^{-47}$  GeV<sup>4</sup>. From a theoretical point of view, at the moment, there is no explanation as to why the cosmological constant should assume the correct value at the scale of the observed Universe.

Rather than dealing directly with the cosmological constant to explain the accelerating phase of the present Universe, a number of alternative approaches and models have been proposed in the last years. Some of these models are briefly summarized below:

- Quintessence models [WETTERICH (1998), RATRA (1998), CARROL (1998)] - These models invoke a time evolving scalar field with an effective potential that provides the observed inflation.
- Chameleon fields [KHOURY (2004), BRAX (2004)] - In this model the scalar field couples to the baryon energy density and is homogeneous, varying across space from solar system to cosmological scales.
- K-essence [CHIBE (2000), ARMENDARIZ-PICON (2000) and (2001)] - Here the scalar field sector does contain a non-canonical kinetic term.
- Modified gravity arising out of string theory [DVALI (2000)] - In this model the feedback of non-linearities into the evolution equations can significantly change the background evolution leading to acceleration at late times without introducing DE.
- Chaplygin gases [KAMENSHCHIK (2001), BILIC (2002), BENTO (2002)] - This model attempts to unify DE and DM in a unique setting, by allowing for a fluid with an equation of state which evolves between the two.
- $f(R)$ -gravity [CAPOZZIELLO (2011), NOJIRI (2007)] - In this model one considers the Hilbert-Einstein action as a generic function of the scalar curvature  $R$ , not necessarily linear in  $R$  as in the conventional General Relativity.  $f(R)$  gravity contains many features which make these models very attractive, as for example: 1) they provide a natural unification of the early-time inflation and the later-time acceleration of the Universe owing to the different role of the gravitational terms relevant at small and large scales; 2) they allow to unify DM and DE; 3) they provide a framework for the explanation of the hierarchy problem and unification of Grand Unified Theories (GUT) with gravity. However, some  $f(R)$  models of gravity are strongly constrained (or ruled out) by solar system tests restricting the possible models.
- Phantom Dark Energy [Caldwell (2002)].

Many of the models proposed in literature are characterized by the fact that a scalar field (or more than one scalar field) coupled or not to gravity and ordinary matter are included in the action of gravity.

On a fundamental ground, there are several reasons to introduce a scalar field in the action describing gravity. A scalar field coupled to gravity is an unavoidable aspect of all theories aimed to unify gravity with the other fundamental forces. These theories include Superstring, Supergravity (SUGRA), M theories. Moreover, scalar fields appear both in particle physics and cosmology: the Higgs boson in the Standard

Model, the (string) dilaton entering the supermultiplet of the higher dimensional graviton, the super-partner of spin  $\frac{1}{2}$  in SUGRA. It also plays a non-trivial role in models based on composite bosons condensate. The introduction of a scalar field gives rise typically to a violation of the Einstein Equivalence Principle (EEP) depending on its coupling to the Lagrangian describing ordinary matter.

The above considerations apply to most extended theories of Gravity (scalar tensor theories,  $f(R)$  gravity, and so on), which leaves the foundation of relativistic gravity on a rather shaky ground. That becomes a problem especially when trying to isolate the fundamental properties of classical gravity which should be preserved in approaches to quantum or emergent gravity [CAPOZZIELLO (2011)]. The STE-QUEST experiment will therefore play a crucial role not only for searching possible violation of the EEP, but will shed light also on what effective theories of gravity among those above mentioned is the true theory for describing gravity.

A violation of the EEP in the *dark sector*, i.e. DM and DE sectors, comes also from possible coupling of DM to a scalar field. More precisely, a (light) scalar field coupled to DM could mediate a long-range force of strength comparable to gravity [CARROLL (2009) and (2010), BEAN (2008)]. This kind of investigation is also motivated by the fact that such interactions could account for features related to the DM distribution as well as to DM-quintessence interactions [CARROLL (2009) and (2010), BEAN (2008), DAMOUR (1990), BERTOLAMI (2005), GUBSER (2004)] (limits on such a force have been derived from observations of DM dynamics in the tidal stream of the Sagittarius dwarf galaxy which yields a force with strength less than 20% of gravity for a range of 20 kpc [KESDEN (2006)A and (2006)B]). Moreover, as noted in CARROLL (2009), CARROLL (2010), and BEAN (2008), if a new long-range force will be detected in future, then it would be a signal of the presence of a new mass hierarchy between the light scalar mass  $m_\phi < 10^{-25}$  eV and the weak scale  $m_W \approx 10^2$  GeV, in addition to the one between the weak scale and the Planck scale. The possibility that a scalar field couples to Standard Model particles implies that the force acting on ordinary matter could be composition-dependent [DAMOUR (1996)]. As a consequence, such forces are tightly constrained by Eötvös experiments looking for violations of the weak EEP [SCHLAMMINGER (2008)]. On the other hand, even if  $\phi$  has only an elementary (i.e., renormalizable) coupling to DM, interactions between DM and ordinary matter will still induce a coupling of  $\phi$  to ordinary matter [CARROLL (2009) and (2010), BEAN (2008)]. This can be thought of as arising from the scalar coupling to virtual DM particles in ordinary atomic nuclei. Hence, a fifth force coupled to the Standard Model is naturally expected in the case in which a light scalar couples to a DM field having Standard Model interactions.

Without any doubts, the equivalence of gravitational mass and inertial mass represents one of the most fundamental postulates in nature. Theoretical attempts to connect general relativity to the Standard Model of particles are affected by a violation of the EEP [DAMOUR (1996)]. Therefore, tests of the EEP turn out to be important tests of unification scale physics far beyond the reach of traditional particle physics experiments. The discoveries of DM and DE have provided strong motivation to extend tests of the EEP to the highest precision possible. In this respect, the STE-QUEST experiment will play a significant role.

## 2.2.2 Particle Physics Context

In Sec. 2.2.1, it already becomes clear that the difficulties of GR in cosmology are closely related to those in particle physics. In particular, in a quantum field theory (like e.g. the Standard Model of particle physics), one would expect that the vacuum energy of the fundamental fields should be observed in its gravitational consequences, especially on the large scale of the universe. However, there is a huge discrepancy (121 orders of magnitude, or at least 44 orders of magnitude if one assumes the QCD scale, see Sec. 2.2.1) between the observed vacuum energy density of the universe (dark energy) and the one expected from the Standard Model of particle physics. This has been considered a major problem in modern physics, even before the discovery of dark energy when the “observed” value of the cosmological constant (or vacuum energy) was compatible with zero [WEINBERG (1989)]. And one might argue that this problem has become even worse since the discovery of the accelerated expansion of the universe, and the associated small *but non-zero* value of  $\Lambda$ , as now one requires a mechanism that does not completely “block” the gravitational effect of vacuum energy, but suppresses it by a huge factor, i.e. some extreme fine tuning mechanism is required that is difficult to imagine.

As already mentioned in the introduction, another conceptual problem is that the Standard Model of particle physics requires a number of dimensionless coupling constants to be “put in” by hand, which seems somewhat arbitrary and is not very satisfactory [DAMOUR (2012)]. One of the aims of theoretical developments is then to replace these constants by some dynamical field that provides the coupling constants (e.g. moduli fields in string theory, dilaton, etc...), similarly to the Higgs field giving rise to the mass of

fundamental particles. As a consequence the coupling constants become dynamical quantities that vary in space-time (e.g. space-time variation of the fine structure constant  $\alpha$ ), which necessarily leads to violations of the EEP (violation of LPI, but also of WEP/UFF and LLI). However, the resulting phenomenological consequences are such, that in most approaches one requires some mechanism to stabilize these fields in order to be compatible with present day constraints from EEP tests [TAYLOR (1988), DAMOUR (1994)]. Although no firm predictions exist, this makes the discovery of the effect of such fields (e.g. EEP violation) a distinct possibility [DAMOUR (2012)].

The recent discovery of the Higgs particle at LHC confirms the existence of the first fundamental scalar field, at least fundamental down to the scale probed by the Standard Model. As discussed in the previous section, scalar fields are ubiquitous in cosmology because they easily provide a diffuse background: they play a central role in most models of inflation or of dark energy. It is thus important to have identified at least one fundamental scalar field. There has been attempts to make the Higgs field itself play a role in cosmology, by coupling it to the curvature of space-time. This is for example the model of Higgs inflation [BEZRUKOV (2008)]. At first glance, this might seem to lead to violations of the equivalence principle but, going to an Einstein frame, this gives rise to nonlinear interactions of the Higgs field, which are down by powers of the Planck mass (or more precisely  $M_p/\xi$  if  $\xi$  is the coupling of the Higgs to curvature) [BEZRUKOV (2011)].

Even if one disregards gravity, the Standard Model of particle physics still does not address all the fundamental questions: in particular, whereas it attributes the origin of mass to the Higgs non-vanishing vacuum value, it does not explain the diversity of the masses of the fundamental particles, i.e. it does not explain the diversity of the couplings of the matter to the Higgs field. One thus has to go to theories beyond the Standard Model in order to answer these questions. Most of these theories make heavy use of scalar fields, the most notable examples being supersymmetry, which associates a scalar field to any spin  $\frac{1}{2}$  matter field, string theory and higher-dimensional theories. Some of these scalar fields may be extremely light, or even massless, which leads to new types of long range forces, and thus potential EEP violations, unless these fields are universally coupled, a difficult property to achieve.

Moreover, the values of these scalar fields often have a predictive role in setting the value of fundamental constants or ratios of mass scales. Because they are weakly coupled to ordinary matter, they may not have reached their fundamental state, in which case they are still evolving with time. This leads to a time dependence of the corresponding constants or mass scales, and thus again to a potential violation of the equivalence principle.

### 2.2.3 Quantum Mechanics and the Einstein Equivalence Principle

Quantum tests of the Equivalence Principle differ from classical ones because classical and quantum descriptions of motion are fundamentally different. In particular, the Universality of Free Fall (or WEP) has a clear significance in the classical context where it means that space-time trajectories of test particles do not depend on the composition of these particles. How UFF/WEP is to be understood in Quantum Mechanics is a much more delicate point. The subtlety of discussions of the Einstein Equivalence Principle in a quantum context is also apparent in the debate about the comparison of various facets of the EEP, in particular the UFF and the Local Position Invariance [MÜLLER (2010), WOLF (2011), GIULINI (2012)]. More generally, considering quantum phenomena in the context of gravity poses many conceptual and fundamental difficulties as discussed below. Although not all of these are directly explored by STE-QUEST, they provide a broad picture of the limits of our knowledge in this domain and thus the interest of experiments like STE-QUEST that have the discovery potential for expected and unexpected results that might shed light on this frontier of physics.

Let us first discuss the case where no distinction is made between classical and quantum tests, by evaluating different UFF tests with respect to non-standard theories, as was done for example by Damour & Donoghue for the specific case of couplings to a light dilaton [DAMOUR (2010)]. The same type of argument is also valid for a vector field like the  $U$  boson [FAYET (1986) and (1990)]. In that case a similar absolute value for the precision (say  $10^{-15}$  for instance) leads to a larger sensitivity for the free fall of Titanium ( $^{48}\text{Ti}$ ) and Platinum ( $^{196}\text{Pt}$ ) test masses (e.g. the MICROSCOPE mission) than for STE-QUEST where the two isotopes of rubidium ( $^{85}\text{Rb}$  and  $^{87}\text{Rb}$ ) are compared. To be more quantitative, in a model such as DAMOUR (2010), the sensitivity depends on the difference in  $E_i/M$  ratios between the two test masses with  $E_i$  a particular type of nuclear binding energy (volume, surface, Coulomb, asymmetry and pairing energies). The difference in sensitivities then simply stems from the locations of these atoms along the sequence of stable heavy elements

in the  $(N,Z)$  plane as shown in Figure 2-2, with the Pt-Ti pair being between 5 and 60 times more sensitive (depending which  $E_i$  is considered) than  $^{85}\text{Rb}$ - $^{87}\text{Rb}$ .

However, this conclusion holds for a variation along the main sequence of stable nuclei (and for a specific non-standard model). With a wider phenomenological point of view, the  $^{85}\text{Rb}$ - $^{87}\text{Rb}$  test has to be considered as exploring a variation in the table of nuclei, which is complementary to that along the main sequence. In this context, the precision of STE-QUEST has to be compared to existing tests between two Rb isotopes rather than to MICROSCOPE. This is similar to methods used in the context of particle physics when the CERN Scientific Council has accepted experiments [DOSER (2010), PEREZ (2012)] for testing the free fall of cold anti-hydrogen atoms at a level of the order of  $10^{-2}$ . With most non-standard theories used to compare

the interest of experiments, the targeted precision is far from what is already known from classical tests of the EEP. The fact that the experiments have been judged to be worthy shows the peculiar interest of tests of UFF performed with non-classical objects like antimatter or quantum objects.

Let us now discuss a number of physical hypothesis one is implicitly making when doing the classical comparison in the previous section, simply looking at the different locations of the tested materials in Figure 2-2, i.e. assuming that there is nothing special about quantum tests.

The first implicit assumption is that quantum mechanics is valid in the freely falling frame associated with classical test bodies in the definition of WEP. Indeed, the usual definition of the EEP states that special relativity holds in the freely falling frame of WEP without reference to quantum mechanics (and relativistic quantum mechanics did not exist at the time of the earliest formulation of the EEP by Einstein in 1911). Of course, this extension of the notion of freely falling frame to quantum mechanics is always implicit and “obvious”. It is used when one computes the phase shift of a matter wave interferometer in a gravity field, using the full machinery of quantum mechanics, for instance Feynman's path integral formalism [STOREY (1994)].

Another important implicit assumption is that any possible violation of the EEP must be due to a new fundamental interaction (which superposes to the gravitational force), and that fundamental interactions are described in the framework of quantum field theory (QFT) by bosonic fields. In particular, the formalism of QFT must be true for that field, e.g. the procedures of second quantization and of renormalization. The consequence is that the violation of the EEP is either due to a scalar spin-0 field (dilaton) or a vector field (for instance the  $U$  boson [FAYET (1986) and (1990)]). Indeed, recall that higher-order spin fields ( $s \geq 2$ ) yield difficulties, for instance the coupling of an additional spin-2 field to the spin-2 field of general relativity is problematic. Of course there are theorems that fundamental interactions in the framework of relativistic quantum mechanics necessarily proceeds with the notion of fields, but as physicists we also want to prove our theorems experimentally.

The previous statements represent the state-of-the-art of Physics that we have today; if one of these would turn out to be wrong this would provoke a major crisis in Physics. Nevertheless, because they are so fundamental, these statements are worth to be experimentally verified wherever possible. It is true that they are tested every day in particle accelerators, but in a regime where the gravitational field plays essentially no role. Testing the EEP for quantum waves in the presence of gravity represents a new way of testing some of our deepest beliefs in Physics at the interplay between QM and GR.

Additionally, there are a number of other concerns regarding the quantum to classical comparison in general, which illustrate the difficulties in this region of physics and thus the interest of any experimental guidance.

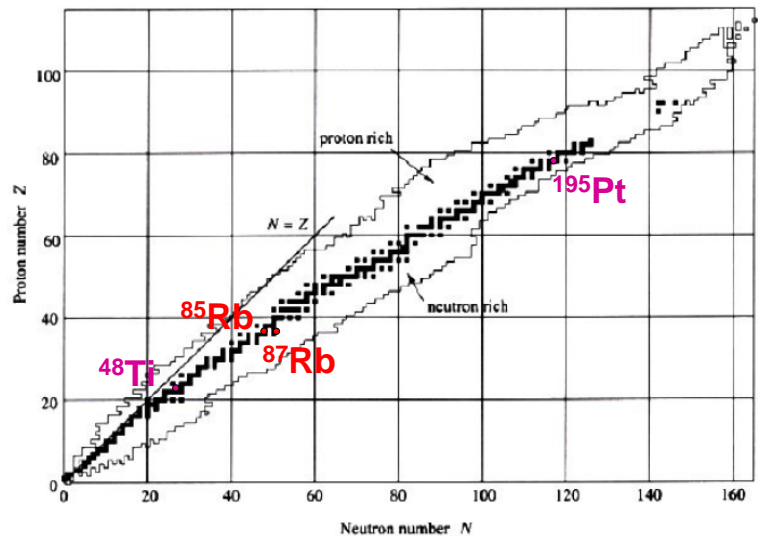


**Figure 2-2:** The valley of stable nuclei in the  $(N,Z)$  plane, with the nuclei used in STE-QUEST in red, and those of MICROSCOPE in violet.

The variety of quantum states is much larger than that of classical ones and it seems therefore plausible that quantum tests may ultimately be able to see deeper details of couplings between matter and gravity than classical ones. When considering non-standard couplings of matter to gravity, there might be a difference between how the wave packet centre is moving and how it is deforming [KAJARI (2010), BOURDEL (2011), UNNIKRIISHNAN (2012)]. As an illustration in a concrete example, let us consider the free fall in a gravitational field of a particle in QM described by the wave function  $\psi$ . We assume that the wave function is initially Gaussian. Schroedinger's equation with Hamiltonian operator

$$\hat{H} = \frac{\hat{p}_z^2}{2m} + mg\hat{z} \quad (2-2)$$

is satisfied, where the second term is the usual Newtonian gravitational potential. We compute the time of flight of this particle from some initial position  $z_0$  up to  $z = 0$ , the initial position being determined by the expectation value  $z_0 = \langle \hat{z} \rangle_{\psi_0}$  of the position in the Gaussian initial state  $\psi_0$ . The time of flight is statistically distributed with the mean value agreeing with the classical universal value,

$$T = \sqrt{\frac{2z_0}{g}}. \quad (2-3)$$

However, the standard deviation of the measured values of the time of flight around  $T$  depends on the mass of the particle

$$\sigma = \frac{\hbar}{\Delta_0 mg}, \quad (2-4)$$

where  $\Delta_0$  is the width of the initial Gaussian wave packet. In this sense the quantum motion of the particle is non-universal, as it depends on the value of its mass [LÄMMERZAHN (1996), VIOLA (1997), DAVIES (2004)]. Another example is the role of intrinsic spin of quantum probes, that has no classical equivalent. For classical particles, the EEP is implemented by the rule of the minimal coupling (see e.g. WEINBERG (1972)): In the presence of the gravitational field we replace the Minkowski metric  $\eta_{\mu\nu}$  in the Lagrangian of special relativity by the curved space-time metric  $g_{\mu\nu}$  of general relativity. Suppose that a classical body is made of  $N$  particles with positions  $\mathbf{x}_a$  and velocities  $\mathbf{v}_a$  interacting through the classical electromagnetic field  $A_\alpha$ , with dynamics obeying the Lagrangian  $L_{SR}[\mathbf{x}_a, \mathbf{v}_a, A_\alpha, \eta_{\mu\nu}]$  in special relativity. Then the Lagrangian describing the dynamics of this body in general relativity will simply be  $L_{GR}[\mathbf{x}_a, \mathbf{v}_a, A_\alpha, g_{\mu\nu}]$ . The procedure to couple a quantum field to gravity is much more complex and, we argue, more fundamental than for the coupling of classical fields. The Lagrangian of the quantum field (e.g. the Dirac field) depends on the derivative of the field because of the intrinsic spin, and requires additional formalisms like tetrads and the spinorial representations of the Lorentz group and the associated spinorial derivative. So, while classical matter is coupled to gravity by using only the metric ( $\eta_{\mu\nu}$  replaced by  $g_{\mu\nu}$ ), quantum fields associated with electrons and other fermions are coupled to gravity through tetrads, which may be considered as a deeper representation of space-time (the metric is immediately deduced from the tetrads, but the inverse is not true). Of course, atom interferometry tests of the Equivalence Principle are usually performed with spin-less states ( $m_F = 0$ ) because the latter are insensitive to magnetic fields at first order. They can also be performed with other Zeeman sublevels with a somewhat reduced precision due to the first-order coupling with magnetic fields. This possibility of performing spin-dependent tests is an obvious advantage of quantum tests over classical versions of EP tests though the latter may of course perform tests with spin-polarized matter [HOEDL (2011)]. Comparing these various tests could be done by following the line already opened for spin-dependent clock measurements [WOLF (2006)], using the Standard Model Extension framework [KOSTELECKÝ (2011)A].

Our main concern about the frontier between QM and GR is of course the absence of a consistent quantum theory of gravity. As a result fundamental questions remain unanswered, such as: What is the gravitational field generated by a quantum system described by some quantum wave function  $\psi$ ? The best answer we have at the moment is the so-called semi-classical theory, which states that the gravitational field obeys the Einstein field equation

$$G_{\mu\nu} = \frac{8\pi G}{c^4} \langle \hat{T}_{\mu\nu} \rangle, \quad (2-5)$$

but with the expectation value of the stress-energy quantum operator  $\hat{T}^{\mu\nu}$  in the given quantum state  $\psi$  at the right-hand side. It is known (see e.g. [WALD (1984)]) that the semi-classical Eq. (2-5) is inconsistent with the process of measurement in quantum mechanics and the collapse of the wave packet. Suppose that we have a

state of matter made of the superposition of two states (each with probability 1/2) in which the matter is localized, respectively, into two different disjoint regions. According to Eq. (2-5) the gravitational field will be generated by half the matter in the first region and by half the matter in the other distinct region. However, this is incompatible with a measurement of the location of the matter (and the associated collapse of the wave function), since after measurement all the matter will be either located entirely in the first region *or* entirely in the other. Such paradoxes are simply the result of the fact that the semi-classical theory is only an approximation to the more fundamental quantum theory of gravity. It is an effective description of quantum systems under gravity, including their own field, and as such it makes sense and has interesting physical consequences like the back reaction of Hawking's radiation on black holes, or that of quantum fields in the early Universe. Although the semi-classical theory will not be checked directly by quantum tests of the EEP, the above paradoxes remind us that we do not dispose of a consistent quantum theory of gravity and that experimental evidence exploring the relationship between QM and GR is direly needed.

In summary, although there is no established theory that favors quantum tests of the EEP, there are nonetheless a number of difficulties in the frontier between QM and GR due to the absence of a quantum theory of gravitation that call for experiments that lie at that frontier, like quantum tests of the EEP proposed by STE-QUEST.

On the experimental side, quantum mechanical tests have to be considered as opening a new technological channel based on quantum sensors, which is probably the best solution for future much improved tests. Whereas macroscopic tests approach their ultimate limits after years of scientific research and technical development, this is not the case for atomic tests. In particular, the accuracy of the atom interferometry test in STE-QUEST ( $2 \cdot 10^{-15}$ ) shows an improvement by 8 orders of magnitude over the best existing test ( $10^{-7}$ ) between two Rb isotopes. With this improvement, it already reaches the level of accuracy of MICROSCOPE [TOUBOUL (2001)], while still having possibilities for future improvements.

## 2.3 STE-QUEST Tests of the Einstein Equivalence Principle

In this section, we discuss specifically the tests of the EEP carried out by STE-QUEST. We first describe a general theoretical framework for the WEP/UFF and LPI tests that allows a classification and comparison of the different experiments and clarifies the complementarity between the different types of tests. We then use that framework to compare each of the planned STE-QUEST experiments to existing and expected measurements in the same domain and point out the improvements expected from STE-QUEST. Finally we address the possible STE-QUEST tests of Lorentz Invariance and CPT symmetry using another theoretical framework particularly adapted for that purpose.

### 2.3.1 Different Tests of the EEP

Tests of the different aspects of EEP (i.e. WEP, LLI, and LPI), and the relations between them, are best discussed within the “modified Lagrangian framework”, which is a powerful formalism allowing deviations from GR and metric theories of gravity, but at the same time permitting a coherent analysis of various experiments [NORDVEDT (1975), HAUGAN (1979), WILL (1993), WOLF (2011)]. The formalism describes a large class of non-metric theories in a way consistent with Schiff’s conjecture and energy conservation. This class of theories is defined by a single Lagrangian, in which the coupling between gravitation and different types of mass-energies is generically not universal. In a simplified variant of the formalism, we consider a composite body of mass  $m$  (e.g. an atom in a STE-QUEST experiment) in the Newtonian gravitational potential  $U(\mathbf{x}) = GM/r$  of the Earth, where  $r = |\mathbf{x}|$ , thus obeying the Lagrangian

$$L = -mc^2 + mU + \frac{1}{2}m\mathbf{v}^2. \tag{2-6}$$

We postulate that the mass  $m = m(\mathbf{x})$  of this body depends on the position  $\mathbf{x}$  through a violation of the LPI. This is modeled by assuming that a particular internal energy of the body,  $E_X = E_X(\mathbf{x})$ , behaves anomalously in the presence of the gravitational field, where  $X$  refers to the type of interaction involved (electromagnetic, nuclear, spin-spin, spin-orbit, etc.). For simplicity, because we have in mind the discussion of the complementarity between red-shift tests and tests of the UFF, both being performed by STE-QUEST, we consider only a dependence on  $\mathbf{x}$  to model the violation of the LPI. It could be possible to include also a dependence on the velocity  $\mathbf{v}$  to model a violation of LLI. Separating out  $E_X(\mathbf{x})$  from the other forms of energies  $E_Y$  composing the body and which are supposed to behave normally, we write

$$m(\mathbf{x}) = \bar{m} + \frac{1}{c^2} \left[ E_X(\mathbf{x}) + \sum_{Y \neq X} \bar{E}_Y \right]. \quad (2-7)$$

Here  $\bar{m}$  denotes the sum of the rest masses of the particles constituting the body;  $\bar{m}$  and all  $\bar{E}_Y$  are constant. The violation of LPI is modeled in the simplest way by assuming that at the leading order

$$E_X(\mathbf{x}) = \bar{E}_X + \beta_X^{(a)} \bar{m} \Delta U(\mathbf{x}), \quad (2-8)$$

where  $\Delta U = U_{\oplus} - U(\mathbf{x})$  is the potential difference with respect to some reference point. The parameter  $\beta_X^{(a)}$  is dimensionless and characterizes the violation of LPI. It depends on the particular type of mass-energy or interaction under consideration, e.g.  $\beta_X^{(a)}$  would be different for the electromagnetic or the nuclear interactions, with possible variations as a function of spin or the other internal properties of the body ( $a$ ), here labeled by the superscript ( $a$ ). Thus  $\beta_X^{(a)}$  would depend not only on the type of internal energy  $X$  but also on the body ( $a$ ). Defining now the “normal” contribution to the total mass,

$$m_0 = \bar{m} + \sum_Y \frac{\bar{E}_Y}{c^2}, \quad (2-9)$$

and replacing  $m(\mathbf{x})$  by its explicit expression into the Lagrangian of Eq. (2-6) we obtain

$$L = -m_0 c^2 + m_0 \left( U - \beta_X^{(a)} \Delta U \right) + \frac{1}{2} m \mathbf{v}^2, \quad (2-10)$$

where we have neglected higher order terms, which are of no relevance for the discussion here.

We can now analyze the traditional free fall and red-shift experiments. By varying Eq. (2-10), we obtain the equation of motion of the body as

$$\frac{d\mathbf{v}}{dt} = \left( 1 + \beta_X^{(a)} \right) \nabla U, \quad (2-11)$$

which shows that the trajectory is affected by the violation of LPI and is not universal. In fact, we see that  $\beta_X^{(a)}$  measures the non-universality of the ratio between the body's passive gravitational mass and inertial mass. Thus, in this framework, the violation of LPI implies a violation of UFF (and WEP), and  $\beta_X^{(a)}$  is the WEP-violating parameter. This is a classic proof of the validity of Schiff's conjecture [SCHIFF (1960)].

The violation of LPI is best reflected in classical red-shift experiments, which can be analyzed using a cyclic Gedanken experiment based on energy conservation. This was done in [NORDVEDT (1975)] extending a famous argument by Einstein in 1911. The result for the frequency shift  $z$  in a Pound-Rebka type experiment [POUND (1960)] is

$$z = \left( 1 + \alpha_X^{(a)} \right) \frac{\Delta U}{c^2}, \quad (2-12)$$

where the LPI-violating parameter  $\alpha_X^{(a)}$  is again non-universal. The important point is that, within the framework of the modified Lagrangian, the LPI-violating parameter  $\alpha_X^{(a)}$  is related in a precise way to the WEP-violating parameter  $\beta_X^{(a)}$  (see NORDVEDT (1975)),

$$\beta_X^{(a)} = \alpha_X^{(a)} \frac{\bar{E}_X}{\bar{m} c^2}. \quad (2-13)$$

Therefore tests of LPI and WEP are not independent, and we can compare their different qualitative meanings. Since for typical energies involved we have  $\bar{E}_X \ll \bar{m} c^2$ , this means that  $\beta_X \ll \alpha_X$ , where  $\beta_X$  and  $\alpha_X$  denote some typical values of the parameters. For a given set of LPI and WEP tests, their relative merit is given by Eq. (2-13) and it is dependent on the model used, i.e. the type of anomalous energy  $\bar{E}_X$  and the employed materials and bodies.

For example, let us assume a model in which all types of electromagnetic energy are coupled in a non-universal way, i.e.  $\beta_{EM} \neq 0$  (with all other forms of energies behaving normally), and where the clock transition is purely electromagnetic. The WEP test between two materials ( $a$ ) and ( $b$ ), both containing electromagnetic energy (e.g. binding energy), is carried out with an uncertainty of  $|\beta_{EM}^{(a)} - \beta_{EM}^{(b)}| \approx |\beta_{EM}| \leq 10^{-13}$  in best current experiments [SCHLAMMINGER (2008)]. On the other hand, the LPI test for a clock of

type (c) based on an electromagnetic transition<sup>1</sup> is carried out with an uncertainty of  $|\alpha_{EM}^{(c)}| \approx |\alpha_{EM}| \leq 10^{-4}$  in the GPA experiment [VESSOT (1979)]. For macroscopic test bodies, the nuclear electromagnetic binding energy contributes typically to  $\bar{E}_{EM}/(\bar{m}c^2) \approx 10^{-3}$  of the total mass, so from (2-13) we have  $|\beta_{EM}| \approx 10^{-3} \cdot |\alpha_{EM}|$ , which means that the WEP test yields  $|\alpha_{EM}| \leq 10^{-10}$ , a much more stringent limit than the red-shift test ( $|\alpha_{EM}| \leq 10^{-4}$ ).

However, that result depends on the particular model used. If we assume another model in which the nuclear spin plays a role leading to a non-universal coupling of atomic hyperfine energies, i.e.  $\beta_{HF} \neq 0$  (with other forms of energies and properties of the body behaving normally), the result is different. Atomic hyperfine energies are of order  $10^{-24}$  J (corresponding to GHz transition frequencies), which for typical atomic masses leads to  $\bar{E}_{EM}/(\bar{m}c^2) \approx 10^{-16}$ . As a consequence, WEP tests set a limit of only  $|\alpha_{HF}| \leq 10^3$ , while LPI tests using hyperfine transitions (e.g. H-masers) set a limit of about  $|\alpha_{HF}| \leq 10^{-4}$ . The conclusion is therefore radically different in this model where LPI tests perform orders of magnitude better than WEP tests.

To summarize, the two types of tests, WEP (or UFF) and LPI (red-shift), are complementary, and need to be pursued with equal vigor, because depending on the model used either one of the tests can prove significantly more sensitive than the other. The main goal of STE-QUEST is to perform at once the different types of tests of the EEP, with good and in some case unprecedented precision: the WEP/UFF test, which will be done by mean of atom interferometry, the red-shift/LPI test through clock comparisons with optical and microwave links, and also a test of LLI (whose comparison with the WEP and LPI tests could be discussed in a way similar to what was presented above).

### 2.3.2 STE-QUEST Test of the Weak Equivalence Principle

The atom interferometer (ATI) of STE-QUEST is described in detail in Sec. 4.1.1. Here we only recall the main principle and some key numbers in the operation and measurements. The STE-QUEST ATI is a dual species atom interferometer using the two isotopes of Rb (<sup>85</sup>Rb and <sup>87</sup>Rb) which are simultaneously trapped and cooled by a sequence involving atoms manipulation by lasers and magnetic fields. Atoms are cooled to temperatures below the critical temperature (few nK) for Bose-Einstein Condensation (BEC), which allows operation of the interferometer with degenerate quantum gases (BECs). The complete trapping and cooling process lasts about 10 s. The two isotopes are then released into free fall and subjected simultaneously to a Mach-Zender interferometer. Each isotope undergoes three laser pulses that coherently split, redirect, and recombine the wave packets during another 10 s. The actual separation of the coherent wave packets during the interferometer sequence is of the order 10 cm and larger than their respective size by more than 3 orders of magnitude. During each of the pulses the laser phase is “printed” onto the matter wave phase, so that on re-combination the interference of the two waves (read out via the measured populations of internal states) provides the information of the acceleration of the freely falling matter waves with respect to the laser source. The final observable is then the difference between the measured accelerations of the two isotopes, i.e. the differential acceleration of the <sup>85</sup>Rb and <sup>87</sup>Rb matter waves.

The STE-QUEST AI thus provides a test of the universality of free fall or weak equivalence principle (UFF/WEP). Such tests are generally quantified by the Eötvös ratio  $\eta_{AB}$  for two test objects A and B and a specified source mass of the gravitational field:

$$\eta_{AB} = 2 \cdot \frac{a_A - a_B}{a_A + a_B} = \beta_A - \beta_B, \quad (2-14)$$

where  $a_i$  ( $i = A, B$ ) is the acceleration of object  $i$  with respect to the source mass and  $\beta_i$  is the parameter introduced in Sec. 2.3.1 (see Eq. (2-11)). Note that for a same experiment the data can be interpreted with respect to different source masses [e.g. SCHLAMMINGER (2008)] with corresponding different results for  $\eta$ , and Eq. (2-14) can be further refined in a model dependent way when searching violations linked to particular types of mass-energy (see Sec. 2.3.1).

---

<sup>1</sup> We assume in this example that electromagnetism plays the same role in the nuclear binding energy and the hydrogen hyperfine transition.

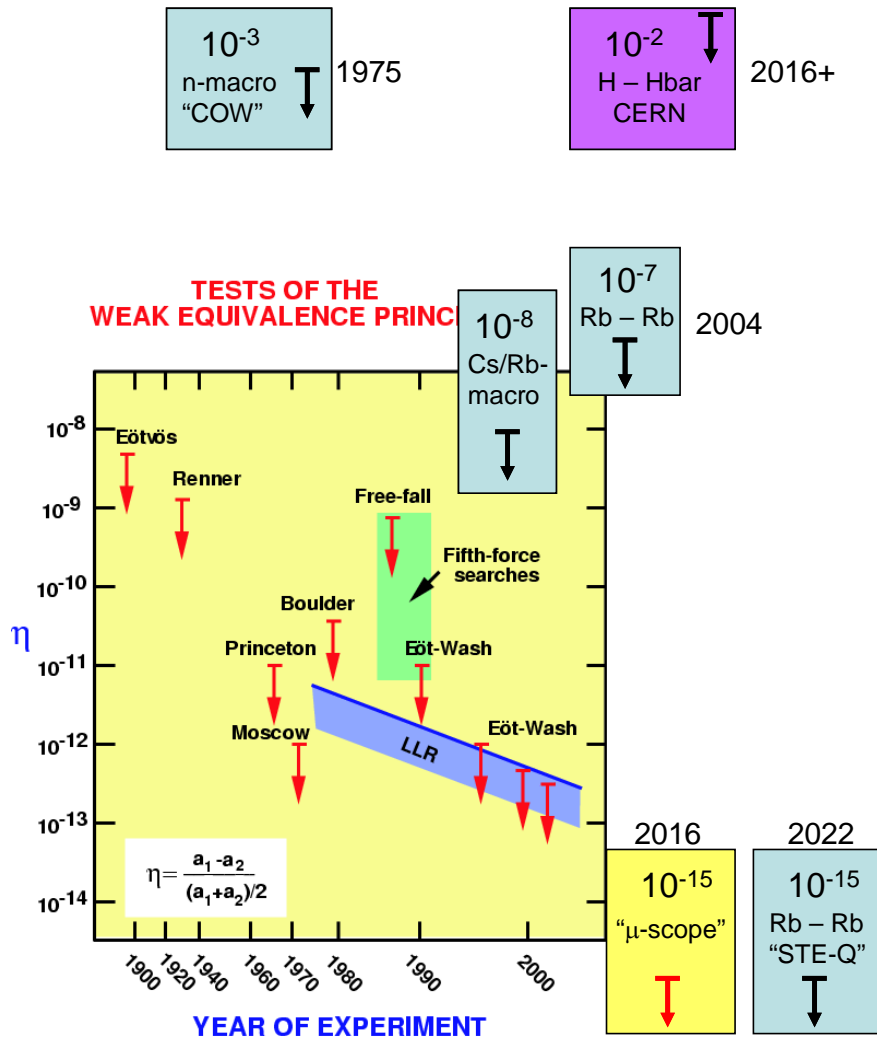


**Figure 2-3:** Present and upcoming tests of WEP/UFF in the Earth field (except for LLR, which is in the Sun field) adapted from [WILL (2006)]. Experiments using macroscopic test masses are represented by red arrows on a yellow background, experiments involving at least one quantum object by black arrows on a blue background. COW is the Collela-Overhauser-Werner experiment [COLELLA (1975)] using neutron interferometry compared to macroscopic test masses. Cs/Rb-macro [PETERS (1999) and MERLET (2010)] are the similar atom interferometry experiments. For completeness the violet entry is the hydrogen vs. anti-hydrogen test in progress at CERN.

The useful ATI measurements are performed during about 1700 s around perigee when the sensitivity is largest. When taking into account all perturbing effects (gravity gradients, vibrations, magnetic fields etc...) the single shot (20 s cycle time) precision is about  $2.9 \cdot 10^{-12} \text{ m/s}^2$  in differential acceleration of the two isotopes, and is dominated by the atomic shot noise. As a consequence, with the STE-QUEST baseline orbit, the goal of  $2 \cdot 10^{-15}$  in the Eötvös ratio can be reached in less than 1.5 years (see Sec. 3.3.1 for details) with good prospects for reaching  $1 \cdot 10^{-15}$  in the mission lifetime. Meanwhile, systematic effects are estimated to be below the  $2 \cdot 10^{-15}$  level once calibrated, with the possibility of carrying out some of the calibrations during the rest of the orbit (away from perigee) thus not impacting the useful measurement time (see Sec. 4.1.1). The final uncertainty of the UFF/WEP test can be compared to present and upcoming tests, by looking directly at the corresponding Eötvös ratios. Figure 2-3 presents such a comparison for different tests in the Earth field (except LLR which is in the sun field).

When examining Figure 2-3, one should bear in mind that the compared experiments all use different test masses, and that thus a direct comparison can be misleading, as discussed in Sec. 2.2.3 and 2.3.1. The only experiment that the STE-QUEST UFF/WEP test can be compared to directly is the ground measurement of the differential free fall of the two Rb isotopes [FRAY (2004)] with respect to which STE-QUEST represents an improvement by impressive 8 orders of magnitude. Even when comparing to macroscopic tests, with best present ground tests from the Eöt-Wash group [SCHLAMMINGER (2008)] or LLR [WILLIAMS (2004)], both at

the  $2 \cdot 10^{-13}$  level, STE-QUEST still represents an improvement by two orders of magnitude. However, it is important to stress here that STE-QUEST measurement is truly quantum in nature (see Sec. 2.2.3), in particular:

- The observable is the phase difference of interfering matter waves in a coherent superposition;
- The coherent superposition is well separated spatially by  $> 10$  cm, more than 3 orders of magnitude larger than the size of the individual wave packets;
- The atoms are condensed to a quantum degenerate state (Bose Einstein Condensates);
- The coherence length of the atoms is of the order of a micron, many orders of magnitude larger than the de Broglie wavelength of the macroscopic test masses ( $10^{-27}$  m or less).

As discussed in Sec .2.5, ground tests using coherent matter waves are also likely to improve within the STE-QUEST time frame. However, they are not expected to reach performances comparable to those of STE-QUEST because of the inherent limits of the ground laboratory environment (short free fall times, gravity gradients, perturbed laboratory environment, etc.), which will ultimately limit tests on ground. This is somewhat akin to classical tests where the next significant improvement is expected from going into space with the MICROSCOPE mission.

Finally, we note that so far no analysis in the field of other sources (e.g. galactic dark matter [SCHLAMMINGER (2008)]) has been carried out for STE-QUEST. This might lead to further interesting limits and experimental possibilities, e.g. by considering parts of the orbit that are not useful for UFF/WEP in the Earth field, but are useful in the field of more distant bodies. Such analysis and corresponding optimization of the measurement scenario will be carried out as the mission progresses and will further enhance the scientific discovery potential of STE-QUEST.

### 2.3.3 STE-QUEST Test of Local Position Invariance

In the baseline configuration, STE-QUEST will be able to compare distant ground clocks using the microwave link (MWL) in common-view mode. In the common-view technique, two ground clocks are simultaneously compared to the space clock. The difference of simultaneous measurements provides then a direct comparison of the two clocks on the ground. This measurement does not require a high-performance frequency reference on-board the STE-QUEST spacecraft. Indeed, the noise of the space clock, which appears as common mode in the two simultaneous link measurements, is rejected to high degree when the difference of the two space-to-ground comparisons is evaluated. According to the STE-QUEST reference orbit, common-view contacts between USA and Europe, Europe and Japan, Japan and USA have uninterrupted durations longer than 10 hours with each of them repeated every two days. The concept of the LPI test in the gravitational field of the Sun is shown in Figure 2-4. In this example the frequency ratio  $\nu_T/\nu_B$  between two ground clocks in Turin and Boulder is measured.

In the framework discussed in Sec. 2.3.1, with the Sun as the source of the anomalous gravitational coupling,

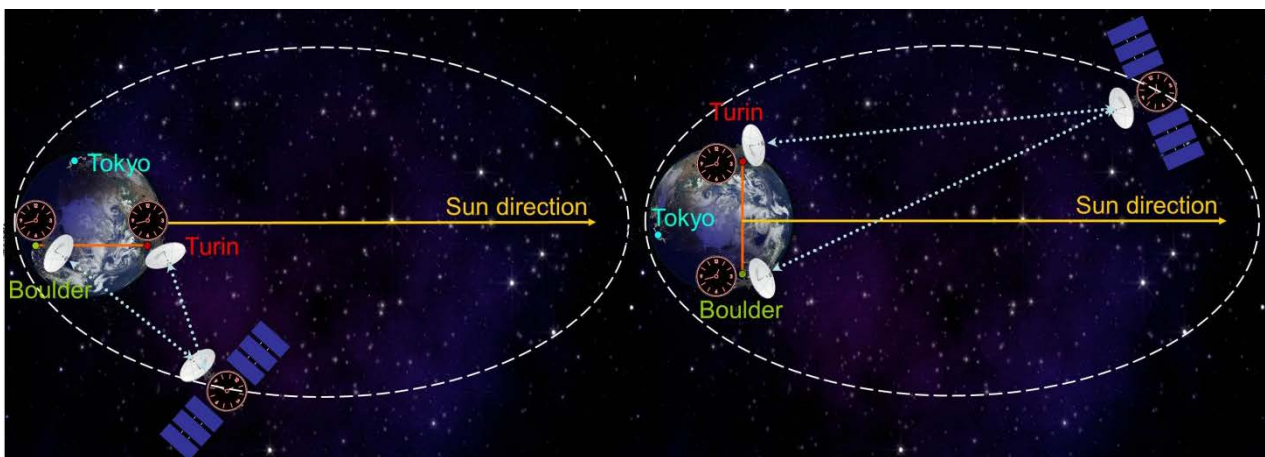


Figure 2-4: Common-view comparison between Torino and Boulder for the test of LPI in the field of the Sun.

the measured frequency ratio of the two clocks can be written as

$$\frac{\nu_T}{\nu_B} = 1 - \frac{1}{c^2} \left[ (U_B - U_T) + \frac{v_B^2 - v_T^2}{2} + (\alpha_B U_B - \alpha_T U_T) \right] + \Delta, \quad (2-15)$$

where  $U_B$  and  $U_T$  are the solar Newtonian gravitational potentials at the locations of the ground clocks and  $v_B$  and  $v_T$  are the corresponding velocities in a solar system barycentric reference frame. The LPI violating parameters  $\alpha_B$  and  $\alpha_T$  depend on the type of transition used in the respective clocks, and  $\Delta$  represents all corrections due to the other solar system bodies (including the Earth) assumed to behave normally, as well as higher order correction terms.

An essential point to note is that, in the absence of an LPI violation ( $\alpha_B = \alpha_T = 0$ ), the leading part in equation (2-15) is equal to zero (up to small tidal correction terms in  $\Delta$  and constant terms from the Earth field). This is a direct consequence of the EEP, as the Earth is freely falling in the Sun field [HOFFMANN (1961)]. The LPI test in the Sun field is thus a null-test, verifying whether the measured frequency ratio is equal to the expected value, i.e.  $1 + \Delta$  in this example.

In general, the types of clocks used at the different ground stations may be of different type so  $\alpha_B \neq \alpha_T$ . In the following, we will assume for simplicity clocks of the same type which simplifies the LPI violating term in (2-15) to  $\alpha \cdot (U_B - U_T)$ , with the aim of the experiment being the measurement of  $\alpha$ . More precisely the experiment will measure the time evolution of the ration  $v_T/v_B$ , which again should be zero in GR (up to correction terms), but will evolve in time if the LPI violating parameters are non-vanishing because of the time evolution of  $U_B - U_T$ , mainly related to the rotation of the Earth. The time evolution of  $(U_B - U_T)/c^2$  will be predominantly periodic with a diurnal period and peak-to-peak amplitude of about  $1 \cdot 10^{-12}$ .

Then, the determination of the LPI parameters boils down to a search of a periodic signal with known frequency and phase in the clock comparison data. As detailed in Sec. 3.3.2, in the baseline configuration the measurement uncertainties of the MWL and the ground clocks should allow a detection of any non-zero value of the LPI violating parameter  $\alpha$  in the Sun field that exceeds  $2 \cdot 10^{-6}$  after four years of integration. In the case that the optional optical link is included in the payload, that goal can be reached in 72 days of integration with the ultimate performance of  $5 \cdot 10^{-7}$  reached in 4 years. Note however, that these results are based on only frequency measurements without making use of the phase cycle continuity provided by the STE-QUEST MWL. When phase cycle continuity is maintained by the link, the measurement duration is not affected by the dead-time between one common-view comparison and the next, resulting in a reduction of the integration time needed to reach the ultimate accuracy. Such a data analysis approach is presently being implemented in the numerical simulations.

The procedure for the LPI test in the Moon field is identical to the sun field test described above. The difference is that the frequency and phase of the signal that one searches for are different and that the sensitivity is decreased by a factor  $\approx 175$  (see below).

In the case where the onboard clock option of STE-QUEST is realized, it will be possible to perform also an LPI test in the field of the Earth. Given that this is only an option, we will discuss the test and the results that can be achieved only briefly. Some more details can be found in Sec. 3.3.2. In this case the MWL (or optical) link is used to compare the onboard clock to ground clocks. In the formalism of Sec. 2.3.1, the frequency ratio can be written as

$$\frac{v_{STE}}{v_B} = 1 - \frac{1}{c^2} \left[ (U_B - U_{STE}) + \frac{v_B^2 - v_{STE}^2}{2} + (\alpha_B U_B - \alpha_{STE} U_{STE}) \right] + \Delta, \quad (2-16)$$

where  $U_B$  and  $U_{STE}$  are the Earth Newtonian gravitational potentials at the locations of the ground clock and the onboard clock, and  $v_B$  and  $v_{STE}$  are the corresponding velocities in a geocentric reference frame. The LPI violating parameters  $\alpha_B$  and  $\alpha_{STE}$  depend on the type of transition used in the respective clocks, and  $\Delta$  represents all corrections due to the other solar system bodies assumed to behave normally, as well as higher order correction terms.

The main difference with respect to the sun LPI test above is that the ground clocks are not freely falling in the field of the Earth, so even in the absence of an LPI violation the frequency ratio is not zero and varying in time with the eccentric orbit of STE-QUEST. The test then compares the theoretically calculated frequency ratio (from the knowledge of the STE-QUEST orbit and the ground station locations) to the actually measured one. This leads to two methods for the measurement, one based on the accuracy of the clocks (so called DC measurement) that searches for an offset with respect to the expected value, and one based on the periodic variation due to the orbit eccentricity (so called AC measurement) that searches for the time varying signature and thus relies on the clock stability. The former is carried out mainly when the satellite is at apogee (when the LPI violating term in (2-16) is largest), the latter uses measurements over the full orbit. As detailed in Sec. 3.3.2, simulations taking into account the MWL and clock noise and accuracy show that with both methods a limit of  $2 \cdot 10^{-7}$  on the LPI violating parameter  $\alpha$  can be reached after 4 days (DC

measurement) and 840 days (AC measurement) of integration. In the case of the DC measurement, the limit is imposed by the clock accuracy rather than the measurement duration. In the case of the AC measurement the limit can be decreased to  $1.5 \cdot 10^{-7}$  when integrating over the whole mission duration. The sensitivities of STE-QUEST estimated above can be compared to present and upcoming LPI tests by looking directly at the limits on the corresponding parameters (see Sec. 2.3.1). Such a comparison is presented in Figure 2-5, adapted and updated from [WILL (2006)].

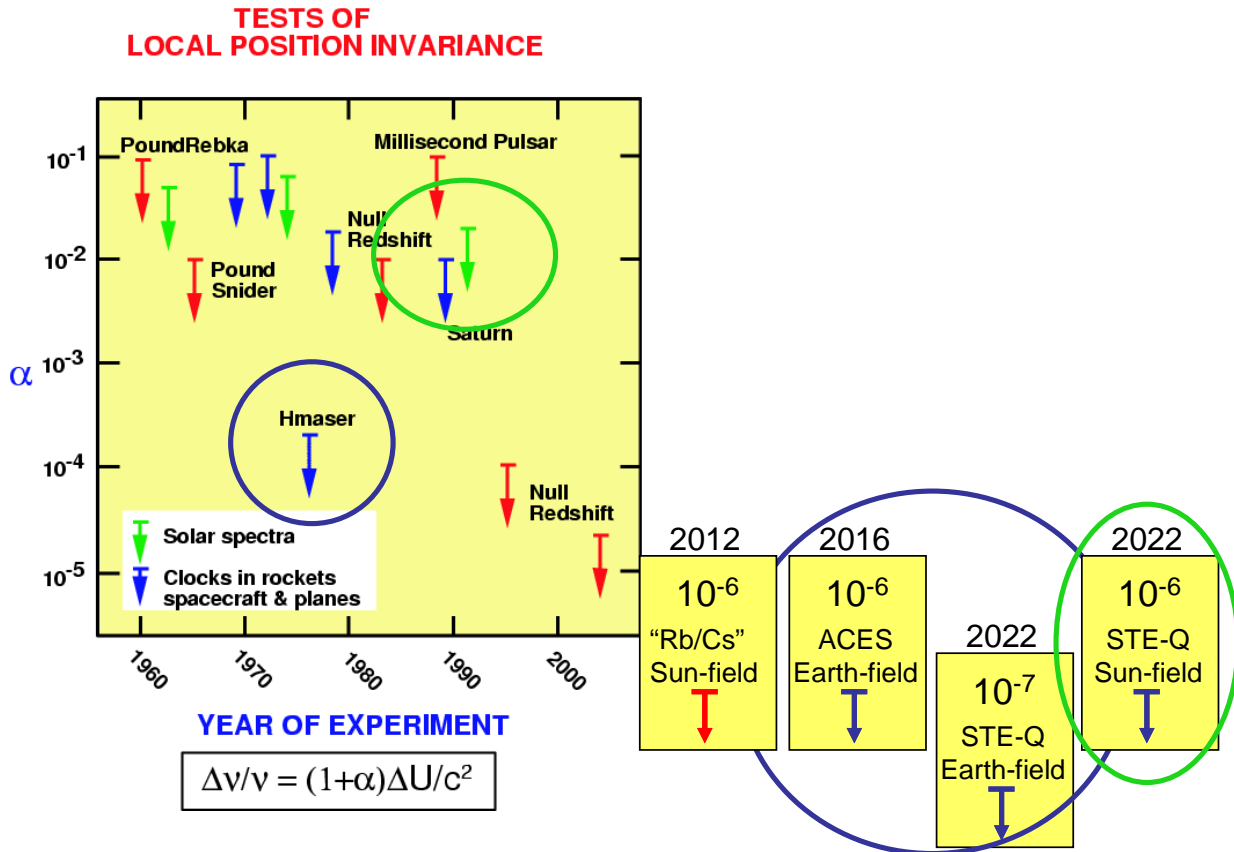


**Figure 2-5:** Present and upcoming limits on LPI violation adapted from [Will 2006]. Red arrows (after 1990) represent “null red-shift measurements” that can only provide the difference  $\alpha_i - \alpha_j$  for two different types of clocks  $i$  and  $j$ . Inside the green circles are the best direct LPI tests in the Sun field providing directly  $\alpha_i$  for the respective transition. Inside the blue circles are the best direct LPI tests in the Earth field (optional in the case of STE-QUEST).

Figure 2-5 shows a number of experiments, including null tests and direct tests. The latter set limits directly on the parameter  $\alpha_i$  for the relevant transition, e.g. the H-maser experiment of 1979 [VESSOT (1979)] sets a limit on  $\alpha_H$  for the hydrogen hyperfine transition. The “Null Red-shift” experiments in Figure 2-5 consist of two co-located clocks of different type in the same laboratory whose relative frequency is monitored as the local gravitational potential varies in time. Thus one measures  $(\alpha_i - \alpha_j)U/c^2$  for two clocks of type  $i$  and  $j$  and sets a limit on the difference  $(\alpha_i - \alpha_j)$ . The most precise such test at present sets a limit of  $(\alpha_{Rb} - \alpha_{Cs}) = (0.11 \pm 1.0) \cdot 10^{-6}$  for the Rb vs. Cs hyperfine transitions [GUENA (2012)], using the annual variation of the solar potential in the laboratory due to the eccentricity of the Earth’s orbit. Depending on the underlying model, the difference  $(\alpha_i - \alpha_j)$  might be much smaller than the individual values, especially when similar transitions are used (both hyperfine or both electronic, i.e. optical), so direct tests are necessary and complementary to co-located tests, which is one of the main drivers for experiments like ACES or STE-QUEST. In the STE-QUEST LPI test, a non-zero signal will be observed (Eq. (2-15)), no matter what the actual values of  $\alpha_T$  and  $\alpha_B$  in Eq. (2-15) are, provided at least one of them is non-zero, because of the different temporal variation of  $U_B$  and  $U_T$ . This is not the case in null-tests with co-located clocks, where one necessarily has  $U_i = U_j$  and thus a signal can only be detected if  $\alpha_i \neq \alpha_j$ , which is not the case for STE-QUEST.

Finally, all Sun LPI science objectives also apply to a test with the Moon as the source mass. STE-QUEST will carry out a direct LPI test in the Moon field using the same methods (and data) as the test in the Sun field described above. Note that the two putative signals can be easily de-correlated in the data due to the different frequency and phase. The sensitivity of STE-QUEST to a possible violation of LPI sourced by the Moon is then simply given by a reduction factor with respect to the Sun effect of

$$(M_{\text{Sun}}/d_{\text{Sun}}^2)/(M_{\text{Moon}}/d_{\text{Moon}}^2) = 175 \quad (2-17)$$

As detailed in Sec. 3.3.2, in the baseline configuration the measurement uncertainties of the MWL and the ground clocks should allow a detection of any non-zero value of the LPI violating parameter  $\alpha$  sourced by the Moon that exceeds  $4 \cdot 10^{-4}$  after four years of integration. In the case that the optional optical link is included in the payload, that goal can be reached in 72 days of integration with the ultimate performance of  $9 \cdot 10^{-5}$  reached in 4 years. Note however, that these results are based on only frequency measurements without making use of the phase cycle continuity requested for the STE-QUEST MWL. When phase cycle continuity is maintained by the link, the measurement duration is not affected by the dead-time between one common-view comparison and the next, resulting in a reduction of the integration time needed to reach the ultimate accuracy. Such a data analysis approach is presently being implemented in the numerical simulations.

Clock tests as described above are sometimes interpreted as searches for a space-time variation of fundamental constants, in particular those of the Standard Model (fine structure constant, electron, proton and quark masses, QCD mass scale, etc...). Such an interpretation is model dependent (one assumes the validity of the Standard Model of particle physics to describe atomic transitions) so we do not use it here as our aim is to remain as general as possible. In order to best constrain all possible variations of constants the comparison of as many different transitions as possible is essential. Comparisons of ground clocks based on different types of transitions repeated during the STE-QUEST mission (see Sec. 2.4.1.1) will provide a wealth of data to search for temporal variations of fundamental constants, the fine structure constant  $\alpha$  and the electron-to-proton mass ratio  $\mu$  in particular. Different clock transitions have different dependency on fundamental constants. Therefore, the results of crossed frequency comparisons repeated in time provides a clear interpretation of any observed drift over time and imposes unambiguous limits on time variations of fundamental constants. Current best limits on time variations of fundamental constants from laboratory experiments are consistent with zero: the  $\alpha$  drift was recently measured to  $\dot{\alpha}/\alpha = (5.8 \pm 6.9) \cdot 10^{-17} \text{ yr}^{-1}$  in the dysprosium experiment of LEEFER (2013); the  $\alpha$  and  $\mu$  drift were determined to  $\dot{\alpha}/\alpha = (-1.6 \pm 2.3) \cdot 10^{-17} \text{ yr}^{-1}$  and  $\dot{\mu}/\mu = (-1.9 \pm 4.0) \cdot 10^{-16} \text{ yr}^{-1}$  in the frequency comparison of a  $\text{Hg}^+$  and an  $\text{Al}^+$  clock [ROSEN BAND (2008)]. At the same time, data obtained from astronomical observation of Quasar absorption spectra are providing complementary information exploring completely different measurement systematics:  $\dot{\alpha}/\alpha = (6.4 \pm 1.3) \cdot 10^{-16} \text{ yr}^{-1}$  [MURPHY (2004)] and  $\dot{\mu}/\mu = (-1.2 \pm 1.5) \cdot 10^{-16} \text{ yr}^{-1}$  [MURPHY (2008)]. Interestingly enough, even if their interpretation is still controversial, these data seem to indicate a time variation of  $\alpha$ . Additional and more precise measurements are clearly needed to better understand and resolve the puzzle. These limits are expected to improve by at least one order of magnitude thanks to STE-QUEST.

### 2.3.4 STE-QUEST Tests of Lorentz Invariance and CPT Symmetry

Lorentz Invariance is the third sub principle of the Einstein Equivalence Principle as described in Sec. 2.1.1. Currently, there is a great deal of interest in Lorentz Invariance and the combined charge conjugation, parity, time reversal (CPT) symmetry - and, in particular, the question of whether these related symmetries are truly exact in nature. Both the Standard Model of particle physics and the general theory of relativity are precisely invariant under Lorentz and CPT symmetries, which makes these symmetries particularly fundamental. Whilst Lorentz and CPT symmetries have been discussed frequently in frameworks similar to the one introduced in 2.3.1, a more general, broad, and complete framework for tests of Lorentz Invariance and combined charge conjugation, parity, time reversal (CPT) symmetry has been developed over the last decade or so, the Standard Model Extension (SME) [COLLADAY (1997) and (1998)] and we will use that framework to analyze Lorentz Invariance tests that will be carried out with STE-QUEST. The first estimates presented here give a general idea of the potential of STE-QUEST in this field. A more thorough analysis and simulation will be carried out as the mission progresses.

Many candidate theories of quantum gravity suggest the possibility of Lorentz and CPT symmetry breaking in certain regimes. For example, the symmetries could be broken spontaneously, either in string theory [KOSTELECKÝ (1989) and (1991)] or in quantum field theories with fundamental tensor fields [ALTSCHUL

(2005) and (2010)]. There could also be Lorentz-violating physics in loop quantum gravity [GAMBINI (1999), ALFARO (2002)] and non-commutative geometry theories [MOCIOIU (2000), CARROL (2001)]; Lorentz violation through spacetime-varying couplings [KOSTELECKÝ (2003), FERRERO (2009)]; or breaking of Lorentz and CPT symmetries by quantum anomalies in certain spacetimes with nontrivial topologies [KLINKHAMER (2004)]. Moreover, since CPT violation in a well-behaved low-energy effective quantum theory automatically requires Lorentz violation as well [GREENBERG (2002)], any predictive theory that entails violations of CPT will also include violations of Lorentz Invariance.

So far, there is no compelling evidence that Lorentz and CPT symmetries are not actually exact in nature. In fact, there have been numerous experimental tests of these theories, using a very wide variety of techniques. Recent experimental tests have included studies of matter-antimatter asymmetries for trapped charged particles and bound state systems, measurements of muon properties, analyses of the behavior of spin-polarized matter, frequency standard comparisons, Michelson-Morley experiments with cryogenic resonators, Doppler effect measurements, measurements of neutral meson oscillations, polarization measurements on the light from cosmological sources, high-energy astrophysical tests, precision tests of gravity, and others (see KOSTELECKÝ (2011)A for a compilation of the present experimental constraints).

A general effective field theory that describes Lorentz violation for elementary particles is the Standard Model Extension (SME) [COLLADAY (1997) and (1998)]. As a quantum field theory, the SME contains all Lorentz-violating operators that can be written down using Standard Model fields, along with coefficients for Lorentz violation that parameterize the Lorentz-violating effects. These coefficients vanish in a perfectly Lorentz-invariant theory. It has also been expanded (as a classical field theory) to give a systematic way of studying Lorentz- and CPT-violating gravitational interactions [KOSTELECKÝ (2004)]. The SME gravitational action includes both spacetime curvature effects and spacetime torsion phenomena; some of the torsion effects turn out to be equivalent, at least locally, to spin-dependent Lorentz-violating operators in the particle physics sectors of the SME [KOSTELECKÝ (2008)]. Although many theories describing new physics suggest the possibility of Lorentz violation, none of them are understood well enough to make firm predictions. The greatest utility of the SME is the theory's generality. The SME provides a framework for placing constraints on Lorentz and CPT-violating effects, without worrying about the underlying mechanism by which the symmetry violation arises.

In the presence of Lorentz violation, experimental results will depend on the orientation of the apparatus (for violations of spatial isotropy) and the velocity of the apparatus (for violations of Lorentz boost invariance). For Earthbound experiments the changes of orientation and velocity are limited to the Earth rotation and orbital motion or to slow modulations imposed in the laboratory (e.g. turntables). For a satellite experiment, there are new forms of motion, and this enhances the sensitivity to Lorentz violation. The highly eccentric and time-varying orbit of the STE-QUEST satellite will be extremely advantageous for several reasons. Tests of Lorentz boost symmetry require comparisons of data collected in different Lorentz frames. It is necessary to physically boost the experiment into different frames and compare the results observed under the different conditions. The sensitivity to boost invariance violations is then determined by the velocity differences  $\mathbf{v}$  between different observation frames. The direction of  $\mathbf{v}$  determines the specific linear combination that can be constrained by a single comparison. Simultaneously, the speed determines the strength of the constraint; for nonrelativistic relative speeds,  $v/c \ll 1$  is a direct suppression factor. For these reasons, it is advantageous to sample as many frames, moving as rapidly in relation to one-another as possible.

When coupled to gravity, one finds that WEP/UFF tests can provide the best available sensitivity to certain types of Lorentz violation in the SME [KOSTELECKÝ (2011)B]. In fact, several Lorentz-violating possibilities can only be tested using such precision gravitational experiments [KOSTELECKÝ (2009)A]. Hence, the impressive WEP tests of the STE-QUEST mission would provide the best sensitivities to date on an additional set of coefficients for Lorentz violation.

Effective WEP violation in the SME originates from its generality in allowing the possibility of coefficients for Lorentz violation that differ among fermions of different flavors. That is, the degree of Lorentz violation may differ from protons, to neutrons, to electrons, for example. When gravitational couplings are considered for fermions, this species dependence leads to a differing gravitational response. Since the effect is due to Lorentz violation, variation in the size of the effective WEP violation with the orientation and boost direction of the experiment typically results, as do modifications in the direction of the gravitational acceleration. Thus WEP tests such as those on the STE-QUEST mission typically have the ability to distinguish a signal due to Lorentz violation from other sources of WEP violation via the dependence of the signal on orientation and velocity as well as the unique direction dependence of the acceleration.

The proposed WEP/UFF experiment is of the class that was analyzed extensively in KOSTELECKÝ (2011)B. Explicit predictions obtained for experiments on Earth extend naturally to STE-QUEST through replacement of appropriate boost and gravitational factors. Performing such an experiment in space provides the benefits of variable boost orientations and longer free-fall times, but there is no fundamental change in the existing analysis. The results of that analysis along with the WEP sensitivity goals of STE-QUEST imply that sensitivities ranging from the  $10^{-11}$  to  $10^{-7}$  levels per measurement cycle will be possible for up to 8 combinations of SME coefficients. After incorporating data from the large number of orbits throughout the mission, constraints ranging from  $10^{-14}$  to  $10^{-10}$  levels are expected. These sensitivities would provide improvements of up to 5 orders of magnitude over existing constraints.

Another way in which STE-QUEST mission as currently proposed could attain sensitivity to Lorentz violation is through red-shift tests. Coefficients for Lorentz violation, which couple to gravitational fields in the SME lead to modified spacetime curvature [KOSTELECKÝ (2011)B, BAILEY (2006)] as well as additional modifications to clock frequencies, and specific predictions for red-shift experiments have been made [KOSTELECKÝ (2011)B, BAILEY (2009)]. These predictions include that of a variation in the red-shift signal as the clock explores the gravitational potential that is qualitatively different from the conventional red-shift signal [BAILEY (2009)]. This effect arises due to the impact of rotation-invariance violation on the gravitational field. While the sensitivity to the relevant SME coefficients available via red-shift tests will not exceed the maximum reach currently available via other types of experiments, such tests are still interesting from a SME perspective for several reasons. The sensitivities to Lorentz violation achieved in a given experiment often constrain or measure a large combination of coefficients from the theoretical framework, hence additional tests can provide the necessary information to disentangle these combinations. Secondly, the present analysis of such experiments considers implications of the minimal gravitationally coupled SME only. Higher dimension operators [KOSTELECKÝ (2009)B and (2012)] for which specific predictions for experiments of this type have not yet been made may result in additional effects that can be measured in this way.

Additional tests of Lorentz Invariance are possible if the optional onboard clock is flown. The dependences of the atomic clock frequencies on the minimal SME parameters is already known [KOSTELECKÝ (1999)A, BLUHM (2003)]. These dependences were determined using the effective Hamiltonian that may be derived from the SME Lagrangian [KOSTELECKÝ (1999)B]. The algorithm for calculating the frequency shifts is quite general and can be applied to virtually any atomic clock transition. In the context of the Schmidt model, all the angular momentum  $I$  of odd-even nucleus is carried by a single unpaired nucleon. The principal sensitivities (given by the Schmidt model and the atomic shell structure) are to Lorentz violation coefficients in the proton sector, with secondary sensitivities in the electron sector. Searching for modulations in the transition frequency with the characteristic satellite orbital frequency will make it possible to place constraints on up to 25 coefficients in the proton sector, with sensitivity levels ranging from  $10^{-21}$  down to  $10^{-28}$ . A further 18 electron-sector coefficients may be constrained with potentially  $10^{-19}$  to  $10^{-27}$  level sensitivities. For most of these coefficients, these are unprecedented levels of sensitivity. There are also dependences on additional SME coefficients, which are not captured by the Schmidt model. These include dependences on neutron coefficients and dependences that exist because of the relatively rapid movement of the nucleons inside an atomic nucleus [ALTSCHUL (2009)]. The extremely sensitive data provided by STE-QUEST would promote interest in these additional dependences, which could be teased out of the data with some additional theoretical work.

In conclusion, STE-QUEST offers the possibility to explore a large parameter space of the SME and to thereby constrain, or uncover, violations of Lorentz and CPT symmetry. In particular, coefficients in the proton and electron sector will be constrained from the clock measurements, while the  $^{85}\text{Rb}$ - $^{87}\text{Rb}$  atom interferometer will provide new constraints in the gravitational sector, with expected improvements of up to 5 orders of magnitude on present limits.

## 2.4 STE-QUEST Legacy Science

STE-QUEST also has important applications in domains other than fundamental physics. In this section, we provide a list of topics that will be investigated by STE-QUEST providing a major scientific contribution in the field. With the present payload and platform capabilities, the following topics will be addressed:

## 2.4.1 Time and Frequency Metrology

### 2.4.1.1 Clock Comparisons

Time and frequency are today’s best realized physical units. Currently many different types of optical clocks are being developed worldwide reaching fractional frequency uncertainties down to  $7\text{-}8\cdot 10^{-18}$  and instabilities, expressed as Allan deviation, of  $\sigma_y(\tau) = 4\cdot 10^{-16}\cdot \tau^{-1/2}$ . The steady improvement in performance will provide clocks with at least one order of magnitude better accuracy and stability by the time STE-QUEST will fly. At that time, novel types of clocks like those based on Mössbauer transitions in nuclei [PEIK (2003)] might already become available. As all these clocks are developed at different locations, means for their evaluation and for their comparison need to be made available.

For comparisons over short distances of around 1000 km, stabilized optical telecommunication fiber links have demonstrated accuracies and stabilities well suited to these clocks [PREDEHL (2012)]. A European fiber network between a few National Metrology Institutes (NMI) is currently planned and similar networks are expected to become available in Northern America and Japan. However, even in several years from now, these techniques will not be able to cover intercontinental distances, as the necessary bidirectional optical amplifiers and regeneration station are today incompatible with long-distance under-water cables.

Thus, the intercontinental connection of separated “local” networks has to rely on satellite-based techniques. At present both GPS and geostationary telecommunication satellites (TWSTFT) are employed, reaching frequency instabilities around  $10^{-15}$  and timing accuracies slightly below 1 ns. A first improvement on this performance is expected by the ACES mission. There, a dedicated microwave link will allow timing stability better than 300 fs after 300 s of integration time when comparing ground clocks in common-view. However, the low Earth orbit of the International Space Station does not allow for common-views over intercontinental distances. In this case, the ACES on-board clock needs to act as a flywheel oscillator during the dead time needed by the ISS to fly from one continent to the next. The time error accumulated by the clock during the dead time is thus adding to the overall budget, reducing the time stability of the transfer system (non-common-view comparisons).

STE-QUEST is addressing the needs of already existing and future clocks on ground. The mission is providing microwave links that allow for the simultaneous comparison of up to four ground clocks over very long common-view contact durations (> 10 h).  $5\cdot 10^{-19}$  frequency accuracy and 50 ps timing accuracy with high stability will be provided to the institutes participating to the STE-QUEST network of ground clocks (Figure 2-6). Optionally, an optical link could provide even better short-term stability in the common-view comparison of two ground clocks.

The high quality of the link will allow rapid progress in different areas of research: metrological applications and fundamental science as well as clocks synchronization, realization of coordinated time scales, and their distribution.

The long common-view durations and the high performance of the STE-QUEST links are precious tools for comparing state-of-the-art atomic clocks distributed worldwide. The comparison between two ground clocks can reach a relative frequency uncertainty of  $2\cdot 10^{-18}$  in a single common-view with a link based on microwave technology and down to the  $5\cdot 10^{-19}$  level if the optical link technology is used. More importantly, the capability of comparing clocks in common-view is not simply limited to the atomic frequency standards directly connected to the link ground terminals. Indeed, by making use of local fiber links, several additional clocks can be connected to the network and simultaneously compared among themselves. Evaluation of atomic clocks at the  $1\cdot 10^{-18}$  uncertainty level will allow to precisely characterize and correct systematic

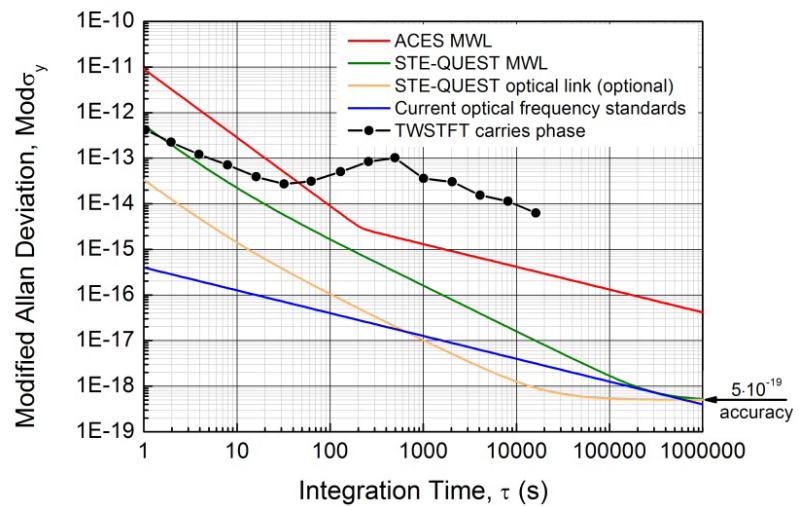


**Figure 2-6:** Stability performance of optical clocks and frequency transfer links expressed in modified Allan deviation: TWSTFT [FONVILLE (2004)], ACES [DELVA (2012)] and STE-QUEST [CACCIAPUOTI (2013)].

frequency shifts, to identify unknown effects, finally leading to the establishment of a reliable uncertainty budget, as needed in all precision measurements and metrological applications.

The availability of highly accurate clocks and well characterized links is also essential to perform relativistic geodesy experiments (see Sec. 2.4.3) and evaluate the corrections due to the Earth gravitational red-shift. With the help of a well-characterized transportable optical clock during the STE-QUEST mission, differences in the Earth gravitational potential between any desired user location and a reference clock could be measured and the correction to be applied to the frequency signal received at that location from the reference clock determined.

Finally, with high-performance atomic clocks based on different types of transition (atomic, molecular, or even nuclear) compared through the STE-QUEST network, a matrix of the frequency ratios between all the standards available worldwide can be established at the lowest possible level of uncertainty. Such measurements can be used towards a redefinition of the SI second as unit of time.

**2.4.1.2 International Atomic Time Scales, Clocks Synchronization, and Time Dissemination**

A large number of time scales already exists and is routinely maintained by metrology institutes and international organizations (see Figure 2-7). Universal Time (UT), derived from the observation of the Earth’s rotation period, standardises the biological time based on the day and night life cycle.

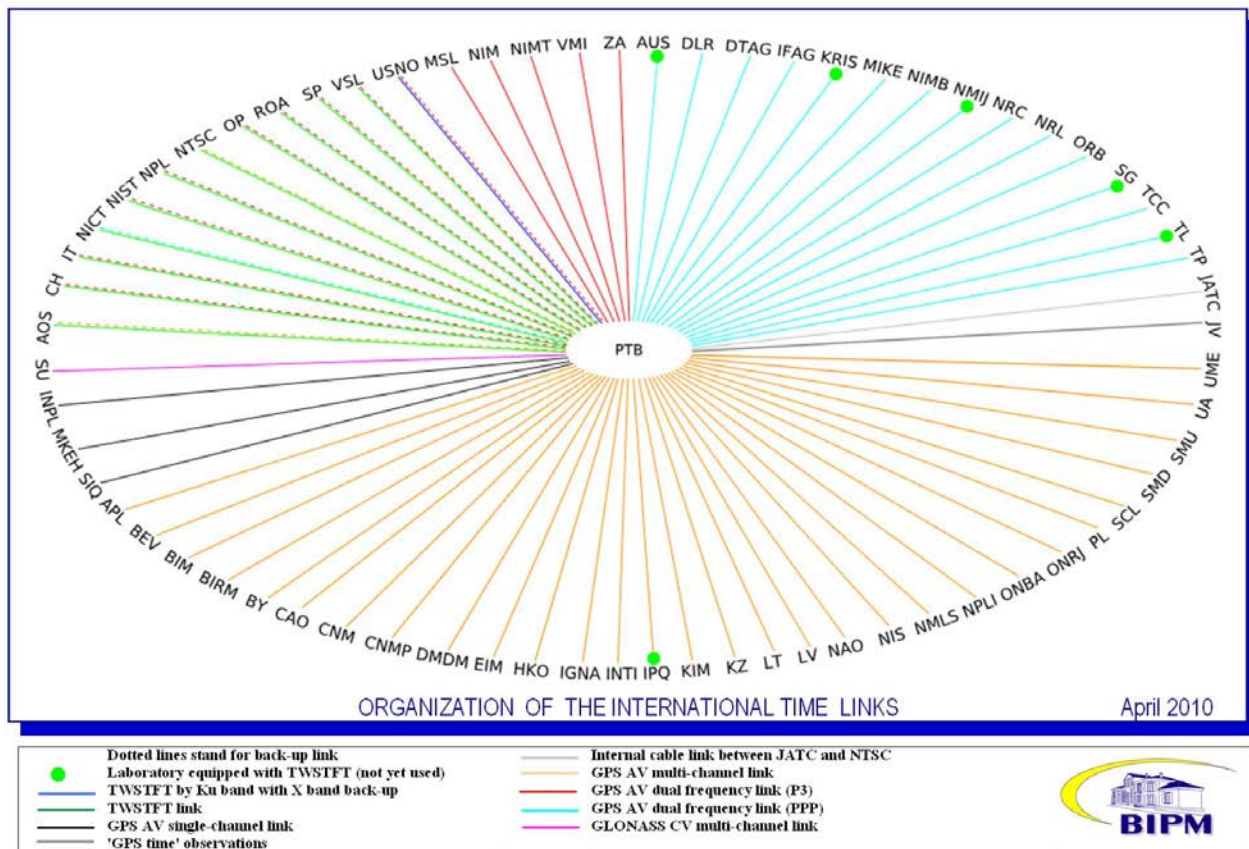


**Figure 2-7:** Time transfer links for EAL construction. At present, comparisons use common-view transfer via GPS and TWSTFT.

On the other side, time scales can be built out of atomic clocks. As an example, we can mention the time scale disseminated by GPS satellites or the International Atomic Time scale (TAI). TAI is built by the Bureau International des Poids et Mesures (BIPM). It plays a major role as it enters in the definition of UTC (Universal Time Coordinated), recognized worldwide as the official international time.

The STE-QUEST mission will offer the possibility to compare ground clocks to a frequency uncertainty better than  $10^{-18}$ . Such accuracy levels have profound influence on the international timescales TAI and UTC, which are currently constructed out of about 350 atomic clocks from about 70 institutes worldwide. At present, about ten primary fountain clocks contribute to UTC with an uncertainty at a few units in  $10^{16}$ . With the upcoming generation of optical clocks, that uncertainty could be reduced to the  $1 \cdot 10^{-18}$  level and below,

but only over regional scales, where fibre links are available. STE-QUEST would allow extending that to a global scale by providing intercontinental comparisons to better than  $1 \cdot 10^{-18}$ .

Establishing timescales at that level on the rotating solid Earth that continuously deforms under tidal forces from the Moon and the Sun will require including relativistic effects at a better approximation and also accurate modelling and monitoring of the dynamic Earth. Finally these developments can lead to a more precise realization of TAI taking into account the effects induced by the geoid and its dynamics.

Besides frequency comparisons, i.e. the measurement of frequency ratios between remote clocks, time transfer experiments are also very important for the synchronization and the distribution of time scales. Available systems, based on TWSTF and GNSS in common-view, presently reach accuracies slightly below one nanosecond (Figure 2-8). On regional scale, timing signals can also be distributed by fiber links that today can provide about 200 ps accuracy [LOPEZ (2013), WANG (2012), ROST (2012)].

Time transfer and clock synchronization experiments are extremely demanding as they require knowledge and control of all the individual delays experienced by the timing signal being distributed, whereas in the frequency comparisons of clocks those delays are only required to be constant over the averaging time. Using the microwave link of STE-QUEST, synchronization better than 50 ps will become possible, corresponding to more than one order of magnitude improvement with respect to available free-space techniques.

The availability of a coordinated timescale with tens of picoseconds accuracy can provide timing information for many application.

Starting from VLBI, Earth rotation and the connection to the galactic reference system can be improved as well as the resolution in observation (see Sec. 2.4.3). In radio astronomy, availability of better timescales can benefit the pulsar timing, e.g. in the low frequency gravitation waves detection in the international pulsar timing array (IPTA) [HOBBS (2012)] or by probing the ultimate limits of pulsar timing [OSŁOWSKI (2011)].

In recent times, also precision timing for elementary particle experiments has become an issue, as illustrated by the erroneous claim of superluminal neutrino speeds [OPERA (2013)]. The availability and increased use of precision timing equipment will help the development of timing techniques with higher confidence and reliability.

Furthermore, the atomic time scale could be distributed over a distance of several hundreds of kilometers from the receiver to a large number of users by means of an optical link based on a distributed fiber network in which one node is an STE-QUEST ground station. STE-QUEST would then provide means for testing an integrated space-to-ground network concept for time and frequency distribution.

## 2.4.2 Terrestrial and Celestial Reference Frame of the Earth

The highly elliptical orbit of the STE-QUEST mission can be used for the realization of terrestrial and celestial reference frames of the Earth by means of the existing onboard precise orbit determination tools: GPS/Galileo receiver, passive Satellite Laser Ranging (SLR) reflector, and the radio source of the STE-QUEST science link observed by the ground network of VLBI antennae. By upgrading the onboard GPS/Galileo receiver for an additional DORIS tracking, the Space Geodesy part of STE-QUEST mission will be able to contribute to the highly accurate realization of the terrestrial reference frame of the Earth [BAR-SEVER 2009]. The highly elliptical orbit of the STE-QUEST mission is well suited for reference frames determination (coordinate system). Indeed, while the STE-QUEST spacecraft is orbiting around apogee, the on-board radio source (MWL) can be observed for very long uninterrupted durations (about 10 h) against the extragalactic radio-sources (quasars) defining the celestial reference frame. In comparison,

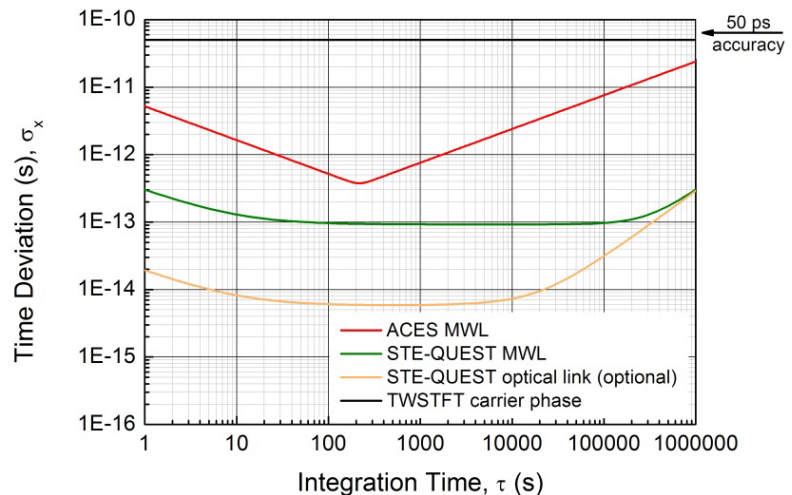


**Figure 2-8:** Stability of time transfer /TADEV of present ACES and STE-QUEST links and a 20 MChips/s modulated TWSTFT link [Piester2008] and the absolute accuracy of time transfer of STE-QUEST.

VLBI observations of satellites orbiting at LEO altitudes is by far more challenging. This opens the STE-QUEST mission to a number of investigations related to reference frames determination. In particular:

- Meeting the GGOS (Global Geodetic Observing System) goals for the terrestrial reference frame of the Earth, i.e. 1 mm accuracy and 0.1 mm/yr stability;
- Realization and unification of the terrestrial and the celestial reference frame of the Earth;
- Proper alignment of the GAIA optical reference frame against the unified terrestrial and celestial reference frame and common optical/radio quasars observed at higher VLBI frequencies (that are closer to optical positions);
- Determination of the long-wavelength variability in the gravity field of the Earth, including the central term and the low-degree spherical harmonic coefficients that are either not observed or poorly observed by GRACE and GOCE gravity field missions (e.g. dynamical flattening of the Earth);
- Improvement of satellite altimetry (Jason-2, Sentinel-3) and tide gauge records of the global mean sea level rise by using the highly accurate terrestrial reference frame from the STE-QUEST mission;
- Contributing to the study of mass transport in polar regions (ice mass loss) by referencing altimetry (Cryosat, ICESat) and gravity data (GOCE and GRACE gravity missions) to the common terrestrial reference frame from the STE-QUEST mission;
- Contributing to the monitoring of the Earth rotation and orientation parameters by making use of the highly elliptical orbit of the STE-QUEST mission (UT1, length of day variations, etc.) and VLBI tracking from the ground;
- Improving the orbit accuracy of GNSS satellites (GPS, GLONASS, GALILEO) by tracking their orbits against the STE-QUEST highly elliptical orbit (differential SLR/GNSS/VLBI);
- Providing a common time scale for space geodesy techniques (GNSS, DORIS, VLBI and SLR);
- Disseminating the terrestrial/celestial reference frame anywhere on Earth or in space (altimetry/gravity missions in LEO orbit, BepiColombo, etc.).

The geodetic scientific community is currently establishing a Global Geodetic Observing System (GGOS) [RUMMEL (2000)]. Its objectives are the measurement of temporal changes of land, ice and ocean surfaces as well as the monitoring of mass transport processes in the Earth system and the early detection of natural hazards. Space Geodesy and GGOS provide the foundation for most Earth observations and planetary missions as well as for the monitoring the Earth's geometry, its gravity field, and rotation. They are all related to mass transport phenomena in the Earth system and to climate changes. Realizing the importance of the geodetic terrestrial reference frame and the contribution of geodesy to Earth observations, GEO (Group on Earth Observations – currently about 75 member countries) has included a specific task “Global geodetic reference frames” in its Work Plan [GEO (2005)]. The main purpose of GEO is to facilitate the implementation of the Global Earth Observation System of Systems (GEOSS), see e.g. [GEO (2005)].

The most demanding requirements for the terrestrial reference frame are imposed by the monitoring the water cycle at global to regional scales and the monitoring and modelling of the sea surface, and ocean mass changes. In order to monitor system Earth processes, such as changes in the ocean currents, volume, mass, and sea level, the background terrestrial reference frame needs to be accurate at a level of 1 mm RMS and stable to 0.1 mm/yr [GROSS (2009)]. Several decades of altimetry missions like Topex/Poseidon, ERS-1/2, Jason-1/2, Envisat, Sentinel-3 and gravity field missions like GRACE and GOCE are providing observations of the Earth system. However, the accuracy of the background terrestrial reference frame is much worse than required to fully exploit the potential of all those missions. Global change processes are small and therefore difficult to quantify, thus requiring a reference frame of sufficient accuracy. On the other hand, the celestial reference frame is fundamentally important for the tracking of interplanetary satellites, for navigation, and planetary sciences [ROTHACHER (2009)]. The highly elliptical orbit of STE-QUEST and the unique suite of instruments could demonstrate the unification of the terrestrial and celestial reference frames of the Earth as well as of all the space geodesy techniques used for their realization (GNSS, VLBI, SLR and DORIS). In this way, the STE-QUEST mission has a high potential to significantly improve the current accuracy of the conventional reference frames of the Earth and meet GGOS requirements for the terrestrial reference frame.

The highly elliptical orbit is a sensor, not only for Earth rotation and orientation, but also for the estimation of low degree spherical coefficients of the Earth gravity field (e.g. Earth dynamic flattening) that are either not observed or poorly observed by GRACE and GOCE gravity field missions. Geometrical mapping of the STE-QUEST orbit against extragalactic radio-sources (quasars) can be realized by observing quasars at approximate locations of the STE-QUEST satellite. This is similar to Delta-DOR approach used for the

tracking of interplanetary satellites. The STE-QUEST satellite dwells for a long time in its apogee, thus becoming a very good target for a ground network of about 30 VLBI radio-telescopes in order to map its orbit and the associated terrestrial frame against the positions of extra-galactic radio sources. Such measurements will allow to combine the geometrical celestial frame from VLBI and the dynamical terrestrial reference frame from the GNSS constellations, SLR, and DORIS satellites. In a similar way, using double-difference of SLR and GNSS measurements, orbits of GNSS satellites and SLR reference frame satellites can be dynamically mapped against the highly elliptical orbit of the STE-QUEST mission. From this point of view, STE-QUEST allows to combine different space geodesy techniques such as GNSS, VLBI, SLR and DORIS, and to contribute to the unification of celestial and terrestrial reference frame of the Earth.

Since optically bright quasars ( $V < 18$  mag) that are covered by the GAIA mission can also be observed by the ground network of VLBI radio-telescopes, combined terrestrial and celestial reference frames from the STE-QUEST mission could also be used to properly align the optical GAIA reference frame. With a suite of different frequencies, the STE-QUEST metrology link allows differential VLBI observations of optically bright quasars at higher frequencies (Ka). Quasar positions in Ka-band are closer to optical positions (GAIA) compared to the conventional celestial frame (ICRF2) defined with quasar positions based on S/X-band. As a bottom line, we may draw a conclusion that unified terrestrial and celestial reference frames from the STE-QUEST mission will serve Earth Observation sciences, as well as planetary sciences at the same time (GAIA, BepiColombo, etc.).

### 2.4.3 Relativistic Geodesy: Reference Frames for Positioning, Timing, and Temporal Gravity

The use atomic clocks for *in situ* determination of gravity potential difference of the Earth's gravity field was proposed for the first time by [BJERHAMMAR (1985)], taking over Einstein's theory of relativity that two atomic clocks will tick at different rates due to different gravity potential at different locations. However, due to difficulties in comparing frequencies of remote clocks at the  $10^{-18}$  relative accuracy level, this concept has not been demonstrated so far, nor found a practical application.

The geoid (Figure 2-9) is the true physical figure of the Earth, a particular equipotential surface of the gravity field of the Earth that accounts for the effect of all subsurface density variations. Its shape approximates best (in the sense of least squares) the mean level of oceans, but the geoid is more difficult to determine over continents. Satellite missions carry out distance measurements and derive the gravity field to provide geoid maps over the entire globe. However, they require calibration and extensive computations including integration, which is a non-unique operation. Today, the geoid is known with a typical uncertainty of about 30-50 cm.

By the time of the STE-QUEST mission launch, ground clocks will have reached a precision of about one part in  $10^{18}$ . With its metrology link, the STE-QUEST mission

will allow comparisons of clocks distributed worldwide with the accuracy required to demonstrate operational relativistic geodesy at 1 cm level resolution on the geoid.

Recently [BONDARESCU (2012)], it has been argued that combining gravitational acceleration data and geopotential measurements at the same points, as these two quantities have different dependencies on the distance  $R$  to a given inhomogeneity lying beneath Earth's surface, would add information towards imaging density structure at depth. This would thus be a very powerful tool in mapping density anomalies within the Earth going to depths of the order of few kilometers. Indeed, synthetic calculations show that the geoid perturbation caused by a 1.5 km radius sphere with 20% density anomaly buried at 2 km depth in the crust of the Earth is already detectable by atomic clocks of the above assumed accuracy. Other potential applications include using successive measurements of geopotential and gravity to understand underground water or

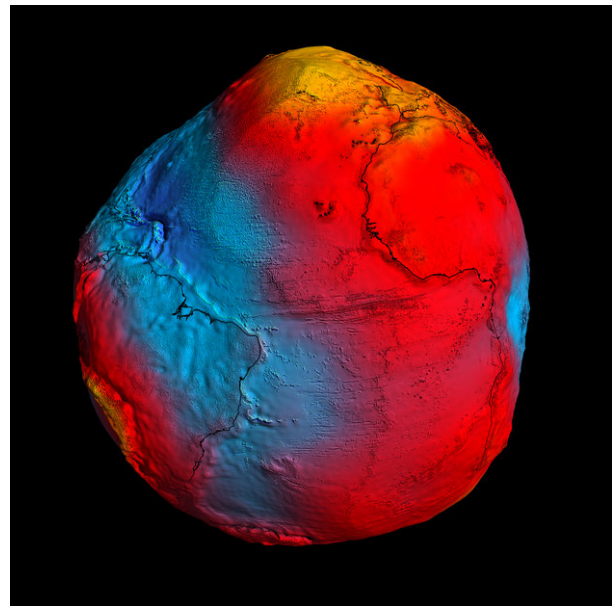


Figure 2-9: Earth gravity as seen by GOCE.

magma movements. Such measurements might also be used in post-earthquake analysis to map the related structural changes.

The orbit of the STE-QUEST mission is designed to allow for long common-view frequency comparison between clocks located in different continents. Such measurements can be used to establish a global reference frame for time and the gravitational potential of the Earth. This reference frame could be used for the realization of TAI (International Atomic Time), as well as to support realization of the global height system. GPS is measuring geometrical heights against the global ellipsoid, not physically defined heights above the geoid. Temporal gravity field maps are provided on routine basis by the GRACE mission, however with significantly lower resolution compared to the static gravity field. Therefore, it will be very interesting to use the STE-QUEST mission to establish a unified terrestrial reference frame for positioning, time, and temporal gravity field of the Earth.

The terrestrial reference frame needs to be complemented with a globally defined uniform height system of similar precision. The current precision level of continental or regional height systems, in terms of gravity potential differences, is in the order of  $1 \text{ m}^2/\text{s}^2$  (10 cm) with inconsistencies between these various systems up to several  $10 \text{ m}^2/\text{s}^2$  (several meters). The actual requirement in the context of GGOS is  $0.1 \text{ m}^2/\text{s}^2$  (1 cm), with the need of a permanent, i.e. dynamical control. The GOCE mission has significantly contributed to the unified global height system by increasing the spatial resolution of the satellite-based gravity field of the Earth. Clock comparisons can additionally provide *in situ* measurements of gravitational potential differences.

The precision measurement of heights is important to understand, on a global scale, processes such as sea level change, global and coastal dynamics of ocean circulation, ice melting, glacial isostatic adjustment and land subsidence as well as the interaction of these processes. Only by monitoring in terms of gravity potential changes at the above level of precision, the change of ocean levels can be understood as a global phenomenon and purely geometric height changes (from GPS/Galileo) can be complemented by information about the associated mass changes. Therefore, it is expected that the STE-QUEST metrology link with ground optical clocks will play an important role in this direction and unify all three reference frames: for positioning, time, and temporal gravity field.

## 2.5 Need for Space

A space-based laboratory provides unique experimental conditions, necessary to exploit the ultimate limits of quantum sensors and push the measurements accuracy to levels not accessible on ground. Space can ensure:

- Infinitely long and unperturbed “free fall” conditions;
- Long interaction times;
- Quiet environmental conditions and absence of seismic noise;
- Huge free-propagation distances and variations in altitude;
- Large velocities and velocity variations;
- Large variations of the gravitational potential.

The atom interferometry test of WEP performed by STE-QUEST is based on a differential measurement between two simultaneous atom interferometers. The level of sensitivity of this test depends on the sensitivity of each measurement to accelerations, on the ability to reduce asymmetries between the two interferometers, and eventually to calibrate the systematic effects. Compared to a ground-based experiment, the space environment leads to significant improvements in all the three points mentioned above.

In space, the experimental setup as well as the test masses, i.e. the atoms, are in free fall. This allows to achieve very long measurement times and very high sensitivities in a compact apparatus. Increasing the sensitivity and subsequently the accuracy of atom interferometry measurements requires large scaling factors  $kT^2$ , where  $k$  denotes the effective wave vector and  $T$  is half of the free evolution time during the atom interferometric sequence.  $T$  can be increased by operating the instrument on freely falling platforms (in drop-towers, on-board parabolic flight, rockets, or spacecrafts) or in long baseline atomic fountains on the ground. As an example, going from  $2T = 1.4 \text{ s}$  of interrogation time, corresponding to a free fall of 10 m on ground, to a 10 s interrogation time, as in STE-QUEST, leads to a 50 times better sensitivity, which has to be compensated by a 2500 times longer averaging time. In a similar way, assuming the same momentum transfer  $k$ , the target interferometer time of  $2T = 10 \text{ s}$  foreseen within the compact apparatus of STE-QUEST (only  $465 \text{ cm}^3$ ) can be achieved on ground only when atomic fountains of at least 100 m or more are used. Shorter ground atomic fountains (10 m) relying on large momentum transfer (LMT) beam splitters are

proposed in DIMOPOULOS (2008), DICKERSON (2013), and HOGAN (2008). However, when attempting at performance levels comparable with STE-QUEST, these experiments become extremely challenging due to the systematics proper to LMT interferometers [CLADÉ (2010)] and to the strict environmental requirements, such as the control on the ambient gravitational field, field gradients, and magnetic disturbances (see Sec. 4.1.1.1), that need to be fulfilled over the very large volume of the instrument.

Another key aspect is represented by the background gravitational acceleration. Differential measurements are certainly easier to perform in the presence of small DC accelerations, as in space ( $< 4.10^{-7} \text{ m/s}^2$  in STE-QUEST), rather than in the presence of the large background signal due to Earth gravity ( $9.8 \text{ m/s}^2$ ), as for ground-based experiments. On ground, the scaling factor of the interferometer needs to be controlled about  $2.5 \cdot 10^7$  times better with respect to space-based instruments. This includes the control on the absolute frequency of the lasers used to manipulate the atoms and the intensity of the laser beams during the Raman pulses. A similar argument can be developed for the rotation signal, although only at the  $10^2$  level.

A third point concerns the control and calibration of systematic effects. In a ground-based experiment, the atomic clouds move with respect to the instrument platform. Indeed, while the atoms are in free fall, the laboratory itself rotates due to the Earth motion. The relative displacement between the atoms and the instrument platform is responsible for an amplification of the systematic effects induced by magnetic field gradients, wave-front aberrations on the laser beams, self-gravity gradients produced by the experimental apparatus. In STE-QUEST, these systematic effects are reduced because of the absence of displacements of the centre of the interferometer compared to the apparatus. More importantly, they can be calibrated, taking advantage of the satellite motion around the Earth. During the orbital motion, the projection of the gravitational acceleration of the Earth along the sensitive axis of the atom interferometer changes its direction and sign modulating an eventual WEP-violating signal. This is a powerful tool that can be used to control the measurement systematics. Science measurements would be implemented both during perigee and apogee passes. During the perigee pass, the eventual WEP-violating signal is maximum. At apogee, the signal originating from Earth gravity vanishes, leading to an effective null-measurement, not possible to realize on ground.

Finally, several systematic effects are specific to ground-based experiments and disappear in zero-g. In a freely falling platform, the quantum immiscibility and gravitational sag ( $\sim 0.67 \text{ nm}$ ) do not impose additional constraints to the co-location requirement ( $< 1.1 \text{ nm}$ ) of the two atomic clouds (see Sec. 4.1.1.1). On the contrary, in a ground-based experiment any perturbation that couples to the initial separation between the barycentre of the two atomic clouds makes those requirements very stringent, limiting the use of the delta-kick cooling (DKC) technique [MÜNTINGA (2013)], crucial in the preparation phase of the ultra-cold atomic samples (see Sec. 4.1.1.1). Moreover, while in a freely falling instrument the barycentres of the two atomic clouds coincide with the centre of the trapping potential, the gravitational acceleration on ground is responsible for a sag of the samples that depends on their atomic mass. This leads to relative displacements between the two atomic clouds that can be calculated to be at the level of  $100 \text{ nm}$ . For a similar reason, the effective release time of the atoms is slightly different for the two species when switching-off the trapping potential under gravity, introducing non-zero displacements and differential velocities between the two clouds. In addition, in a Mach Zehnder configuration [KASEVICH (1991)], the centre of the atom interferometer moves with respect to the freely falling reference frame with a velocity corresponding to one photon recoil, which depends on the atomic mass ( $0.14 \text{ mm/s}$  of differential recoil velocity between  $^{85}\text{Rb}$  and  $^{87}\text{Rb}$ ). This is responsible for a relative displacement between the centres of mass of the two atom interferometers, requiring a very high level of knowledge of the gravity gradients and magnetic field gradients. In STE-QUEST, thanks to the free fall conditions, it is possible to use a more symmetric interferometer, namely the double diffraction scheme [LÉVÈQUE (2009)], in which the centres of the interferometers are at rest for both species and stay superimposed. At last, the possibility to prepare the atomic ensembles in weak traps (few tens of Hz) allows using up to  $10^6$  atoms in each BEC in a dilute regime of interactions.

All these aspects are essential points in the ability to perform the WEP test at the best level and are reduced by many order of magnitude in a freely falling experiment compared to ground-based instruments.

Several test activities are presently on-going in ground-based zero-g facilities. Atom interferometers are routinely operated in the drop-tower environment or on-board parabolic flights. Such experiments are important to investigate the dynamics of atom interferometry measurements in weightlessness conditions. However, due to the limitations on the duration of the free fall conditions and on the residual accelerations that can be achieved in these facilities, they are certainly not suitable for a tests of the Einstein Principle of

Equivalence to the uncertainty levels targeted by STE-QUEST. As an example, the ICE project funded by CNES and regrouping laboratories at the Observatoire de Paris, the Institut d'Optique, and ONERA is performing tests on the noise suppression between two atom interferometers in a very moderate environment ( $< 10^{-2} g$ ). The project aims at a test of the WEP to an uncertainty in the  $10^{-11}$ – $10^{-10}$  range on-board the A-300 zero-g Airbus of Novespace [VAROQUAUX (2009)]. On this specific platform, residual accelerations become prohibitive for reaching the STE-QUEST performance levels. Nevertheless, the experiment will demonstrate new techniques for correlating atom interferometry measurements with classical accelerometers readouts for optimal rejection of the platform acceleration noise [GEIGER (2011)].

Complementary tests are being performed within the DLR-funded QUANTUS (quantum gases in microgravity) project, where atom interferometry experiments are carried out at the ZARM drop-tower in Bremen. This facility can ensure up to 9 s of  $\mu g$  conditions when operated in the catapult mode. The first Bose-Einstein condensate in free fall was demonstrated in 2007 [VAN ZOEST (2010)]. Recently, it was possible to implement Mach-Zehnder interferometers with a free evolution time up to 675 ms [MÜNTINGA (2013)]. The second generation experiment QUANTUS II targets a measurement of the differential acceleration between  $^{87}\text{Rb}$  and K atoms with a sensitivity of  $6 \cdot 10^{-11} \text{ m/s}^2$  [RUDOLPH (2011)]. Based on this technology, a rocket-borne atom interferometer is being developed for a flight to 250 km apogee in November 2014. These experiments are severely challenged by the short free fall durations, which limit the available statistics, necessary to study in detail the systematic effects. As such, they shall be considered as precursors for space-borne experiments, demonstrating the short-term stability of the instrument as well as key techniques in space-like operation regimes.

Space is also crucial for connecting the best atomic clocks in a global network capable of comparing them to ultimate frequency stability and accuracy levels.

Atomic clock performances have improved by about 1 order of magnitude per decade throughout the 20th and into the current century. This trend is likely to continue in the foreseeable future. In effect, the availability of optical frequency combs for more than a decade has led to the rapid improvement of optical clocks, which now outperform microwave clocks. The best optical clocks now have systematic frequency errors of less than  $10^{-17}$ , with  $10^{-18}$  expected to be reached in the next few years.

However the means of comparing clocks over long distances have evolved considerably more slowly. The two most widely-used methods are based on GNSS signals for the first, and on the exchange of microwave signals via telecommunications satellites for the second, called TWSTFT for Two-Way Satellite time and Frequency Transfer. Both of these methods allow frequency comparisons with an uncertainty a little smaller than  $10^{-15}$  over one day, meaning that of the order of 100 s to 1000 s of days of comparison would be necessary to reach the uncertainty of the best optical clocks, if this were feasible. This is a major handicap for the applications of the new generation of clocks, which require the realisation of such comparisons within times of 1 to a few days.

A new comparison method, based on the transfer of ultra-stable signals by optical fibre, has demonstrated the capability to achieve frequency comparison uncertainties of the order of  $10^{-19}$  over one day, which is fully satisfactory, and is starting to be deployed in continental networks. However this method is not thought to be applicable to intercontinental comparisons, due to the need for dedicated signal amplification equipment at intervals from a few tens of km up to 100 km all along the fibre. Another possibility which is currently envisaged is the use of transportable optical clocks themselves to compare distant clocks by clock transport. Such transportable clocks are being developed in view of diverse applications, such as clock-based relativistic geodesy. Nevertheless it seems likely that their performances will be somewhat less good than those of the best clocks permanently installed in laboratories. Still other methods are being explored, such as the use of VLBI observations for time transfer, but do not yet appear to offer a significant improvement over current methods.

This brings us back to the possibility of improving satellite-based methods. GNSS-based methods are improving, but do not seem likely to provide the required gains of 2-3 orders of magnitude. A modest improvement of the TWSTFT method may be obtained by the use of the phase of the carrier signal, but is likely to be limited by the use of a space segment which is not optimised for this application. However a TWSTFT-like method, the microwave link (MWL) developed for the ACES mission, has demonstrated the capability for a very significant improvement of clock comparison uncertainties. The use of this link in the ACES mission will be somewhat limited by the low orbit of the ISS, meaning that common-view comparisons over very long distances will not be possible.

The inclusion of such a link on STE-QUEST, thanks to its very high orbit, will allow it to be used to its full potential for intercontinental comparisons between the best ground clocks. The free-space optical link proposed for STE-QUEST will also allow such long-distance comparisons, even more rapidly due to its better stability. The placement of such a microwave or optical link on a high-orbit satellite is currently the most promising strategy for enabling intercontinental comparisons at the uncertainty level required for the best optical clocks.

### 3 Scientific Requirements

STE-QUEST makes use of differential accelerometers, high-performance clocks, and links to characterize the space-time metric and to test the Einstein Equivalence Principle. This section summarizes the logical flow that, starting from the primary science investigations of STE-QUEST, defines the measurement accuracy and identifies the top-level performance requirements of the main mission elements.

Measurement requirements have an impact on the spacecraft orbit, instruments performance, and science ground segment. Therefore, it becomes mandatory to define a performance model including the different mission elements and, based on that, run a forward calculation of the accuracy that can be achieved in the fundamental physics tests of STE-QUEST.

According to this rationale, this chapter is organized as follows: Sec. 3.1 identifies the STE-QUEST scientific investigations and defines the corresponding measurement requirements; Sec. 3.2 presents the orbit characteristics and discusses the constraints used for their optimization; Sec. 3.3 describes the measurement methods, derives the performance requirements of the STE-QUEST instruments, subsystems, and science ground segment, and finally demonstrates the system compliance with the STE-QUEST measurement requirements through a numerical simulation.

#### 3.1 Science Investigations vs. Measurement Requirements

The top level science investigations of the STE-QUEST mission are in the fundamental physics domain. As discussed in Sec. 2, they address precision tests of the Einstein Equivalence Principle.

Science Investigation	Measurement Requirement
<b>Weak Equivalence Principle Tests</b>	
<i>Universality of propagation of matter-waves</i>	#PSO-01: Test the universality of the free propagation of matter waves to an uncertainty in the Eötvös parameter better than $2 \cdot 10^{-15}$ .
<b>Gravitational Red-shift Tests</b>	
<i>Sun gravitational red-shift</i>	#PSO-02: Measurement of the Sun gravitational red-shift effect to a fractional frequency uncertainty of $2 \cdot 10^{-6}$ , with an ultimate goal of $5 \cdot 10^{-7}$ .
<i>Moon gravitational red-shift</i>	#PSO-03: Measurement of the Moon gravitational red-shift effect to a fractional frequency uncertainty of $4 \cdot 10^{-4}$ , with an ultimate goal of $9 \cdot 10^{-5}$ .
<i>Earth gravitational red-shift (Optional)<sup>3</sup></i>	#PSO-04: Measurement of the Earth gravitational red-shift effect to a fractional frequency uncertainty of $2 \cdot 10^{-7}$ .
<b>Local Lorentz Invariance and CPT Tests</b>	
<i>LLI and CPT</i>	#SSO-01: Provide significant improvements on the determination of several parameters of the Lorentz and CPT symmetry violating Standard Model Extension.

In addition, STE-QUEST has important applications in domains other than fundamental physics. The table below shows the list of topics that shall be investigated by STE-QUEST.

Science Investigation	Measurement Requirement
<b>Clock Comparisons and International Atomic Time Scales</b>	
<i>Common-view comparisons of ground clocks</i>	#SSO-02: Common-view comparison of ground clocks at the $1 \cdot 10^{-18}$ fractional frequency uncertainty level after a few days of integration time with the STE-QUEST microwave link and a few hours by using the optical link.
<i>Space-to-ground time transfer</i>	#SSO-03: Space-to-ground time transfer with accuracy better than 50 ps.
<i>Synchronization of ground clocks</i>	#SSO-04: Synchronization of clocks on ground to better than 50 ps.

<sup>3</sup> This scientific investigation can be performed only if the STE-QUEST payload is equipped with a high-stability and accuracy atomic clock.

<i>Atomic time scales</i>	#SSO-05: Contribution to the generation of atomic time scales to fractional frequency inaccuracy lower than $1 \cdot 10^{-16}$ .
<i>GNSS clocks and time scales (Optional)<sup>4</sup></i>	#SSO-06: Monitoring of the stability of on-board GPS, GALILEO, and GLONASS clocks.
<b>Geodesy</b>	
<i>On-site differential geopotential measurements</i>	#SSO-07: Differential geopotential measurements between two points on the Earth's surface with resolution in the gravitational potential $U$ at the level of $0.15 \text{ m}^2/\text{s}^2$ (equivalent to 1.5 cm on the geoid height difference).
<b>Reference Frames</b>	
<i>Earth terrestrial and celestial reference frame</i>	#SSO-08: Realization and unification of the terrestrial and the celestial reference frame of the Earth.

### 3.2 STE-QUEST Orbit Characteristics

With the purpose of providing an estimate of the accuracy levels achievable in the STE-QUEST tests and experiments, it is necessary to identify a reference orbit. The nature of the tests conducted by STE-QUEST requires a highly elliptic orbit with:

1. Large gravitational accelerations around perigee;
2. Low gravity gradient and non-gravitational disturbances;
3. Long common-view contacts of the spacecraft from ground stations in different continents;
4. Large variations of the gravitational potential between apogee and perigee.

The analysis conducted in the frame of the STE-QUEST assessment study has identified an orbit compatible with the scientific objectives and the mission requirements. The low perigee altitude is compatible with the operation of the differential atom interferometer for tests of the Weak Equivalence Principle. The high apogee altitude provides long contact times at the selected ground stations and long common-view durations between ground stations, important for performing clock red-shift tests.

The orbit optimization process takes into account the constraints imposed by gravity gradient ( $< 2.5 \cdot 10^{-6} \text{ s}^{-2}$ ) and non-gravitational acceleration ( $< 4 \cdot 10^{-7} \text{ m/s}^2$  along the sensitive axis of the atom interferometer and  $< 1 \cdot 10^{-6} \text{ m/s}^2$  along the remaining two orthogonal direction) at the STE-QUEST instruments. Once orbit feasibility from the point of view of spacecraft control and fuel consumption is verified, the ground track is fine-tuned to maximize visibilities at the selected ground station locations. This orbit is considered here as a reference for evaluating STE-QUEST science performance.

The Keplerian elements at the beginning of the mission are reported in the following table. The values of some key quantities relevant for the STE-QUEST experiments are also provided both at apogee and perigee.

Keplerian elements	Value	Parameter	Apogee	Perigee
Reference epoch	01-Jun-2022 20:11	Height	51018 km	700 km
Major axis	32090 km	Velocity	1.2 km/s	10.0 km/s
Eccentricity	0.779	Angular velocity	$2.2 \cdot 10^{-5} \text{ s}^{-1}$	$1.4 \cdot 10^{-3} \text{ s}^{-1}$
Inclination	62.59 deg	Gravitational potential (in $c^2$ units)	$7.7 \cdot 10^{-11}$	$6.3 \cdot 10^{-10}$
RAAN	265.37 deg	Gravity gradient	$4.2 \cdot 10^{-9} \text{ s}^{-2}$	$2.2 \cdot 10^{-6} \text{ s}^{-2}$
Argument of perigee	271.95 deg	Drag	$< 1 \cdot 10^{-6} \text{ m/s}^2$	
True anomaly	28.65 deg	Eclipses	Duration up to 66 min	

The reference orbit has an inclination of about 63 deg and a 16-hour period. The orbit ground track is stable and has a 2-day repeat time. Third-body perturbations alter the eccentricity of the orbit, resulting in a change of the perigee altitude from about 700 km to 2200 km and then back to 700 km during the mission lifetime. Figure 3-1 shows the STE-QUEST spacecraft elevation above the selected stations, Boulder (US), Torino (IT), and Tokyo (JP). The argument of perigee is selected to have the apogee in the northern hemisphere, high above the baseline ground stations. In this way, very long visibility times can be achieved. Having the

<sup>4</sup> This scientific investigation can be performed only if the STE-QUEST payload is equipped with a high-stability and accuracy atomic clock.

apogee in the northern hemisphere also allows for long common-view durations (between 40000 s to 46000 s) over the entire mission, important for measuring the clock red-shift effect in the field of the Sun and of the Moon. The long visibility time (~ 53000 s) from the ground terminals over a wide range of distances from Earth is also compatible with the science objective based on the measurement of the gravitational red-shift in the field of the Earth. Depending on the availability of additional resources from the corresponding international partners, other ground stations may be included improving the overall visibility and reliability of the ground terminals network. For example, there is strong interest for a ground station in Australia, which then would allow good visibility during perigee from the southern hemisphere.

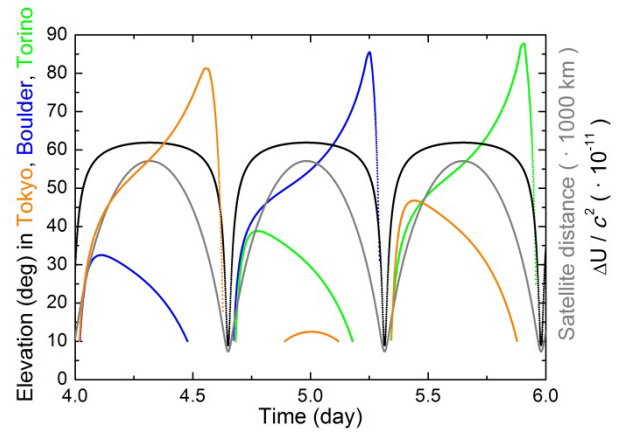


**Figure 3-1:** Elevation angle of STE-QUEST at Tokyo (orange), Boulder (blue), and Torino (green). Satellite distance is from the Earth centre (grey). The gravitational red-shift between satellite and ground is shown in black.

### 3.3 Performance Requirements and Measurement Modelling

The requirements numbering reported below follows the STE-QUEST Science Requirements Document [CACCIAPUOTI (2013)]. Mission performance against the optional scientific objectives are also analysed. The scientific requirements applicable to the optional payload elements are appropriately labelled in the text.

#### 3.3.1 Atom Interferometry Measurements

The STE-QUEST test of the Weak Equivalence Principle relies on an atom interferometry instrument probing the differential acceleration experienced by two freely falling atomic clouds of different species. The parameter historically used to quantify a deviation from the WEP of two test bodies with different composition (*A* and *B*), inertial mass  $m_i$  and gravitational mass  $m_g$ , is the so called Eötvös parameter:

$$\eta_{AB} = 2 \cdot \frac{a_A - a_B}{a_A + a_B} = 2 \cdot \frac{(m_g/m_i)_A - (m_g/m_i)_B}{(m_g/m_i)_A + (m_g/m_i)_B} \quad (3-1)$$

$\eta \neq 0$  would disprove the Universality of Free Fall and violate Einstein Equivalence Principle.

The STE-QUEST atom interferometer will compare the free fall of the two rubidium isotopes while it orbits around perigee. The use of  $^{85}\text{Rb}$  and  $^{87}\text{Rb}$  significantly simplifies the instruments, at the same time ensuring a better control on common-mode noise sources and on measurement systematics. Around apogee, calibration measurements will be performed to validate the instrument sensitivity.

Due to its high symmetry, the double-diffraction scheme [LÉVÈQUE (2009)] is particularly suited for high-sensitivity acceleration measurement in free fall conditions. In the interferometer, atomic wave packets made out of cold atoms are coherently split, re-directed and re-combined to generate matter-wave interference. Beam splitting is achieved by atom-light interaction. The differential phase accumulated by the two simultaneous atom interferometers provides a measurement of the differential acceleration between by the two atomic clouds. A non-null differential acceleration would then be the signature for a violation of the Weak Equivalence Principle.

##### 3.3.1.1 Measurement Modelling and Assumptions

Testing the universality of free fall at the  $10^{-15}$  level implies a measurement of the differential acceleration between the two atomic species at the same level of precision.

To maximize an eventual WEP-violating signal, the measurement axis of the accelerometer needs to be oriented along the spacecraft-Earth direction during a perigee passage. The measurement is performed while the spacecraft is in inertial motion with respect to a non-rotating freely falling reference frame and pointed towards nadir when crossing perigee. This spacecraft attitude introduces a modulation in the eventual WEP-violating signal, important to control the measurement systematics. The inertial motion is maintained for the orbital arc dedicated to the differential atom interferometry measurements, which extends around perigee and up to altitudes of about 3000 km. The sensitivity of the atom interferometry instrument to differential acceleration measurements is specified in the following requirement:

SciRD Ref.	Requirement
#SR-PL-15	<b>Differential Atom Interferometer Sensitivity:</b> The STE-QUEST atom interferometry instrument shall have a sensitivity to differential accelerations better than $(13 \cdot 10^{-12} \text{ m/s}^2)/\sqrt{\tau}$ , for integration times $\tau$ , expressed in seconds, between 20 s and $3.5 \cdot 10^6$ s both in the external and internal operational modes.

The numerical simulations developed for estimating the integrated measurement sensitivity, also accounting for the measurement dependence on the spacecraft altitude and attitude with respect to Earth, are discussed in the next section.

### 3.3.1.2 Numerical Simulations

The single-shot sensitivity to Eötvös ratio measurements  $\sigma_\eta$  is obtained by dividing the sensitivity to differential accelerations measurements  $\sigma_{\Delta a}$  (see #SR-PL-15) by the projection of the position-dependent gravitational acceleration  $\vec{g}(\vec{r})$  along the sensitive axis of the instrument (as defined by the effective wave vector  $\vec{k}$  of the Raman lasers):

$$\sigma_\eta = \frac{\sigma_{\Delta a}}{g(\vec{r}) \cdot \cos(\nu)}, \quad (3-2)$$

with  $\nu$  being the true anomaly. As gravity gradients affect the interferometer contrast  $C$ , the single-shot sensitivity to differential acceleration measurements is proportional to  $C$  and also depends on  $\nu$  and  $r$  according to the formula

$$\sigma_{\Delta a} \propto C, \text{ where } C = \exp\left\{-\frac{1}{2}(k\sigma_r\Gamma_{zz}T^2)^2\right\} \exp\left\{-\frac{1}{2}(k\sigma_\nu(t_0 + T)\Gamma_{zz}T^2)^2\right\}, \quad (3-3)$$

where  $\Gamma_{zz} = \cos(\nu)\Gamma_{zz} + \sin(\nu)\Gamma_\perp$  is the effective gravity gradient along the sensitive axis of the instrument,  $\Gamma_{zz} = -2GM_E/r^3$  is the Earth gravity gradient, and  $\Gamma_\perp = \Gamma_{zz}/2$ ; here,  $G$  denotes the Newtonian gravitational constant and  $M_E$  is the mass of the Earth. Because of these dependencies, the single-shot sensitivity to the Eötvös ratio  $\sigma_{\eta,i}$  has to be calculated for each individual measurement  $i$ . If  $N$  is the number of measurements in one orbit and  $M$  is the number of identical orbits:

$$\sigma_\eta^{(M \text{ orbits})} = \frac{1}{MN} \sqrt{\sum_{i=1}^N M \cdot \sigma_{\eta,i}^2} = \frac{1}{\sqrt{M}} \sigma_\eta^{(1 \text{ orbit})} = \frac{1}{\sqrt{M}} \cdot \sqrt{\frac{1}{N(N-1)} \sum_{i=1}^N \sigma_{\eta,i}^2} \approx \frac{1}{N\sqrt{M}} \sqrt{\sum_{i=1}^N \sigma_i^2}. \quad (3-4)$$

A numerical orbit propagator, which iteratively solves Kepler's equation by using Newton's method, was implemented in the simulation code. The orbit propagator is adjusted to a precision of  $\Delta r \leq 16$  cm for the STE-QUEST baseline orbit. The natural evolution of the STE-QUEST orbit was introduced into the simulation by varying the perigee altitude according to the STE-QUEST reference orbit (Sec. 3.2), while keeping all Keplerian elements not depending on the perigee altitude.

The simulation program executes the following steps:

- I. It solves the STE-QUEST orbit with respect to position and true anomaly as a function of time;
- II. At each measurement cycle, it calculates  $\vec{g}(\vec{r})$  and its projection on the instrument sensitive axis, assuming inertial pointing of the STE-QUEST spacecraft while orbiting around perigee;
- III. It calculates the single-shot sensitivity for Eötvös ratio measurements  $\sigma_{\eta,i}$  along the orbit;
- IV. It determines the sensitivity  $\sigma_\eta^{(1 \text{ orbit})}$  by averaging over the measurements for each orbit.

The total number of orbits  $M$  as well as the measurement time needed to reach the ultimate accuracy in the test of the Weak Equivalence Principle can then be evaluated.

### 3.3.1.3 Simulation Results

#### #PSO-01: Test the universality of the free propagation of matter waves to an uncertainty in the Eötvös parameter better than $2 \cdot 10^{-15}$

The STE-QUEST reference orbit has a perigee altitude that varies between 700 km and 2200 km. A higher perigee altitude translates into a lower gravitational acceleration, but also into a higher contrast due to a decrease of the effective gravity gradient. These two effects nearly cancel each other resulting in a sensitivity to the Eötvös ratio between  $5.0 \cdot 10^{-14}$  (for a 700 km perigee) and  $5.3 \cdot 10^{-14}$  (for a 2200 km perigee) per orbit, obtained by averaging between 75 to 100 differential acceleration measurements respectively. As a result, an integrated sensitivity of  $2 \cdot 10^{-15}$  can be reached in less than 1.5 years with good perspectives for reaching the  $1 \cdot 10^{-15}$  uncertainty level within the mission lifetime.

Tracking the propagation of matter waves extends classical free fall experiments in the conceptually different domain of quantum objects. The measurement involves external and internal degrees of freedom, therefore addressing different aspects of the Einstein Equivalence Principle. Laser ranging [WILLIAMS (2013)] and

torsion balance experiments [SCHLAMMINGER (2008)] on the ground have tested the WEP validity on macroscopic objects to a few parts in  $10^{13}$ . The space mission MICROSCOPE is designed to reach a sensitivity of 1 part in  $10^{15}$  [TOUBOUL (2001)]. To date, matter-wave tests of the equivalence principle have been performed with neutrons [LITTREL (1997)] and samples of laser cooled atoms [FRAY (2004)]. While experiments based on neutrons are essentially limited by problems related to the coherent beam splitting, cold atom interferometry has demonstrated inaccuracy levels of  $1 \cdot 10^{-7}$ . STE-QUEST aims at a quantum test of the Weak Equivalence Principle with an uncertainty down to  $2 \cdot 10^{-15}$ .

### 3.3.2 Clock Measurements

The gravitational potential experienced by ground and space clocks is the sum of three major contributions:

$$U(\mathbf{x}) = U_{\text{Earth}}(\mathbf{x}) + U_{\text{Sun}}(\mathbf{x}) + U_{\text{Moon}}(\mathbf{x}). \quad (3-5)$$

Since the time variations of the individual contributions with the position  $\mathbf{x}(t)$  of the space or ground clocks have different signature, it is possible to independently measure each of the three red-shift effects.

The concept of the Earth time dilation measurement is shown in Figure 3-2 (left). The STE-QUEST clock is continuously compared with one or more clocks on ground. The comparison provides the frequency ratio between the satellite clock and the ground clock as measured at the same location (either on the satellite or on ground). This value arises from a procedure involving corrections stemming from the velocity of the ground and satellite clocks (second-order Doppler effect) that need to be evaluated. Two different measurement modes can be implemented, the first based on an absolute comparison between the space clock and the ground clock (DC measurement), the second measuring the variations of the Earth red-shift effect experienced by the space clock while orbiting between perigee and apogee (AC measurement).

As shown in Figure 3-2 (right), the red-shift measurement in the gravitational field of the Sun and the Moon relies on the common-view comparison of terrestrial clocks. This measurement does not require a high-performance frequency reference on-board the STE-QUEST spacecraft. When two ground clocks are simultaneously compared to the space clock, the difference of simultaneous link measurements rejects the common-mode noise of the space clock and provides a direct comparison of the two clocks on the ground. A putative violation of LPI will then show up as a modulation of the relative frequency of the two clocks that is synchronous to the orientation of the baseline with respect to the source (Sun or Moon).

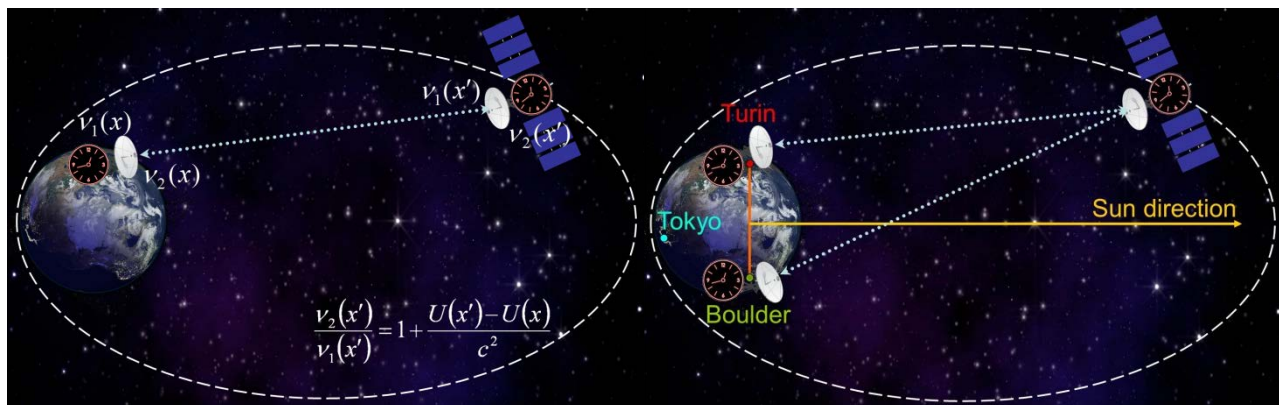


**Figure 3-2:** (Left) Measurement principle of the gravitational time dilation effect in the field of the Earth.  $\nu_1$  ( $\nu_2$ ) is the frequency of the wave emitted by the ground (space) clock. The formula shows the result of a frequency comparison performed at the spacecraft location  $\mathbf{x}'$ . (Right) Measurement principle of the gravitational time dilation effect in the field of Sun or Moon, using two ground clocks. Here, the satellite and its links act as a transponder.

#### 3.3.2.1 Measurement Modelling and Assumptions

The accuracy of gravitational time dilation tests depend on the combination of several effects:

1. STE-QUEST orbit and ground terminals positions;
2. STE-QUEST operational constraints;
3. Clocks and links performance;
4. Orbitography.

The constraints imposed by 1 to 4 are discussed in the following sections and included in the numerical simulations developed to verify the mission performance against the STE-QUEST scientific objectives. Results are provided also for the optional optical link technology.

**Orbit and Ground Terminal Positions**

The “frozen” orbit presented in Sec. 3.2 is a suitable choice for what concerns gravitational potential differences between apogee and perigee and between apogee and ground. The baseline locations of the ground stations are taken to be close to major metrology institutes: Turin (Europe), Boulder (USA), and Tokyo (Japan). In these centres, high-performance atomic clocks are currently available and will be further developed and operational at the time of the STE-QUEST mission. Visibility durations are optimized with respect to the selected ground stations and change only moderately during the course of the mission due to perigee altitude changes. Thus, the behaviour during the 2-day repeat period of the orbit ground track at the beginning of the mission can be taken as representative of the whole mission (see Figure 3-1).

An important parameter that is taken into account in the simulations is the visibility of the ground stations, based on long-term weather observations. For the microwave link, 100% visibility is assumed, since microwave frequencies show very limited sensitivity to weather conditions and the link budget can be designed to ensure availability even during cloudy weather conditions. For the optical link, we assume 25% average probability that any pair of ground clocks can perform a continuous common-view comparison when the satellite is in the appropriate phase of the orbit; this figure was derived on the basis of historical weather data on cloud coverage at the baseline ground station locations. In addition, both STE-QUEST links are considered to be in full tracking mode at elevations higher than 10 deg. Therefore, orbit segments corresponding to a line-of-sight in the space-to-ground link lower than 10 deg over the horizon are not considered in the simulation of clock red-shift experiments.

**Operational Constraints**

The duration of the STE-QUEST routine science phase is limited to 4.5 years. During this phase, mission operations shall ensure the minimum measurement time needed for averaging the uncertainty in the clock red-shift tests down to its ultimate limit. This requires the identification of windows along the STE-QUEST orbit to be dedicated to spacecraft manoeuvres that are not compatible with clock measurements. They also include the spacecraft manoeuvres needed to gain inertial pointing during the perigee passage to perform WEP tests (see Sec. 5.3.1.1). Orbit segments characterized by an altitude between 3000 km and 7000 km are reserved for that purpose and therefore they are assumed not to contribute to the measurements.

**Clocks and Links Performance**

The performance of the STE-QUEST clock and links is specified in the following requirements:

SciRD Ref.	Requirement
#SR-PL-11 (Optional)	<b>STE-QUEST Atomic Clock Instability:</b> The fractional frequency instability of the STE-QUEST atomic clock expressed in Allan deviation shall be smaller than $8 \cdot 10^{-14} / \sqrt{\tau}$ , both in the external and internal operational modes, for integration times $\tau$ , expressed in seconds, between 1 s and $7 \cdot 10^5$ s.
#SR-PL-12 (Optional)	<b>STE-QUEST Atomic Clock Inaccuracy:</b> The STE-QUEST atomic clock fractional frequency inaccuracy shall be smaller than $1 \cdot 10^{-16}$ .
#SR-PL-16	<p><b>(a) Microwave Link Instability for Space-to-ground Clock Comparisons (Optional):</b> The modified Allan deviation of the noise introduced by the STE-QUEST microwave link in the comparison of the on-board clock with clocks on the ground shall be smaller than</p> $\sqrt{(5.0 \cdot 10^{-13} / \tau^{3/2})^2 + (1.6 \cdot 10^{-13} / \tau)^2 + (7.1 \cdot 10^{-15} / \tau^{1/2})^2}$ <p>for integration times <math>\tau</math>, expressed in seconds, between 10 s and <math>7 \cdot 10^5</math> s.</p> <p><b>(b) Microwave Link Instability for Ground-to-ground Clock Comparisons (b):</b> The modified Allan deviation of the noise introduced by the STE-QUEST microwave link in the comparison of two clocks on the ground shall be smaller than</p> $\sqrt{(5.0 \cdot 10^{-13} / \tau^{3/2})^2 + (1.6 \cdot 10^{-13} / \tau)^2 + (5.9 \cdot 10^{-17} / \tau^{1/2})^2 + (5.0 \cdot 10^{-19})^2}$ <p>for integration times <math>\tau</math>, expressed in seconds, between 10 s and <math>7 \cdot 10^5</math> s.</p>
#SR-PL-17 (Optional)	<p><b>(a) Optical Link Instability for Space-to-ground Clock Comparisons:</b> The modified Allan deviation of the noise introduced by the STE-QUEST optical link in the comparison of the on-board clock with clocks on the ground shall be smaller than</p> $\sqrt{(3.2 \cdot 10^{-14} / \tau^{3/2})^2 + (1.0 \cdot 10^{-14} / \tau)^2 + (7.1 \cdot 10^{-15} / \tau^{1/2})^2}$ <p>for integration times <math>\tau</math>, expressed in seconds, between 10 s and <math>10^5</math> s.</p> <p><b>(b) Optical Link Instability for Ground-to-ground Clock Comparisons:</b> The modified Allan variance of the noise introduced by the STE-QUEST optical link in the comparison of two clocks on the ground shall be smaller than</p> $\sqrt{(3.2 \cdot 10^{-14} / \tau^{3/2})^2 + (1.0 \cdot 10^{-14} / \tau)^2 + (5.9 \cdot 10^{-17} / \tau^{1/2})^2 + (5.0 \cdot 10^{-19})^2}$ <p>for integration times <math>\tau</math>, expressed in seconds, between 10 s and <math>10^5</math> s.</p>

#SR-PL-18	<b>Time and Frequency Transfer Links Inaccuracy:</b> The STE-QUEST time and frequency transfer links shall be able to compare the space clock and clocks on ground to a fractional frequency inaccuracy smaller than $3 \cdot 10^{-17}$ (optional) as well as to compare ground clocks to a fractional frequency inaccuracy smaller than $5 \cdot 10^{-19}$ .
#SR-GS-01	<b>Ground Clocks Instability:</b> The fractional frequency instability of the ground clocks participating to the STE-QUEST mission expressed in Allan deviation shall be smaller than $2.5 \cdot 10^{-16} / \sqrt{\tau}$ , for integration times $\tau$ , expressed in seconds, between 1 s and 250000 s.
#SR-GS-02	<b>Ground Clocks Inaccuracy:</b> The fractional frequency inaccuracy of the ground clocks participating to the STE-QUEST mission shall be smaller than $1 \cdot 10^{-18}$ .

Figure 3-3 shows the STE-QUEST links performance for space-to-ground and ground-to-ground comparisons against the modified Allan deviation specified for PHARAO and for clocks on the ground.

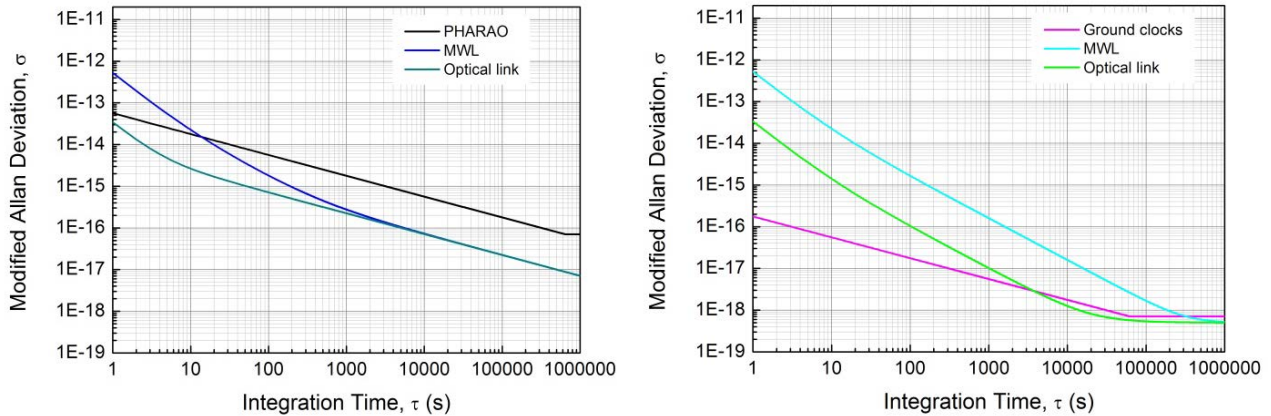


Figure 3-3: STE-QUEST links performance for space-to-ground (left) and ground-to-ground (right) comparisons.

**Orbitography and Gravitational Potential Determination**

Positioning of the clocks and of the link reference points in space and on the ground as well as precise knowledge of the gravitational potential at the space and ground clocks are essential to perform clock redshift tests. These requirements are summarized in the table below.

#SR-PL-41 and #SR-GS-16 account for time errors in the evaluation of the relativistic time and frequency shifts induced by positioning errors at the clock in space and on the ground. #SR-PL-40 and #SR-GS-15 define boundaries for errors in the calculation of the difference between up and down travel time of the clock signal between the link reference points on ground and in space (e.g. antenna phase centre of the STE-QUEST microwave link). As also shown in DUCHAYNE (2009), the positioning requirements imposed by #SR-PL-41 and #SR-GS-16 are by far the most stringent ones, with the space segment related requirement #SR-PL-41 only required for the optional Earth redshift measurement.

SciRD Ref.	Requirement
<b>In space</b>	
#SR-PL-40 (Optional)	<b>Orbit Determination of the Link Reference Points in Space:</b> The uncertainty in the orbit determination (position, velocity, time) of the STE-QUEST links reference points (e.g. antenna phase centre) in space shall introduce a noise in the comparison between the STE-QUEST clock and ground clocks that, expressed in Allan deviation, shall be 3 times smaller than the links noise (see #SR-PL-16, #SR-PL-17).
#SR-PL-41 (Optional)	<b>Orbit Determination of the STE-QUEST Atomic Clock:</b> The uncertainty in the orbit determination (position, velocity, time) of the STE-QUEST clock reference point (i.e. centre of the PHARAO Ramsey cavity) shall introduce a noise in the evaluation of the clock relativistic frequency shifts that, expressed in Allan deviation, shall be 3 times smaller than the STE-QUEST clock noise (see #SR-PL-11).
#SR-PL-42 (Optional)	<b>Gravitational Potential at the STE-QUEST Atomic Clock:</b> The error in the determination of the gravitational potential at the space clock location shall lead to a fractional frequency uncertainty due to the red-shift effect smaller than $3 \cdot 10^{-17}$ .
<b>On ground</b>	
#SR-GS-15	<b>Position of Link Reference Points on Ground:</b> The uncertainty in the determination of position, velocity, and time of the STE-QUEST links reference points (e.g. antenna phase centre) on ground shall introduce a noise in the comparison between the STE-QUEST clock and ground clocks that, expressed in Allan deviation, shall be 3 times smaller than the links noise (#SR-PL-16, #SR-PL-17).

#SR-GS-16	<b>Ground Clocks Position:</b> The error in the determination of the ground clock position and velocity shall introduce a relative frequency uncertainty in the evaluation of the gravitational red-shift and of the second-order Doppler effect smaller than $5 \cdot 10^{-19}$ .
#SR-GS-17	<b>Gravitational Potential at the Ground Clocks:</b> The error in the determination of the gravitational potential at the ground clock location shall lead to a fractional frequency uncertainty due to the red-shift effect smaller than $3 \cdot 10^{-17}$ .
#SR-GS-18	<b>Daily Variations of the Earth Gravitational Potential at the Ground Clocks:</b> Daily variations of the Earth gravitational potential at the ground clock location shall be modelled to a fractional frequency uncertainty smaller than $5 \cdot 10^{-19}$ , with the ultimate goal of $2 \cdot 10^{-19}$ .

Following the approach described in DUCHAYNE (2009), the requirements can be translated into positioning accuracies at the reference points of both the space and ground clocks. In particular, the uncertainty in the determination of position and velocity of the reference point at the optional atomic clock shall be smaller than 2 m and 0.2 mm/s respectively, along the tangential, radial, and normal directions of the STE-QUEST orbit. The accuracy levels calculated above are stringent limits that only apply for the optional Earth redshift test while the clock is orbiting around perigee and are less stringent during apogee passages. Similar figures apply to the positioning accuracies of the ground clocks. The positioning accuracies of the ground clocks are constrained by the knowledge of the gravitational potential as explained below.

Knowledge of the gravitational potential at the space and ground clock locations is then required to be better than a corresponding fractional frequency shift of  $3 \cdot 10^{-17}$  (#SR-PL-42 and #SR-GS-17) in order not to affect the measurement uncertainty of clock red-shift tests in the field of the Earth. For a clock on the Earth surface, this corresponds to a determination of the clock height with respect to the geoid with an uncertainty lower than 30 cm. Local gravity measurements at and above the ground clock site might be needed to achieve these uncertainty levels in the local geopotential measurement [PAVLIS (2003)]. The terrestrial contribution is nearly constant in time, with small seasonal variations, e.g. due to the change in the water table level under the ground clocks. These effects need to be modelled to the appropriate level (#SR-GS-18) to perform clock red-shift tests in the gravitational field of the Sun or of the Moon. WOLF (1995) provides a comprehensive discussion of the uncertainties affecting the frequency comparison of clocks on the ground or on-board terrestrial satellites. The requirements discussed here have been derived to contribute negligible noise to the link and therefore they will not be considered in the modelling of clock comparison.

### 3.3.2.2 Numerical Simulations

Numerical simulations are based on the Monte-Carlo method. The code generates synthetic noise samples,  $n_i(t)$  ( $i = 1 \dots i_{\max}$ ), consisting of values of the relative frequency noise  $\Delta f(t)/f$  for the STE-QUEST clocks and links data, and simulates clock comparison measurements in the configurations listed below:

1. PHARAO clock + microwave link + ground clock;
2. PHARAO clock + optical link + ground clock;
3. Ground clock + optical link + ground clock;
4. Ground clock + microwave link + ground clock.

The generation of synthetic noise data follows the requirements discussed in Sec. 3.3.2.1 (see also Figure 3-3) for space-to-ground (study cases 1 and 2) and ground-to-ground comparisons (study cases 3 and 4).

The program executes the following steps:

- I. Selects one of the study cases listed above (1 to 4) and reads the  $\Delta f(t)/f$  noise files corresponding to the selected measurement scenario;
- II. Defines the orbit interval to be simulated and reads the corresponding data;
- III. Computes the noisy signals simulating the clock comparison measurements;
- IV. Extracts the science results and their errors from a global fit to the data.

In the case of the *Earth time dilation measurement*, the relative gravitational frequency shift is calculated from the spacecraft orbit data and from the position of ground clocks on the surface of the Earth. For simplicity, the average Earth radius is used, neglecting the different altitudes at the ground stations. In the *AC measurement of the Earth time dilation effect*, fit parameters include the factor  $\alpha_{E, AC}$ , which multiplies the Earth time dilation signal, and an offset term, which accounts for a frequency error of the on-board atomic clock, expected to vary on time scales much longer than the orbit period. In the *DC measurement of the Earth red-shift effect*,  $\alpha_{E, DC}$  is the fit parameter which multiplies the Earth time dilation signal.

In the case of the *Sun/Moon time dilation measurement*, the relative gravitational frequency shift of each ground clock is calculated on the basis of latitude, longitude, and distance to the Sun. The differential shifts between station 1 and 2, 2 and 3, and 1 and 3 are computed and written into a list that covers three

subsequent orbits (2 days) continuously. Fit parameters include the factor  $\alpha_{S/M}$ , which multiplies the Sun/Moon time dilation signal and an offset term, for instance accounting for the differences in geopotential between the two ground station locations.

The standard deviations  $\sigma(\alpha_{E, AC})$ ,  $\sigma(\alpha_{E, DC})$ , and  $\sigma(\alpha_{S/M})$  computed from the statistical ensemble  $\{i = 1 \dots i_{\max}\}$  represent the best estimate of the respective measurement uncertainties, achievable over a 2-day measurement interval. If  $N$  is the number of 2-day measurement intervals available for the test, averaging further decreases the uncertainty of the final result by a factor  $\sqrt{N}$ . Of course, that averaging is limited by systematic effects having signatures that are correlated with the expected signals. Those effects are constrained by the requirements on clock accuracy and gravitational potential determination given above.

### 3.3.2.3 Simulation Results

#### **#PSO-02: Measurement of the Sun gravitational red-shift effect to a fractional frequency uncertainty of $2 \cdot 10^{-6}$ , with an ultimate goal of $5 \cdot 10^{-7}$**

The gravitational red-shift effect induced by the Sun is measured by comparing ground clocks in common-view. The Sun field contribution varies according to the orientation of the ground clock pair with respect to the Earth-Sun direction. This effect has a 1-day period and a peak-to-peak amplitude of about  $1 \cdot 10^{-12}$  between two ground stations. As the ground clocks are in free fall with respect to the Sun, this effect is cancelled in general relativity by the second-order Doppler shift due to the motion of the ground clocks relative to each other [HOFFMAN (1961)]. The measurement of this null effect is of importance for achieving the primary scientific objective #PSO-02. Indeed, in theoretical frameworks that violate EEP (see Sec. 2.3.1 and 2.3.3), this cancellation might not be perfect, leading to a residual diurnal variation that could be measured.

The analysis of the Sun red-shift test presented here assumes three clocks on the ground, cross-compared via the STE-QUEST high-performance links (study case 3 and 4 of Sec. 3.3.2.1). During the 2-day period of the STE-QUEST orbit ground track, common-view comparisons of the three pairs of ground clocks performed via the microwave link achieve an average resolution of  $6 \cdot 10^{-5}$ . Differently from the optical technology, the microwave link operation is extremely robust with respect to weather conditions. Assuming 100% link availability, 4 years of measurement are then needed to bring the test inaccuracy down to  $2.2 \cdot 10^{-6}$ . Reaching the ultimate goal  $5 \cdot 10^{-7}$  within the mission lifetime is then not possible with the microwave technology. Performing the same test with the optical link (optional) would provide an average fractional frequency resolution of  $6 \cdot 10^{-6}$  after 2 days. In this case, 72 days of integration time would be sufficient to reach the target resolution of  $2 \cdot 10^{-6}$ . The estimated measurement duration is assuming 25% average probability of clear sky conditions, simultaneously at any pair of two ground stations, to ensure availability of the optical link during the common-view comparisons. The ultimate goal of  $5 \cdot 10^{-7}$  can then be reached by integrating over 4 years of measurement.

This analysis is not making use of the phase cycle continuity requested for the STE-QUEST link measurements. When phase cycle continuity is maintained by the link, the measurement duration is not affected by the dead-time between one common-view comparison and the next, resulting in a reduction of the integration time needed to reach the ultimate accuracy. Such a data analysis approach is presently being implemented in the numerical simulations.

In comparison, the best current results for the solar gravitational frequency shift are at the few % level [KRISHER (1993), LOPRESTO (1991)]. The improvement compared to the ACES mission is between a factor 10 and 30, due to the better accuracy of ground clocks by the time of the STE-QUEST mission and to the better stability of the STE-QUEST links compared to ACES.

#### **#PSO-03: Measurement of the Moon gravitational red-shift effect to a fractional frequency uncertainty of $4 \cdot 10^{-4}$ , with an ultimate goal of $9 \cdot 10^{-5}$**

The STE-QUEST mission also provides the possibility to measure the gravitational time dilation induced by the Moon. For the analysis of the resolution of the Moon time dilation measurement, a simplified treatment can be proposed. The Moon is assumed to be stationary with respect to the Earth, as was the case in the simulation of the Sun effect. This is a reasonable assumption, since the period of the Moon orbit (27 days) is much longer than the period of the Earth rotation (1 day). Thus, the motion of the Moon with respect to the Sun direction is very limited during the time interval for which the measurement simulation is performed (2 days). When considering the comparison of ground clocks, the time dilation effect of the Moon can be

clearly differentiated from that of the Sun on the time scale of a lunar period because of the phase shift of the lunar effect. The Moon effect is also reduced, by a factor  $(M_{\text{Sun}}/d_{\text{Sun}}^2)/(M_{\text{Moon}}/d_{\text{Moon}}^2) = 175$  compared to the effect of the Sun. The square dependence on the distance  $d$  between Earth and Moon or Earth and Sun stems from the fact that in a modulation-type measurement, where the distance change of each ground clock to the Moon and the Sun is much smaller than  $d$ , a Taylor expansion can be used to estimate the result.

The peak-to-peak Moon effect on the comparison of ground clocks is expected to be at the  $6 \cdot 10^{-15}$  level for the Torino-Tokyo and Boulder-Tokyo comparisons. Using the results of the clock red-shift measurement in the field of the Sun, a resolution of  $4 \cdot 10^{-4}$  in the measurement of the Moon time dilation effect can be expected after 4 years of averaging with the microwave link. Reaching the ultimate goal  $9 \cdot 10^{-5}$  is then not possible with the microwave technology within the mission lifetime. Performing the same test with the optical link (optional), would require 72 days for reaching a measurement uncertainty of  $4 \cdot 10^{-4}$ . The ultimate goal of  $9 \cdot 10^{-5}$  would then be reached by averaging over 4 years of measurement. To our knowledge, no such measurement has been performed before.

#### **#PSO-04 (Optional): Measurement of the Earth gravitational red-shift effect to a fractional frequency uncertainty of $2 \cdot 10^{-7}$**

This test can be performed only if the cold-atom clock PHARAO is part of the STE-QUEST payload. Two complementary measurement approaches can be implemented.

##### ***DC Measurement of the Earth Time Dilation Effect***

The first measurement approach relies on the absolute comparison between the space clock and clocks on ground, in particular while the STE-QUEST spacecraft is orbiting around apogee, where the space-to-ground gravitational red-shift effect is maximized. The numerical simulation, based on a space clock with fractional frequency instability of  $8 \cdot 10^{-14}/\sqrt{\tau}$  and fractional frequency inaccuracy of  $1 \cdot 10^{-16}$  and compared to ground clocks via the STE-QUEST microwave link (study case 1 of Sec. 3.3.2.2), indicates that a resolution of  $4 \cdot 10^{-7}$  in the measurement of the gravitational red-shift effect can be reached in 32 hours (2 orbits) over a single ground station. 6 days of measurements are then needed to reach a resolution of  $1.5 \cdot 10^{-7}$ , limited by the specified clock inaccuracy. The simulation does not assume averaging over several simultaneously obtained space-to-ground comparisons. The use of an optical link (study case 2 of Sec. 3.3.2.2) does not improve the measurement resolution as that is limited by the performance of the space clock (see Figure 3-2).

##### ***AC Measurement of the Earth Time Dilation Effect***

This measurement mode relies on the stability rather than the accuracy of the satellite clock. As such, it is complementary to the previous approach for achieving the primary scientific objective #PSO-04. The variations of the gravitational red-shift during the orbital motion are measured continuously for the maximum possible observation time during each orbit and repeated over  $N$  orbits. Systematic shifts at the STE-QUEST atomic clock, if not correlated with the orbital motion, are expected to average out, leading to a gain in sensitivity of up to  $\sqrt{N}$ . The numerical simulation based on a space clock with fractional frequency instability of  $8 \cdot 10^{-14}/\sqrt{\tau}$  and the STE-QUEST microwave link (study case 1 of Sec. 3.3.2.2) indicates that a resolution of  $5 \cdot 10^{-6}$  can be reached in 32 hours (2 orbits) in the measurement of the gravitational red-shift effect over a single ground station. 840 days of measurements are therefore needed to reach a resolution of  $2 \cdot 10^{-7}$ . Averaging over the whole mission duration for about 1460 days improves the resolution down to  $1.5 \cdot 10^{-7}$ . The simulation does not assume averaging over the signals obtained from simultaneous space-to-ground comparisons. Also in this case, the use of an optical link (study case 2 of Sec. 3.3.2.2) does not improve the measurement resolution as it is limited by the performance of the space clock (see Figure 3-3).

Both the DC and AC measurement of the Earth time dilation effect, are performed by comparing the measured clock frequency shift with the value expected from general relativity (gravitational red-shift and second order-Doppler effect). Therefore, orbit data of both space and ground clock are needed for the evaluation of relativistic effects. In comparison, the best current results for the Earth gravitational frequency shift are at the  $7 \cdot 10^{-5}$  level [VESSOT (1980)], bringing a measurement improvement of a factor 350. With respect to ACES, the more favourable orbit of the spacecraft and the slightly better performance of the STE-QUEST clock are expected to bring a factor 30 improvement.

## 4 Payload Design

The architecture of the STE-QUEST payload is presented in Figure 4-1. The schematic shows the core instruments required to conduct the scientific investigations discussed in Sec. 3 and the optional payload elements identified to enlarge the STE-QUEST science outcome with additional experiments and tests.

The core instruments of the STE-QUEST payload are:

- Differential atom interferometer;
- Science link operating in the microwave;
- GNSS receiver.

The atom interferometer provides differential acceleration measurements between ultra-cold samples of  $^{85}\text{Rb}$  and  $^{87}\text{Rb}$  in free fall. The microwave link, driven by the frequency reference provided by the internal ultra-stable oscillator or eventually by the cold-atom clock, is used to perform clock comparisons.

The optional payload elements include:

- High-performance cold-atom clock;
- Optical link.

The availability of a high-stability and accuracy cold-atom clock on-board STE-QUEST opens the possibility to perform space-to-ground clock comparisons, thus allowing a precision measurement of the gravitational red-shift effect in the field of the Earth. The optical link is a complementary technique ensuring outstanding stability and very short averaging times for the comparison of atomic clocks on the ground.

This section presents the design characteristics of both the core instruments and the optional payload elements.

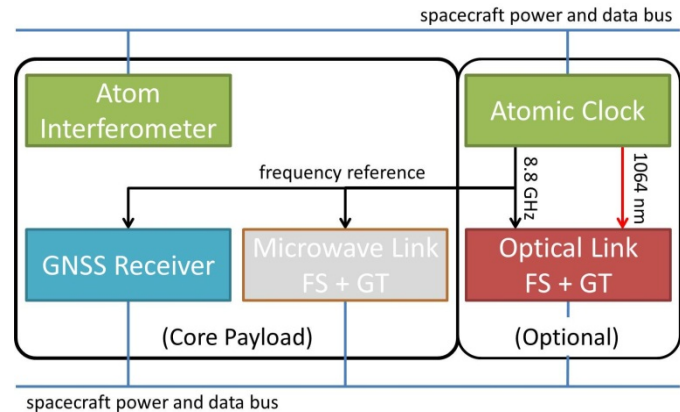


**Figure 4-1:** The STE-QUEST payload architecture. Both core instruments and optional payload elements are shown.

### 4.1 Core Instruments

#### 4.1.1 The Dual Species Atom Interferometer

The dual species atom interferometer (ATI) compares the free evolution of matter waves of ultra-cold rubidium  $^{85}\text{Rb}$  and  $^{87}\text{Rb}$  atoms. The differential acceleration between the two samples is continuously measured, while the spacecraft orbits around perigee where the signal-to-noise ratio of an eventual WEP violating signal is maximized.

##### 4.1.1.1 Design

The ATI measurement cycle consists of the following steps. First, two Bose-Einstein condensates (BEC) of  $^{87}\text{Rb}$  and  $^{85}\text{Rb}$  are simultaneously produced with  $10^6$  atoms in each at an effective expansion temperature of 70 pK. An atom-chip-based magneto-optical trap (MOT) fed by a  $2\text{D}^+$ -MOT captures and cools down the atoms of both species. After that, atoms are transferred into a magnetic trap generated by the chip and pre-evaporated. This ensures high transfer efficiency from the magnetic trap to the optical dipole trap (ODT), which is the next step of the atomic sample preparation. The ODT is used for further evaporation and for reaching the BEC phase. To avoid collapse of the  $^{85}\text{Rb}$  condensate, a strong magnetic field (about 158 G) is used to tune the scattering length of the atoms around the Feshbach resonance [ALTIN (2010)]. A delta-kick cooling (DKC) sequence [MÜNTINGA (2013)] applied in combination with the ODT after release leads to the targeted effective temperature. Shortly after (10 ms), the Feshbach field can be switched-off without any noticeable effect on the expansion dynamics of the  $^{85}\text{Rb}$  BEC. At this point, the two samples are simultaneously interrogated by the atom interferometry sequence. The Raman lasers probing  $^{85}\text{Rb}$  and  $^{87}\text{Rb}$  are appropriately detuned from the respective two-photon transitions to match the effective wave vectors of the two simultaneous atom interferometers. This condition is important to guarantee a  $2.5 \cdot 10^{-9}$  rejection ratio for common-mode vibration noise [TINO (2013)]. The interferometer is realized by three laser pulses tuned on the two-photon Raman transitions of  $^{85}\text{Rb}$  and  $^{87}\text{Rb}$ , which symmetrically split, reflect, and recombine the BECs trajectories [LÉVÈQUE (2009)]. Each atom-light interaction process imprints on the atomic wavefunction information on the distance between the atom and a common retro-reflecting mirror. This

information, depending on the acceleration of the atoms with respect to the mirror, can be read in terms of atomic population at the two output ports of the simultaneous atom interferometers. The laser-induced atomic fluorescence is collected by a CCD camera and used to measure the number of atoms in the two hyperfine levels of the rubidium ground state. The relative acceleration between the  $^{85}\text{Rb}$  and  $^{87}\text{Rb}$  atomic samples can then be extracted by analysing the data as described in FOSTER (2002). One complete experimental cycle lasts 20 s, with a duration of the atom interferometry sequence of  $2 \cdot T = 10$  s.

The ATI instrument consists of three main functional units based on a modular design: the physics package (PP), the laser system (LS), and the electronics package (EP). Surrounded by a four-layer magnetic shield, the PP hosts the atom chip, the optical trap, and a 12 cm baseline interferometer inside an ultra-high vacuum system (see Figure 4-2). Additional coils and optics for atom manipulation, and the CCD cameras for atom detection are attached to the chamber or the chamber mounts. The vacuum pumps are located outside the magnetic shield. The laser system features high power diode lasers at 780 nm for cooling, detection, preparation, and coherent manipulation of both species. A telecom laser at 1560 nm generates the light fields for the ODT and serves, after frequency doubling, as a frequency reference locked to the atomic transition. Both PP and LS rely on the current drivers and controllers of the EP. A data management unit (DMU) executes the experimental sequences in real time, stores the data, and is capable of fitting images, determining atom numbers, and running differential evolution algorithms [GEISEL (2013)] for autonomous optimization of the atomic source parameters.

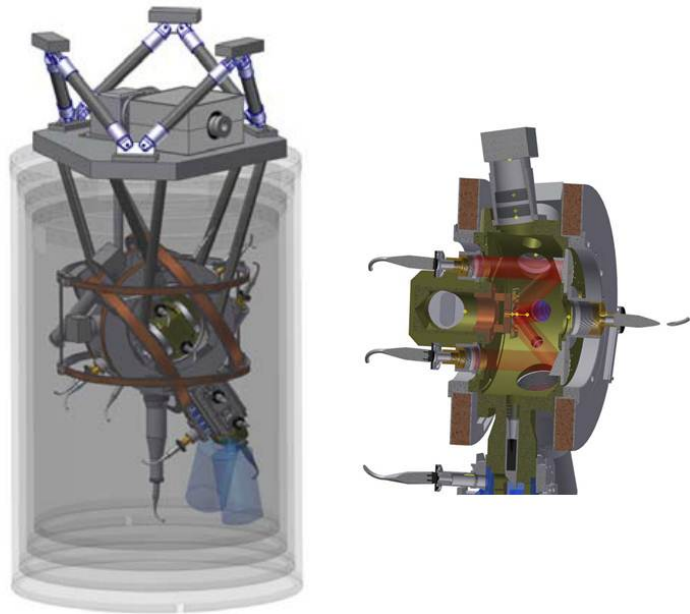


**Figure 4-2:** (Left) Design of the atom interferometer physics package: the science chamber, the coils generating the magnetic fields for the preparation of the atomic samples, and the 4 layers of mu-metal shield are well visible; (Right) Section of the instrument science chamber.

The atom interferometer phase  $\varphi$  is related to the acceleration  $a$  measured along the instrument sensitive axis through the relationship  $\varphi = a \cdot kT^2$ , where  $S = kT^2$  represents the calibration factor of the instrument,  $k$  is the effective wave vector and  $T$  the free evolution time in the atom interferometry sequence. At the quantum projection noise limit, the error on the phase measurement provided by the atom interferometer is proportional to  $C/\sqrt{N}$ , where  $N$  is the number of atoms at detection and  $C$  is the contrast of the atom interference fringes. Due to Earth gravity gradient, a minimum contrast  $C=0.6$  can be expected for an atomic sample of a few micrometres and with a temperature of about 70 pK. Therefore, with  $N = 10^6$  atoms at detection, a total momentum transfer  $\hbar k$  of four photon recoils in the beam splitting process [LÉVÈQUE (2009)], and a free evolution  $T = 5$  s, a sensitivity to accelerations of  $2.1 \cdot 10^{-12}$  m/s<sup>2</sup> can be achieved in a Rb atom interferometer for a single measurement cycle ( $\sim 20$  s). This result leads to a differential acceleration sensitivity on the  $^{85}\text{Rb}$  and  $^{87}\text{Rb}$  atomic samples of  $2.9 \cdot 10^{-12}$  m/s<sup>2</sup> per single measurement cycle. During each orbit, the Eötvös parameter is measured for about 0.5 h, leading to an integrated sensitivity to the Eötvös ratio between  $5.0 \cdot 10^{-14}$  (for a 700 km perigee) and  $5.3 \cdot 10^{-14}$  (for a 2200 km perigee).

The instrument performance budget is detailed in Table 4-1. The main error sources are arising from the relative position and velocity of the atomic samples after release from the ODT, from magnetic field gradients, wave front curvature of the beam-splitter lasers, residual mean-field energy, and spurious accelerations. Stringent requirements on the relative position (1.1 nm) and differential velocity (0.31 nm/s) of the two atomic ensembles at the first beam splitter pulse have been derived. Estimated contributions from gravitational sag, spurious accelerations, Coriolis force, and magnetic fields impose a control on the relative displacements of the two rubidium clouds to better than 1.1 nm for an ODT with a trap frequency of 42 Hz. After release, magnetic field gradients combined with the Feshbach field also affect the overlap, requiring the magnetic field gradients in a reduced volume above the atom chip to be below 0.4 nT/m.

The preparation of the binary quantum mixture and its compliance with the requirements discussed above has been studied in detail. Our numerical simulations, based on the solution of the Gross-Pitaevskii equations for the interacting binary mixture, show that the field of 158.569 G, corresponding to a scattering length of

Error source	Error term $\Delta a = \Phi_{\Delta a}/(kT^2)$	Experimental conditions	Bias $\cdot 10^{-15} \text{ m/s}^2$
Gravity gradient	$-T_{zz} \cdot \Delta z$ $-T \cdot T_{zz} \cdot \Delta v_z$	$\Delta z = 1.1 \cdot 10^{-9} \text{ m}$ $\Delta v_z = 3.1 \cdot 10^{-10} \text{ m/s}$	2.6 3.5
Coriolis acceleration	$-2 \cdot \Omega_y \cdot \Delta v_x$ $-2 \cdot \Omega_x \cdot \Delta v_y$	$\Delta v_x = 3.1 \cdot 10^{-10} \text{ m/s}$ $\Delta v_y = 3.1 \cdot 10^{-10} \text{ m/s}$	$-6.3 \cdot 10^{-1}$ $-6.3 \cdot 10^{-1}$
Other terms: rotations, gradients	$-(\Omega_{orb}^2 - \Omega_c^2) \cdot \Delta z$ $-T \cdot (6 \cdot \Omega_c \cdot \Omega_{orb} - 3 \cdot \Omega_{orb}^2 - 3 \cdot \Omega_c^2) \cdot \Delta v_z$ $T \cdot (2 \cdot \Omega_{orb}^3 + \Omega_c^3) \cdot \Delta x$ $T \cdot T_{xx} \cdot \Omega_{orb} \cdot \Delta x$ $-7/6 \cdot T^2 \cdot T_{zz} \cdot \Omega_{orb} \cdot \Delta v_x$ $-7/6 \cdot T^2 \cdot T_{xx} \cdot \Omega_{orb} \cdot \Delta v_x$ $-\Omega_{orb} \cdot \Omega_z \cdot \Delta y$	$\Delta x = 1.1 \cdot 10^{-9} \text{ m}$ $\Delta y = 1.1 \cdot 10^{-9} \text{ m}$ $T_{zz} = -2GM_e/R^3 = -2.26 \cdot 10^{-6} \text{ s}^{-2}$ $\Omega_c \approx \Omega_{orb} = 1.4 \text{ mrad/s}$ $\Omega_c - \Omega_{orb} \approx \Omega_x = \Omega_y = 1 \text{ } \mu\text{rad/s}$ $T_{xx} = T_{yy} = -T_{zz}/2$	$-3.2 \cdot 10^{-3}$ $1 \cdot 10^{-3}$ $4.9 \cdot 10^{-2}$ $9.1 \cdot 10^{-3}$ $2.9 \cdot 10^{-2}$ $-1.5 \cdot 10^{-2}$ $-1.6 \cdot 10^{-3}$
Photon recoil	$T^4 \cdot T_{zzz} \cdot \hbar^2 k^2 / 16 \cdot (m_{87}^{-2} - m_{85}^{-2})$	$T_{zzz} = 6 \cdot G \cdot M_e / R^4 = -9.57 \cdot 10^{-13} \text{ m}^{-1} \text{ s}^{-2}$	$3.9 \cdot 10^{-2}$
Self-gravity		apogee measurement - subtraction	1
Magnetic field gradients	$B_0 \cdot \delta B \cdot \hbar \cdot (K_{87}/m_{87} - K_{85}/m_{85})$	$B_0 = 100 \text{ nT}$ , $\delta B < 0.1 \text{ nT/m}$ , $K_{87} = 575.15 \text{ Hz/G}^2$ and $K_{85} = 1293.98 \text{ Hz/G}^2$	1
Effective wave front of the beam splitter	$(T_{at,87}/m_{87} - T_{at,85}/m_{85}) \cdot k_B / R_e$	$\lambda/300$ mirror $\rightarrow R_e = 250 \text{ km}$ and $T_{at} = 0.07 \text{ nK}$ , collimation $R_i \sim 400 \text{ m} \rightarrow R_e > 250 \text{ km}$ and $T_{at} = 0.07 \text{ nK}$	$6.3 \cdot 10^{-1}$ $2.8 \cdot 10^{-1}$
Mean field	$\int_0^{2T} dt [\mu \cdot V(0) / (\hbar \cdot V(t) \cdot N^{-1/2})]$	BEC radius at the first beam splitter $300 \text{ } \mu\text{m}$ , expansion rate $82 \text{ } \mu\text{m/s}$ , tuned atom numbers uncertainty of 1000	$2 \cdot 10^{-5}$
Accelerations	CMRR $\cdot a_{spur}$	CMRR = $2.5 \cdot 10^{-9}$ and $a_{spur} = 4 \cdot 10^{-7} \text{ m/s}^2$	1
Detection		$ \eta - 1  < 0.003$	1
<b>Total</b>			<b>14</b>

**Table 4-1:** Error budget for the ATI instrument. The error contributions were evaluated for an altitude of 700 km when the orientations of the sensitive axis and local gravitational acceleration coincide. By introducing the counter rotation  $\Omega_c$  the inertial pointing mode is reflected. For higher altitudes and different orientations, the error terms depending on gravity gradients will be reduced.

900  $a_0$ ,  $a_0$  being the Bohr radius, leads to a sample with a radius of  $50 \text{ } \mu\text{m}$  after about 10 ms of free expansion. Under these conditions, the atomic density and interactions are sufficiently low to switch off the Feshbach field without perturbations. Due to the requirement on the relative positioning of the two atomic ensembles, the quantum mixture needs to be prepared when the system is in the miscible regime. The sequence chosen in our study optimizes the overlap of the two atomic gases and allows to control their expansion dynamics at the desired level (see Figure 4-3). The overlap between the two atomic clouds will be measured by spatial imaging and continuously verified during the mission lifetime (see also Sec. 4.1.1.3).

During the interferometry sequence, the requirement on magnetic field gradients ( $< 0.1 \text{ nT/m}$ ) can be relaxed by a factor of 500 by alternating the interferometer input states for subsequent cycles and averaging out the contribution of this error term. The magnetic shields, enabling a suppression factor of  $> 10000$  of the ambient B-field, saturate at 8000

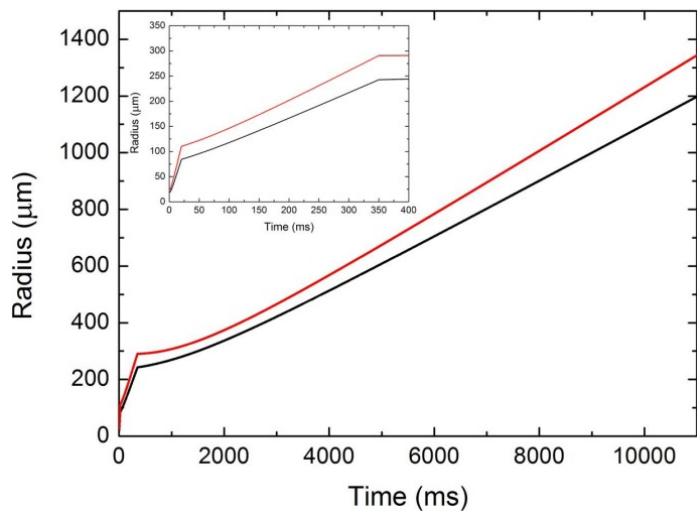


**Figure 4-3:** Expansion of the two BECs obtained by solving a coupled set of two time-dependent Gross-Pitaevskii equations. After release from the ODT, the atoms experience an expansion in a magnetic field of 158.569 G for 10 ms. A series of two DKC pulses significantly reduces the expansion rates (see inset).

G and start to decrease in performance for fields above 30 G. Simulations show that when the Feshbach field is on, the residual field at the mu-metal shields is 30 G along the coils axis and 0.3 G perpendicularly to it. Eventual hysteresis effects will be mitigated by degaussing the shield.

The residual effect of mean-field energy will be minimized by appropriately tuning the atom numbers for the two species to 1:1.697. This leads to a cancellation of the  $^{85}\text{Rb}$ - $^{85}\text{Rb}$  (negative scattering length),  $^{87}\text{Rb}$ - $^{87}\text{Rb}$  (positive scattering length), and  $^{85}\text{Rb}$ - $^{87}\text{Rb}$  (positive scattering length) mean field energy.

**4.1.1.2 Interfaces and resource requirements**

The ATI payload is designed to comply with the constraints set by the spacecraft and the space environment (see Table 4-2). Data rates are assessed as feasible.

The choice of  $^{87}\text{Rb}$  and  $^{85}\text{Rb}$  was specifically made to engineer a high common mode rejection ratio and suppress spurious accelerations and background vibrations below the target threshold [SORRENTINO (2013)]. Using low expansion rates given by the effective temperature of 70 pK allows free evolution times of 10 s. Such low temperatures mitigate a velocity dependent dephasing related to rotations and gravity gradients. Magnetic fields which could affect the interferometry measurement are reduced by a four layer magnetic shield with a suppression factor > 10000.

Instrument mass, power, volume, and data rate budgets are also reported in Table 4-2.

Requirement	Value	Comment
Mass	265 kg	Including margins
Power	Average: 730 W, Peak: 983 W	Including margins
Volume	470 dm <sup>3</sup>	Box design separable over satellite
Data rates	< 110 kb/s	Including margins
Local gravitational acceleration	> 3 m/s <sup>2</sup>	During science measurement
Gravity gradient	< 2.5 · 10 <sup>-6</sup> s <sup>-2</sup>	During science and calibration
Non gravitational accelerations	< 4 · 10 <sup>-7</sup> m/s <sup>2</sup>	Along ATI sensitive axis
	< 1 · 10 <sup>-6</sup> m/s <sup>2</sup>	Along two remaining orthogonal axes
Sensitive axis pointing at perigee	Nadir to better than 3°	
Rotations	< 10 <sup>-6</sup> rad/s	Mean value uncertainty < 10 <sup>-7</sup> rad/s
Magnetic field variations	1 ± 0.1 ± 0.01 ± 0.1 ± 1 G	[0,0.001] ÷ 0.01 ÷ [0.1,10] ÷ 100 ÷ 1000 Hz
Mechanical vibrations PSD	10 <sup>-3</sup> · v ÷ 2 · 10 <sup>-5</sup> ms <sup>-2</sup> Hz <sup>-1/2</sup>	[0.001,0.02] ÷ [0.02,100] Hz
Spurious accelerations rms	< 4 · 10 <sup>-7</sup> ÷ 4 · 10 <sup>-5</sup> · v ÷ 4 · 10 <sup>-4</sup> ms <sup>-2</sup>	[0-0.01] ÷ [0.01,10] ÷ > 10 Hz
Self-gravity of space craft	< Earth's contribution at perigee	
ATI sensitivity	13 · 10 <sup>-12</sup> m/s <sup>2</sup> · 1/τ[s] <sup>1/2</sup>	[20, 3.5 · 10 <sup>6</sup> ] s
Magnetic fields	< ± 10 μG	Inside magnetic shield
Magnetic field gradients	< ± 4 μG/m	Inside magnetic shield
Temperature	10-30° / -40° - 60°	Operation/no operation
Pressure	1 bar – 10 <sup>-10</sup> mbar	2000 Pa/s, peaks of 4500 Pa/s
Measurement time (science)	30 min/orbit	During routine science operations (4.5 y)
Measurement time (calibration)	> 7.5 h/orbit	During routine science operations (4.5 y)
Launch	[20,5000] ÷ 5000 g	[100,2000] ÷ [2000,10000] Hz
Radiation: TID for EEE parts	> 100 krad (Si)	
Radiation: TNID for EEE parts	> 4 · 10 <sup>9</sup> /cm <sup>2</sup> , 10 MeV proton flux	

Table 4-2: Requirements at the ATI instrument.

**4.1.1.3 Operation requirements**

During the science commissioning, the parameters of the instrument are autonomously adjusted for nominal performance, calibrated via differential evolution algorithms [GEISEL (2013)], and transferred into experimental sequences for verification measurements.

In the nominal science phase, 1/2 h per orbit, while the spacecraft is orbiting around perigee, is dedicated to the measurement of the Eötvös ratio. The remaining part of the orbit is used for the evaluation of systematic errors (~ 7.5 h per orbit). Most of that time (~ 5 h) is used to measure the overlap and differential velocity of the two atomic clouds. Several images of the atomic ensembles are taken with alternating time of flight of 1 s and 10 s. The relative position of the centre of mass of the two clouds is obtained by fitting the 2D-images captured by the CCD camera. Averaging over a sufficient number of cycles allows to measure both the relative displacement and the velocity at the required precision (see Table 4-1). In nominal operation, the

ATI executes pre-defined experimental sequences with fixed parameters, which are defined by the Instrument Operation Centre (see Sec. 6) and uploaded via the standard TM/TC channel.

#### 4.1.1.4 Heritage

Several national and international activities are presently addressing atom interferometry tests of the Weak Equivalence Principle in micro-g environments, supporting the development of future space-borne experiments.

The ESA project SAI/Q-WEP (Quantum-Weak Equivalence Principle test) has developed a transportable atom interferometer for ground testing [SORRENTINO (2010)]. In addition, an industrial study has been recently concluded to assess the feasibility of an atom interferometry experiment testing the Weak Equivalence Principle on-board the International Space Station (ISS) [TINO (2013)].

The ICE (Interférométrie Cohérente pour l'Espace) project, funded by CNES is aiming to a WEP test with a dual species  $^{87}\text{Rb}/\text{K}$  atom interferometer on board of an A-300 micro-g Airbus of Novespace [NYMAN (2006)]. Zero-g conditions are obtained during 20 s parabolas. The experiment uses frequency-doubled telecom lasers to manipulate the atoms. An ODT similar to the one designed for STE-QUEST provides the last preparation stage of the atomic clouds. Operation of a dual species  $^{87}\text{Rb}/\text{K}$  MOT, an inertial insensitive single species K interferometer, and an inertial sensitive  $^{87}\text{Rb}$  interferometer has been recently demonstrated during parabolic flights. The  $^{87}\text{Rb}$  interferometer has achieved a sensitivity of  $2 \cdot 10^{-4} \text{ m}/(\text{s}^2\sqrt{\text{Hz}})$  in the noisy environment of the A-300 Airbus resolving accelerations 300 times weaker than the typical 1-g peak-to-peak fluctuations of the aircraft [GEIGER (2011)].

The DLR-funded QUANTUS (QUANTen Gase Unter Schwerelosigkeit) cooperation has demonstrated that quantum degenerate sources and atomic quantum sensors based on atom chips and diode laser technology can be successfully implemented in microgravity. The instrument was tested in the zero-g capsule operated at the Bremen drop-tower test facility. The set-up has already undergone several hundred drops demonstrating the robustness of the technology. Similar tests will be performed in a sounding rocket. The QUANTUS-I apparatus demonstrated the first atom-chip-based  $^{87}\text{Rb}$  BEC under microgravity with free expansion times up to 2 s [VAN ZOEST (2010)]. Bragg interferometers with free evolution times up to  $2 \cdot T = 675 \text{ ms}$  were studied [MÜNTINGA (2013)]. Therein, the contrast was enhanced by a delta-kick cooling (DKC) step applied via magnetic fields from the atom chip lowering the effective temperature to 1 nK. The successor experiment QUANTUS II [RUDOLPH (2011)] aims at extending the capabilities to a test of the WEP with a dual species  $^{87}\text{Rb}/\text{K}$  atom interferometer in the Bremen drop-tower capsule operated in catapult mode (9 s of free fall time). In ground based experiments, the production of a few  $10^5$   $^{87}\text{Rb}$  atoms in 2 s was demonstrated. Since the apparatus and specifically the atom chip were designed for microgravity, higher atom numbers are expected for operation in the drop tower environment. The sounding rocket mission MAIUS will finally explore a new parameter range for cold-atom experiments in microgravity. It will be a test platform for the demonstration of key elements for future long-duration space missions. The rocket will be equipped with an atom laser operated in an extended experimental parameters range compared to the drop tower. The MAIUS facility will carry a degenerate atom source for a total experiment time of 6 min.

### 4.1.2 Microwave Link

#### 4.1.2.1 Design

The MWL design is an evolution of the science link presently under development for the ACES mission. The end-to-end system is composed of a flight segment unit and a distributed network of ground terminals, respectively connected to the clocks on-board the STE-QUEST spacecraft and on the ground. The input clock signal is up-converted and used to coherently generate the microwave signals that are transmitted through the atmosphere and received by the remote terminal at the other end of the link. The space segment provides 4 independent receiving channels capable of performing up to 4 simultaneous comparisons of the space clock with clocks on ground. The comparison of two ground clocks in common-view can be obtained by evaluating the difference of the two simultaneous space-to-ground comparisons. As the noise of the space clock is in common-mode, common-view comparison can be carried out without the need for a high performance on-board clock. A commercial ultra-stable oscillator (USO) is indeed sufficient for this purpose. Primary function of MWL is to measure the desynchronization between the space clock and clocks on the ground, or equivalently the difference between the space clock proper time  $\tau^s$  and the ground clock proper time  $\tau^g$  at a given coordinate time  $t$  (see also Sec. 6.4.2.1).

While propagating from space to ground and vice-versa, the phase of the signal is perturbed by several effects that need to be evaluated and corrected for. They are:

- The range between the ground station and the STE-QUEST spacecraft, responsible for propagation delays that can vary from a few ms at perigee to hundred ms at apogee.
- The propagation delays induced by the troposphere, typically ranging between 10 ns and 100 ns, depending on the local atmospheric conditions and satellite elevation.
- Ionosphere propagation delays, varying between 0.1 ns and a few ns and depending on the frequency.
- Multipath effects: The detection of the direct signal can be disturbed by reflections (multipath signal) generated at surfaces in the immediate vicinities of both the space segment and ground terminal antennae. The multipath signal combines with the direct signal introducing a delay depending on relative phase and amplitude.
- Internal delays due to the ground terminal and flight segment electronics: Such delays need to be carefully calibrated before launch and continuously monitored during the mission.

MWL is an asynchronous three-frequency link based on a two-way geometry, which operates continuously with an up-link in the Ka-band and two down-links in the Ka and X-band (Figure 4-4).

The two-way configuration is important to correct for the range-induced delays, which cancel to first order when the desynchronization between the space and the ground clock is calculated (see also Sec. 6.4.2.1). Residual corrections due to link asymmetries depend on the knowledge of antennae phase centres positions as well as on the two-way geometry of the link (see Sec. 3.3.2.1 for positioning requirements in space and on ground). The two-way configuration is also important to remove the non-dispersive delays introduced by the propagation through the troposphere. Frequency dependent tropospheric delays, if not corrected, can still degrade the performance of the STE-QUEST link. A semi-empirical correction model, similar to the one developed in HOBIGER (2013) for the ACES mission can then be used to estimate this effect and remove it to the required level. Ionospheric delays are frequency dependent and they influence with opposite sign both group and phase velocity of the microwave signal. To this purpose, the link measures the differential delay on the Ku-band and X-band downlink signals to calculate the total electron content (TEC) of the ionosphere and correct for the ionospheric time delay [KAPLAN (1996)].

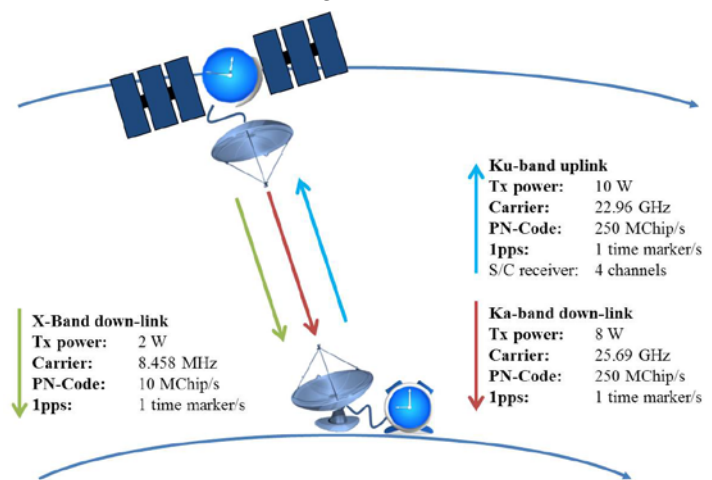


Figure 4-4: MWL architecture.

The two ends of the link transmit a carrier that is phase-modulated by a pseudo-noise code (PN-code) at a rate of 250 MChip/s. Carrier and code are both coherently generated from the local clocks. The code and the carrier phase of the received signal are compared to their local replicas at the space and ground terminals. While the noise on code phase measurements defines the long-term stability of the link, the ultimate performance can only be reached with carrier phase measurements. To this purpose, the code signal is also used to remove phase cycle ambiguities, allowing for continuous phase comparison measurements on the carrier signal. The PN-sequence is also modulated with a PPS (Pulse Per Second) that defines the on-board time scale.

As shown in Figure 4-5, acquisition and tracking is achieved by correlating the incoming signal, down-converted to the intermediate frequency IF, with an early and late replica of the locally generated PN-code sequence [HEJC (2009)]. The use of narrow early-late correlators is important to control multipath effects [VAN DIERENDONCK (1992)]. The 1<sup>st</sup> IF is mixed with a replica of the carrier frequency shifted according to the experienced Doppler effect. After the early-late correlator, the signal is cleaned in a surface acoustic wave (SAW) filter and digitised in a fast A/D converter. A/D conversion as well as signal correlation can be digitally implemented in a field programmable gate array (FPGA). Using fast electronics, internal delays can be precisely controlled with respect to standard analogue beat techniques. Local code and carrier frequencies are generated by direct digital synthesizers (DDS), which are phase locked to the local clock and controlled by the tracking loops.

Following the ACES heritage, the space antenna is designed for circular polarisation to optimally reject multipath and suppress Faraday rotations in the Earth magnetic field. The beam angle shall allow coverage of the Earth in the main lobe at all orbit conditions. Choke rings are used to improve directivity and reduce the effects of signal reflections.

The MWL ground terminal design follows the ACES technology after re-adaptation of the systems to the Ka-band and X-band frequencies. It is a microwave station interfacing the local clock on ground to the STE-QUEST payload (Figure 4-6). To reduce phase instabilities due to the tracking motion, the electronics unit is rigidly attached to the antenna unit. The antenna is a 60 cm offset reflector with a dual-band feed system automatically pointed in azimuth and elevation by a steering mechanism. A computer controls the steering unit based on the STE-QUEST orbit prediction files, collects telemetry and science data both from the local clock and the MWL GT electronics, and interfaces directly with the Mission Operations Center (MOC). The system is housed below a protective radome cover, which also allows to stabilize the temperature by an air conditioning system.

Due to the early-late correlator properties, only multipath signals which result to be time-shifted by less than 1 chip for the carrier and 1.5 chip for the code introduce errors on the phase comparison measurements [ASCARRUNZ (1998)]. Therefore, reflections from surfaces at more than 2 m are strongly attenuated by the PN-code autocorrelation properties. The effect of reflections from shorter distances will have to be minimized through a careful antenna design and its positioning on-board the spacecraft.

The link stability requirement reported in #SR-PL-16 of Sec. 3.3.2.1 translates into a time error with a flicker phase noise as low as 92 fs [AUDOIN (2001)]. Reaching the ultimate link performance requires a control on the delays affecting code and carrier phase measurements at a few tens of femtoseconds. This translates into an optimized thermal design of the end-to-end link. To that purpose, a two-stage temperature control system is foreseen both for the flight segment and ground terminal electronics. In addition, early digitization of the science signal, use of short cables and signal paths, symmetric designs for amplifiers and other critical components become important to meet the scientific requirements. Finally, the calibration of the terminal delays against temperature variation will be performed both in space and on the ground and continuously updated during the mission lifetime thanks to built-in test loop transponders.

The key link parameters have been identified, the link budget at apogee has been calculated for different elevation angles and atmospheric conditions (clear sky or rain), together with the S/N and the expected jitter (white phase noise) of the code and phase comparison measurements. From the design, a link availability better than 99% can be predicted.

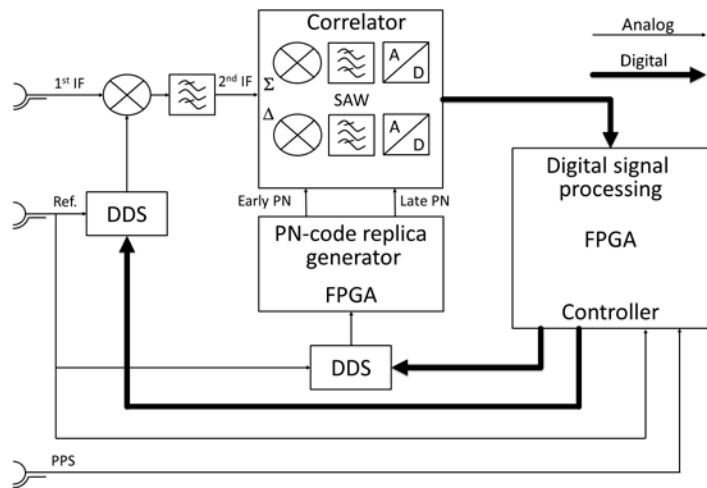


Figure 4-5: Schematic of code signal tracking in MWL.



Figure 4-6: ACES MWL ground terminal under test in compensated compact range facility. The STE-QUEST ground terminals will be based on the ACES technology.

#### 4.1.2.2 Interfaces and resource requirements

The key parameters of the MWL signal are reported in Figure 4-4. The interfaces at the MWL ground terminal and flight segment unit with the signals generated by the local clock (USO or optional atomic clock) include:

- 8.8 GHz reference input signal coherently generated from the local atomic clock;
- 1 PPS input for synchronization, calibration and test purposes;
- 1 PPS output for synchronization, calibration and test purposes.

The connection between the local clock and the MWL input connector shall not degrade the performance of the clock signal itself. This connection is under the responsibility of the institutes operating the ground clocks. Distances of several hundreds of kilometres can today be covered by fibre links introducing negligible noise on the distributed clock signal [PREDEHL (2012)]. The PPS output port is also the reference point for performing time transfer experiments. This connector provides a timing signal synchronously generated from the local atomic clock.

MWL phase comparison measurements are time tagged both in space and on the ground in the local clock timescales. In addition, absolute internal delays at reception and transmission need to be calibrated to 1 ns. This includes the calibration of the MWL flight segment and ground terminal channel delays from reception at the antenna reference point to time stamping in the local time scale and from time stamping in the local time scale to emission at the antenna reference point. Control of internal delays at reception and emission is important to correctly apply the two-way formula and achieve optimal rejection of phase variations due to the Doppler effect. Finally, phase comparison measurements shall be linked to UTC with an uncertainty better than  $1\mu\text{s}$  to correctly retrieve velocity and position of the clocks and the antennae reference points from the orbitography files (see Sec. 3.3.2.1).

MWL is also used to perform time transfer experiments (see Sec. 3.1). To this purpose, the MWL ground terminals need to be calibrated against a transportable unit that will be kept as a reference. Calibration campaigns will take place as a minimum at the beginning and at the end of the mission.

Standard data links are used by the terminals to transfer telemetry, housekeeping, and science data as well as to receive telecommands, orbitography files, etc. Communication between the ground terminals and the MOC takes place through the internet.

The MWL flight segment unit has a mass of 33 kg and a power consumption of 110 W. Both figures include 20% of margin at unit level.

#### 4.1.2.3 Operation requirements

MWL space-to-ground contacts are scheduled on the basis of the visibility windows available at each ground station. As discussed before, weather conditions do not pose any restriction to MWL operation.

MWL uses Code Division Multiple Access (CDMA) to simultaneously connect up to 4 ground terminals to the 4 receiving channels of the flight segment unit. At signal acquisition, frequency and delay of the code oscillator need to be steered on the basis of the predicted range and Doppler shift. Range and Doppler steering files are prepared by MOC and uploaded before the start of each pass to support signal acquisition routines. The MWL ground terminal is automatically pointed in azimuth and elevation by a steering mechanism controlled by a computer on the basis of the orbit prediction files generated by MOC. Signal acquisition is expected to start slightly above the horizon, with the system entering the full tracking mode before reaching 5 deg of elevation.

Both the flight segment unit and the ground terminals are remotely controlled by MOC.

#### 4.1.2.4 Heritage

The development of the STE-QUEST MWL takes full advantage of the ACES heritage. Many of the techniques and procedures discussed before have already been established and tested in the frame of the ACES mission. The ACES MWL engineering model has been completed and tested. The flicker floor of the carrier phase measurements has been measured to 70 fs, compatible with the STE-QUEST needs. The instrument is now undergoing signal simulator tests to characterize the performance under realistic signal dynamics.

The changes identified to upgrade MWL from ACES to the STE-QUEST can be summarized as follows:

- Frequency plan to be re-adapted to Ka-band and X-band;
- Antennae design and power amplification stages to be dimensioned to the STE-QUEST link budget;

- High speed electronics, now available, to be implemented to increase the chip rate to 250 MChip/s (compared to the 100 MChip/s of the ACES MWL) and to perform an early digitization of the regenerated code and carrier signals.

An ESA study has already addressed these issues in a first design iteration of MWL showing compatibility with the STE-QUEST scientific requirement. A second study has recently been initiated to verify the performance through a breadboarding activity of the critical system elements.

### 4.1.3 GNSS Receiver

A GNSS receiver on-board the STE-QUEST payload provides the position and velocity data for orbit prediction and determination. These products are important for the evaluation of the scientific data generated by the on-board instruments as well as to correctly point the MWL antennas at the ground terminals.

The high elliptic orbit of the STE-QUEST satellite restricts the availability of the positioning information to arcs lying below the GNSS constellations (about 20000 km altitude). Dedicated studies have been conducted by industry to assess the capability of providing the required orbitography products through a positioning solution based on the GNSS signals only. Several scenarios corresponding to different combinations of the GNSS constellations (GPS, GALILEO, GLONASS) or GNSS receiver complexity have been exercised.

The required performance in position and velocity accuracy can be met with commercial hardware capable of receiving multi-constellation signals, e.g. from GPS and GALILEO. Receivers based on the Advanced GPS/GALILEO ASIC-4 (AGGA-4) chip are well suited to this purpose. Signals with carrier-to-noise ratios of 35 dBHz and 25 dBHz have been simulated, demonstrating compatibility with the STE-QUEST orbit determination requirements. A receiver capable of operating at 25 dBHz clearly offers additional robustness in signal acquisition beyond the GNSS constellation's orbits.

The received signals are processed on ground together with the standard IGS products to achieve the required orbitography products. Both, quick look and high-performance position and velocity data are made available to the users through the STE-QUEST Archive.

## 4.2 Optional Payload Elements

### 4.2.1 The PHARAO Cold-atom Clock

The atomic clock (ATC) is an optional payload element, which serves to measure the time dilation effect due to the Earth's gravitational potential. It also enables the additional objective of monitoring the stability of on board GPS, GALILEO, and GLONASS clocks.

#### 4.2.1.1 Design and performance

The representative ATC design is a cold-caesium-atom primary frequency standard, closely based on the PHARAO clock developed for the ACES mission on the ISS, scheduled for launch in 2016. It benefits from the experience already acquired in phases A to D of ACES and will benefit further from the demonstration of the ultimate performances of PHARAO in flight.

The main changes in the requirements of ATC compared with PHARAO are the provision of an optical reference signal in addition to the electrical (microwave) reference of PHARAO and an improvement in the clock performances. The main performance requirements, in normal ("external") operating mode, are:

- Short-term frequency instability less than  $3.5 \cdot 10^{-15}$  at 1 s rising to  $5.0 \cdot 10^{-15}$  at 100 s;
- Mid/long-term frequency instability less than  $8 \cdot 10^{-14} \cdot \tau^{-1/2}$  up to  $7 \cdot 10^5$  s;
- frequency accuracy less than  $1 \cdot 10^{-16}$ .

To meet these requirements, ATC augments PHARAO by the addition of a new type of ultra-stable oscillator, based on a cavity-stabilized laser coupled to a femtosecond laser based optical comb. This "Microwave Optical Local Oscillator", or MOLO, provides the required optical output and also provides a microwave local oscillator signal, which has a significantly improved stability compared with the ultra-stable quartz oscillator of PHARAO. MOLO is directly responsible for the short-term stability of the clock. The mid/long-term instability is achieved by stabilizing MOLO on the error signal generated at the ATC Cs resonator. The third requirement, on frequency accuracy, is more stringent than the PHARAO specification, but is the same as the PHARAO ultimate performance goal. The MOLO also partially replaces the Space Hydrogen Maser on ACES, serving as a short-term reference during the evaluation of the clock systematic frequency shifts.

ATC is also required to have a backup (“internal”) operating mode, where MOLO is replaced by a quartz oscillator. In this mode the frequency error limit is relaxed to  $1 \cdot 10^{-15}$ , since without MOLO the systematic errors cannot be well measured.

We note that as for PHARAO, ATC is a frequency standard, not a complete clock. The on-board timescale is expected to be realised in the time and frequency links, in order to facilitate control of absolute timing delays.

The more general requirements and the environmental conditions for ATC are very similar to those of PHARAO, with some exceptions: the ionizing radiation environment of STE-QUEST is much harsher than ACES; the mission duration is longer, 5-6 years instead of 3; finally, the micro-vibration environment is much more favourable in STE-QUEST.

Figure 4-7 shows a high-level block diagram of the ATC. It is composed of seven subsystems grouped into six physical packages (plus 2 small auxiliary electronics boxes), which can be developed and tested separately:

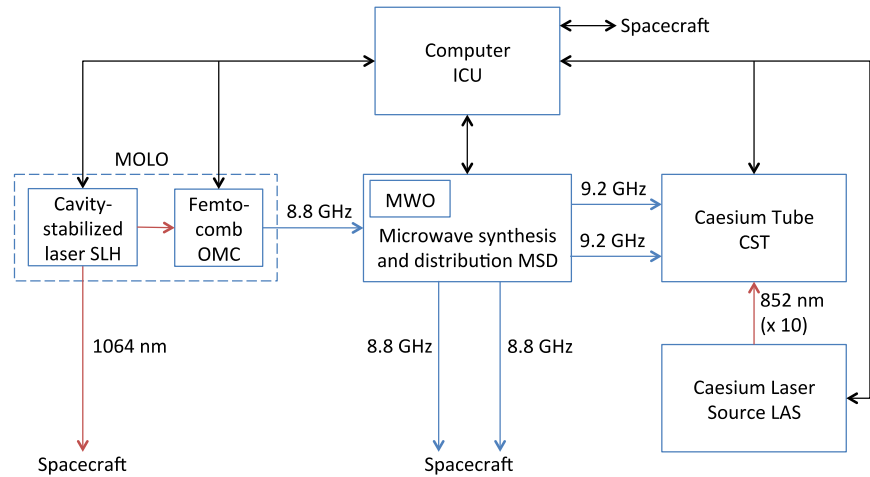


**Figure 4-7:** Simplified ATC block diagram. Red = optical signals. Blue = electrical (microwave). Black = data.

1. Stabilized Laser Head (SLH): Based on a laser stabilized to an ultra-stable cavity. It produces a 1064 nm optical signal, whose frequency is steered (via the servo-loop through the ICU) to the Cs reference transition, thus constituting the optical form of the clock signal. This signal is distributed both to the OMC and to the spacecraft, for use by the optical link. By comparison with ACES it replaces both the H-maser and the quartz oscillator of PHARAO.
2. Optical Microwave Converter (OMC): A femtosecond laser based optical frequency comb, which is locked to the optical signal from the SLH. A harmonic of the comb laser repetition frequency is selected and amplified to provide a signal at 8.8 GHz, which is highly coherent with the SLH optical signal and constitutes the electrical (microwave) form of the clock signal. By comparison with PHARAO, OMC has a similar role to the first stage of the hyperfrequency source.
3. Microwave Synthesis and Distribution (MSD): It takes the 8.8 GHz signal from OMC and uses it to generate two tuneable 9.192 GHz signals for use by the caesium tube. It also distributes the 8.8 GHz OMC signal to the spacecraft for use by the links. It also provides a lower-frequency synchronous signal (not shown in the figure) used to synchronize the operation of the various subsystems through the ICU. By comparison with ACES it replaces the FCDP and the second stage of the PHARAO hyperfrequency source, while having a simpler design.
4. Microwave Oscillator (MWO): Physically included within the MSD package, it consists of a quartz oscillator with frequency multiplication. It provides a backup for the OMC output signal, allowing degraded operation of the clock (internal mode).
5. Caesium Laser Source (LAS): Provides laser signals at 852 nm (10 optical fibres) for the caesium tube. An analogue feedback (not shown) from the CST is used for laser power control. It is very similar to the PHARAO laser source.
6. Caesium Tube (CST): The core of the clock where the atoms are cooled, manipulated and interrogated, using the signals from MSD and LAS, while being protected from the environment. It allows the frequency of the SLH signal to be measured with respect to the reference Cs transition. The design is very similar to the PHARAO Cs tube.
7. Instrument Control Unit (ICU): Controls the feedback loop from CST to SLH (and to MWO in internal mode). Manages data flux within ATC and to the spacecraft. Controls the timing of subsystem operations through dedicated control lines (not shown). Replaces the UGB and a part of XPLC functions of PHARAO and ACES.

Concerning the ATC performance, we first consider the new oscillator, MOLO. Indeed, certain science requirements apply directly to MOLO, considered as an independent subsystem: relative frequency noise power spectral density ( $2.5 \cdot 10^{-29}/\text{Hz}$  at 0.1 Hz,  $2.2 \cdot 10^{-26}/\text{Hz}$  at 1000 Hz), frequency instability ( $< 3.5 \cdot 10^{-15}$  between 1s and 100 s after drift removal), frequency drift ( $< 2 \cdot 10^{-16}/\text{s}$  over 1000 s), optical-microwave frequency offset ( $< 3 \cdot 10^{-17}$ ), and relative instability (3 times below the clock instability as specified in #SR-PL-11). Two representative designs of the ultra-stable optical cavity for SLH were studied (see

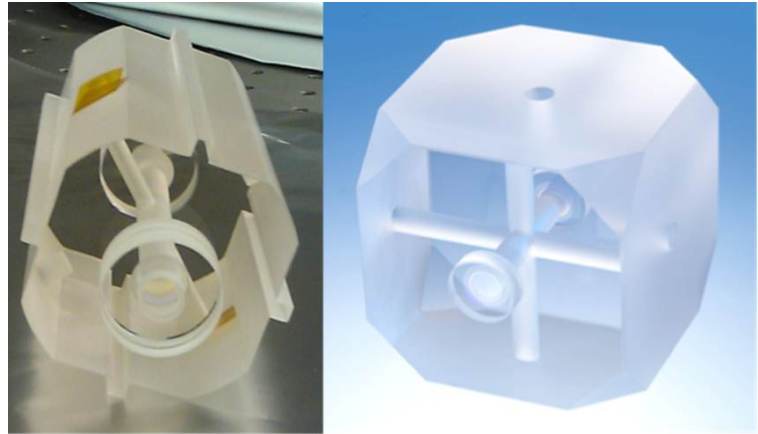


**Figure 4-8:** Optical cavity designs studied (PTB/HHUD and NPL).

Figure 4-8). Their thermal noise floors are sufficiently low to be compatible with the required stability while their vibration sensitivities are low enough that this will not be a significant source of instability in the STE-QUEST environment (Figure 5-4). The necessary active temperature control and vacuum are feasible. Both cavity designs have been used to demonstrate the stabilisation of representative lasers at the required stability, using standard Pound-Drever-Hall locking. Concerning OMC, two methods for locking the femto-comb to the SLH optical reference were studied and shown to be compatible with the MOLO noise requirements. Further, the detection of the relevant harmonic of the comb repetition frequency needed to generate the microwave output signal does not add significant noise, for typical femto-comb characteristics. Two femto-comb technologies were studied (see Sec. 4.2.1.4); both have been used to demonstrate optical to microwave conversion compatible with the MOLO requirements.

We now consider the overall ATC performance. The requirements of MSD are slightly improved compared with the PHARAO hyperfrequency source; the study concluded that this is feasible. CST and LAS have the same performance requirements as PHARAO. The short-term instability of ATC is essentially copied from the MOLO microwave signal and is therefore compliant. The mid/long-term instability contains four contributions:

- Microwave interrogation signal noise, negligible due to the performances of MOLO and MSD;
- Microvibration-induced noise in CST, negligible in the STE-QUEST environment;
- Detection noise, due to LAS, expected to be negligible (to be confirmed on the PHARAO flight model);
- Quantum projection noise, due to the number of atoms captured and detected in CST. The design objective of  $10^6$  atoms is sufficient.

Including the effect of modulation of the number of atoms in order to monitor systematic shifts, the calculated mid/long-term instability is  $6.1 \cdot 10^{-14} \tau^{-1/2}$ , compliant with the requirements.

The frequency inaccuracy results from a number of contributions of which the largest is certainly the cold collisions. Current experimental results justify that the total frequency error can be reduced below  $2 \cdot 10^{-16}$ . Further results from PHARAO are expected to confirm the feasibility of reaching the  $1 \cdot 10^{-16}$  STE-QUEST limit. It should be noted that the magnetic field environment requirement (1 G from DC to 1 mHz, 0.1 G at 10 mHz, 0.01 G between 0.1 Hz and 10 Hz, 0.1 G at 100 Hz, and 1 G at 1 kHz) is necessary for the control of the Zeeman effect uncertainty.

In addition to the clock performance, the amount of instability which can be introduced in the distribution of the optical and microwave clock signals to the time and frequency links is limited to  $3.5 \cdot 10^{-15}$  up to 10 s and 3 times smaller than the Allan deviation of the STE-QUEST clock signal as reported in #SR-PL-11 for longer integration times. Constraints also apply to the internal 1064 nm, 8.8 GHz and 9.2 GHz links.

The study showed that these requirements can be satisfied, subject to assumptions about the maximum rate of temperature variation and on the characteristics of the external interfaces to which the signals are provided.

#### 4.2.1.2 Interfaces and resource requirements

The most important interface signals of the ATC are the 1064 nm optical output and the 8.8 GHz electrical outputs. These signals are extremely accurate and stable frequency references; they constitute the ATC

reference, which is to be compared with ground clocks through the time and frequency link. Other interfaces are less critical:

- Electrical: In addition to the main 28 V or 50 V power supply, ATC requires a stay-alive supply (with spacecraft and ground inputs) for the ion pumps in SLH and CST. ATC has several days of autonomy without stay-alive power.
- Mechanical: ATC is composed of 6 principal units (ICU, SLH, OMC, MSD, LAS, CST) and 2 auxiliary electronics boxes (HVC, EDT), which are to be mounted on the inner surface of the payload module. A nominal layout shows that ATC can be physically accommodated on the payload module.
- Thermal: Thermal transfer takes place by conduction through the baseplate of all units. An MLI enclosure is used around ATC. Active temperature control is used internally in some units.
- Data: Spacewire interface to ICU. Data rate is expected to be  $< 2$  kB/s.

Resource requirements are detailed in the Interface Control Document. As already stated, unit dimensions are compatible with the accommodation. Total mass is 135 kg, power consumption is 328 W average and 362 W peak, including margins, compatible with the EID-A requirements.

#### 4.2.1.3 Operation requirements

The operation requirements of ATC will be similar to those of PHARAO on ACES. Additional command and control is required for MOLO, however this subsystem will be stable over days to weeks and so will not impose strong operational requirements. Operations sequences are predictable and somewhat repetitive and can be planned many days (at least) in advance, although some operating parameters may need to be adjusted on a shorter time scale. The planned mission operations cycle of one contact per day and a minimum delay of 24 hours for uploading modified commands is compatible with the instrument. The Instrument Operations Centre will be closely based on that for PHARAO, adapted to the interface with the Science Operations Centre. As already stated, ATC requires stay-alive power for ion pumps, with several days of autonomy.

#### 4.2.1.4 Heritage

The MOLO is the least mature part of the ATC. The SLH requires a continuous wave laser and an ultra-stable cavity. The space qualified TESAT LCT laser is appropriate. As discussed above, two designs of cavity were studied, reaching TRL 4. Considerable ionizing radiation testing of cavity elements has been carried out, without adverse consequences [CHEN (2013)]. A complement of radiation testing is required, as well as shock and vibration testing and temperature cycling, to reach TRL5. The OMC requires in particular a femtosecond frequency comb. As stated above, two technologies were studied. A diode-pumped crystal-based fs laser was developed and demonstrated to withstand relevant shock and vibration and ionizing radiation levels [LECOMTE (2013)], thus reaching TRL5. In parallel work, a femto-comb using an Erbium-doped fibre laser has been developed by Menlo Systems for the FOKUS experiment, programmed to fly on a TEXUS sounding rocket in November 2013 (see Figure 4-9). Additional work is needed in phase B to replace the Erbium fibre by a radiation-hard doped fibre, thus achieving a TRL  $> 5$ .

MSD reuses much of the PHARAO hyperfrequency source, in particular for generating the two 9.2 GHz signals. Component obsolescence necessitates a significant amount of electronic redesign, also taking account of ionizing radiation tolerance and a small improvement in performance. The other changes are the addition of the 8.8 GHz signal distribution and of a local data acquisition and digital conversion capability, to simplify the interface with ICU. The study showed that this is feasible, without a major change to the budgets compared with PHARAO.

LAS is very closely based on the PHARAO laser source (see Figure 4-10). The main change is the local integration of the thermal regulation control, instead of having this done by the ICU. A small number of components require further qualification or replacement, for reasons of obsolescence, radiation tolerance, etc.



**Figure 4-9:** Er:fibre based comb delivered for the TEXUS sounding rocket test (Menlo Systems).

CST in turn is closely based on the PHARAO caesium tube (Figure 4-10), while integrating some additional electronic drivers (PHARAO coils control, signal acquisition and digital conversion, etc.) in order to simplify the interfaces, in particular with ICU. Again, a small number of components require replacement for obsolescence, radiation tolerance, etc.

ICU will make use of much more modern hardware than the PHARAO computer; systems qualified for the STE-QUEST environment are readily available.

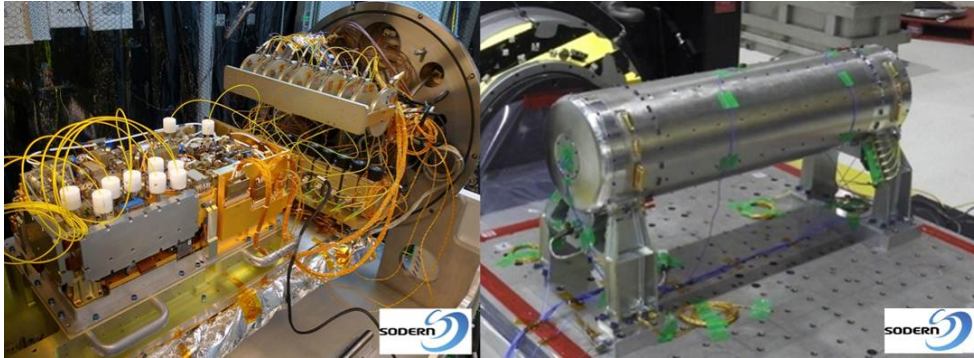


**Figure 4-10:** (Left) Flight model of the PHARAO laser source in qualification testing. (Right) The flight model of the PHARAO caesium tube during vibration testing.

## 4.2.2 Optical Link

### 4.2.2.1 Design

The optical link is an optional payload element able to ensure outstanding stability (see #SR-PL-17, Sec. 3.3.2.1) and significantly shorter averaging time, particularly important to compare ground clocks down to the  $1 \cdot 10^{-18}$  uncertainty level.

The general architecture can be split in two different functional areas: pointing, signal acquisition and tracking (PAT) for establishing the laser links and, once the laser link is operating, the phase comparison measurement between the received signal and the locally generated replica. PAT technologies have been developed during the past years for laser communication terminals (LCT), which are perfectly suited for T&F applications. Therefore, modifications to existing terminals are only required in relation to the T&F metrology functions. Of interest here are the signal generation and analysis that allow the required comparison of remote clocks via the optical signals exchanged through the atmosphere.

The STE-QUEST optical link is a two-way asynchronous link composed of the two on-board terminals and a network of optical ground stations (OGSs). As for MWL, the two-way configuration is important to remove phase delays introduced by the range and the troposphere. Figure 4-11 shows the block diagram of the optical terminal and the proposed signal structure. The EOM sideband modulation is rather standard. In this scheme, the clock signal is contained in

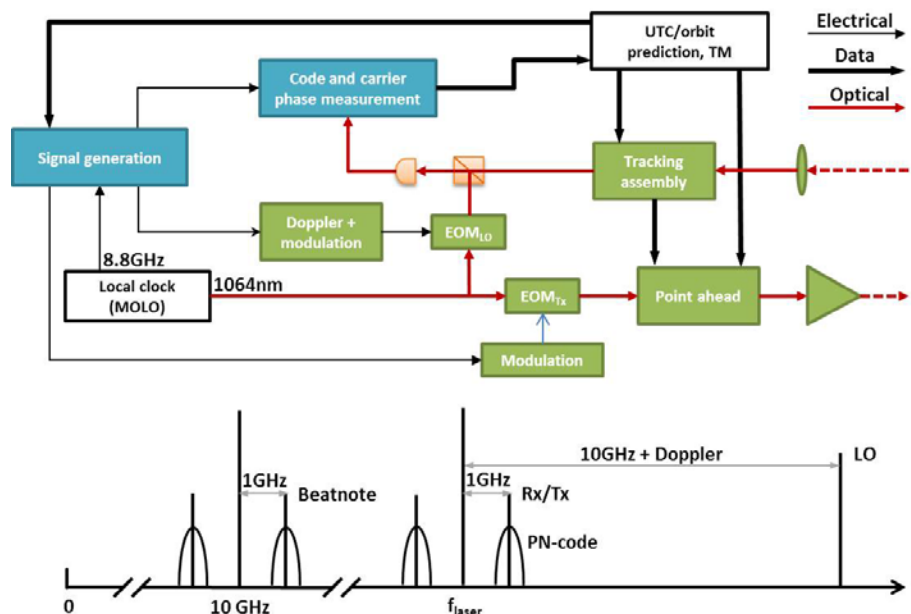


**Figure 4-11:** Block diagram of the optical link terminal. (Bottom) Proposed signal structure.

the optical carrier and in the 1 GHz RF modulation or, more precisely, in the difference between the upper and lower 1 GHz optical sidebands. A PN-code is used to resolve the phase ambiguity of the 1 GHz modulation, at the same time providing a timing signal. Chip rates of e.g. 100 MChip/s are sufficient to this

purpose. The modulation frequencies of the uplink and downlink signals can be further optimized in the final design to avoid interference and maximize the performance. Upon reception, the incoming signal is mixed with a Doppler-corrected local replica, resulting in an optical beatnote that is detected by a fast photodiode. In the STE-QUEST scenario, the Doppler shift can be large even for an apogee pass (up to  $\pm 4$  GHz on the optical carrier). The Doppler compensation obtained through  $EOM_{LO}$  allows the detection of a beatnote at a fixed frequency ( $\sim 10$  GHz) and within the detection bandwidth (3 GHz). This electrical signal is now similar to what is obtained in MWL, out of the first mixing stage of Figure 4-5, and it can be treated by using the same techniques as discussed in Sec. 4.1.2.1. The space segment is tailored on the TESAT LCT with a 0.135 m telescope shared for emission and reception, and 2 W laser power on emission. The ground station architecture is based on a dual telescope set-up, as used by many satellite laser ranging (SLR) stations, with a 0.4 m aperture receive telescope and a 0.09 m aperture emit telescope. As examples, Yaragadee (Australia) uses a 1 m receive and a 0.16 m emit telescope, or Graz (Austria) uses a 0.5 m receive and a 0.1 m emit telescope, both very close to the values proposed here. An alternative could be a shared telescope (as for the space segment) with the emission beam smaller than the full reception one.

Troposphere and ionosphere propagation delays can be better controlled in the optical rather than in the microwave domain. However, optical frequencies are affected by atmospheric turbulence. Smaller atmospheric disturbances, as typical for astronomical observation sites at high altitude, can be corrected with a single tip/tilt mirror. For ground stations in areas with higher turbulences (as in urban settings), a more complex adaptive optical system will be required. Both terminals (ground and space) need to dispose of a steerable tracking mirror that is locked to the incoming signal. This can also serve as tip/tilt correction of turbulence effects. Furthermore, an independent steerable point-ahead mirror on the emission path is required. The point ahead angle can reach 65 mrad at perigee and 10 mrad at apogee.

#### 4.2.2.2 Interfaces and resource requirements

Two optical terminals are accommodated on the outside of the STE-QUEST platform. In order to maximise the use of existing technology within Europe, the TESAT LCTs (see Figure 4-12) were considered as a design baseline. For the ground terminals, existing designs or hardware for satellite laser ranging (SLR) or laser communication can be used. The following table summarizes the main technical design parameters.

Apart from the mechanical, electrical, data and thermal interfaces with the servicing parts of the satellite, an optical (1064 nm) and microwave (8.8 GHz) interface with the atomic clock is required. The optical signal serves as a carrier for the generation of the optical sidebands. The microwave sinusoidal signal is derived from the STE-QUEST clock and does not need to be phase coherent with the optical signal. It is used to generate both the modulation sidebands and the PN-code for cycle ambiguity resolution and time scale definition.

As for MWL, the optical ground terminals need to be within reach of an operating high-performance atomic clock in order to allow distribution of the frequency reference using optical fibre links. As mentioned above, the distance can be several hundreds of kilometres. The link between the atomic clock and the optical ground terminal is under the responsibility of the institute operating the clock.

All emission and reception events at the primary mirror are time tagged in a local time scale on board and on the ground. The required accuracy is 300 ps. This implies knowing all delays on the incoming and outgoing path between the primary mirror reference point and the actual tagging on the local time scale to the same accuracy level. Orbit prediction requires an accuracy of about 1 km on the position and a few % for the velocity, depending on the exact microwave modulation scheme used. A rough UTC prediction of about 1  $\mu$ s is required for initial ambiguity resolution.

Each of the space optical terminals has a mass of 53 kg and an average power consumption of 160 W, including a 5% margin applicable for a recurrent unit.

	Parameter	Heritage
<i>Wavelength</i>	1064 nm (Nd:YAG)	TESAT LCT
<i>Space telescope diameter</i>	135 mm	TESAT LCT
<i>Ground receive telescope diameter</i>	400 mm	SLR heritage
<i>Ground transmit telescope diameter</i>	90 mm	SLR heritage
<i>Emitting laser power (space)</i>	2 W	LISA PF
<i>Emitting laser power (ground)</i>	25 W	COTS

#### 4.2.2.3 Operation requirements

The operation of the optical link is limited by weather conditions at the ground stations. Based on long-term weather data, about 25% of the common-view passes will be usable to establish a laser link for ground-to-ground clock comparisons. The operation of the optical link therefore requires a short-term (few days) weather forecast to identify the passes where a link will be established. For these passes, the rough orbit prediction will be calculated by MOC and transmitted to the spacecraft and to the ground stations to optimise the pointing, acquisition, and tracking sequence. The on-board terminals will be switched from standby to operational mode in advance to allow self-calibration and for reaching thermal equilibrium. Power, thermal, pointing, or microvibrations constraints may limit the use of the atom interferometer during this time. On ground, especially for an OGS in urban environments, limitations due to air traffic safety regulations may impose limits on the time window or pointing direction of the lasers.

Signal acquisition procedures start once the satellite moves into the field of view of the OGS. A short time is needed for establishing the rough pointing. Afterwards, the fine pointing mode is entered to optimise the signal quality. The T&F signals are then transmitted until the end of the link and tracked.

In case of a common-view T&F comparison between two ground clocks, the second terminal executes the same sequence as soon as the second OGS moves into the field of view.

The science, telemetry, and housekeeping data produced by the optical terminals in space and on the ground are stored and downloaded through the established communication links.

#### 4.2.2.4 Heritage

Laser Communication Terminals (LCT) have been deployed and tested in space-to-ground links by JAXA and JPL since 1995 (ETS-IV satellite). Inter-satellite links for data-relay applications were first demonstrated by ESA in 2001 (between ARTEMIS and SPOT-4 satellites) and later by JAXA in 2006 (between ARTEMIS and OICETS satellites). After these technology demonstrations, a second generation of LCTs was developed, being smaller, lighter, and providing higher data rates. Three of these second-generation terminals are already deployed in space (on TerraSAR-X, NFIRE and Alphasat satellites) and more will be used for inter-satellite links of the European Data Relay Satellite (EDRS) system.

These second-generation LCT are perfectly suited to transfer time and frequency information with ultra-high accuracy and relatively few modifications to the existing systems are necessary. While the baseline design of the optical link is using the European technology developed by TESAT, suitable terminals also exist in the US and could be used in case of a collaboration with NASA.

Technologies for the optical ground stations are very similar to the OGS equipment used for laser communication and no further development is needed.

The most critical part of the optical T&F transfer link is the performance in the presence of atmospheric turbulence (e.g. in proximity of urban areas). A first ESA study has shown by analysis and simulations that the STE-QUEST performance requirements are within reach. A second study is already planned to improve the simulations of atmospheric turbulence effects and finally verify the performance using a breadboard operated under representative test conditions.



**Figure 4-12:** (Left) The TESAT Laser communication terminal is a technology demonstration payload carried by TerraSAR-X, NFIRE, and Alphasat. (Right) An optical ground station with a 40 cm telescope and open clam-shell dome.

## 5 Mission Design

The mission study has been sized on the complete STE-QUEST payload, including both the core instruments and the optional payload elements (see Sec. 1). Demonstration of mission feasibility for the complete payload also provides evidence of the end-to-end system compatibility with the scenario based on the core instruments. The core configuration has been identified and selected with the specific purpose of reducing costs, development risks, and ensuring significant margins on the mission resource budgets.

### 5.1 Mission Profile

A highly elliptic orbit ensures sufficient measurement time for the differential atom interferometer at altitudes below 3000 km as well as long common-view durations from the science link terminals on the ground and large variations of the gravitational potential.

The orbit, shown in Figure 5-1 (left), has a semi-major axis of about 32000 km, a perigee altitude initially around 700 km and an inclination of 62.59 deg. Over the mission duration, third-body perturbations vary the eccentricity of the orbit, resulting in a change of the perigee altitude (see Figure 5-1 (right)). The orbit has

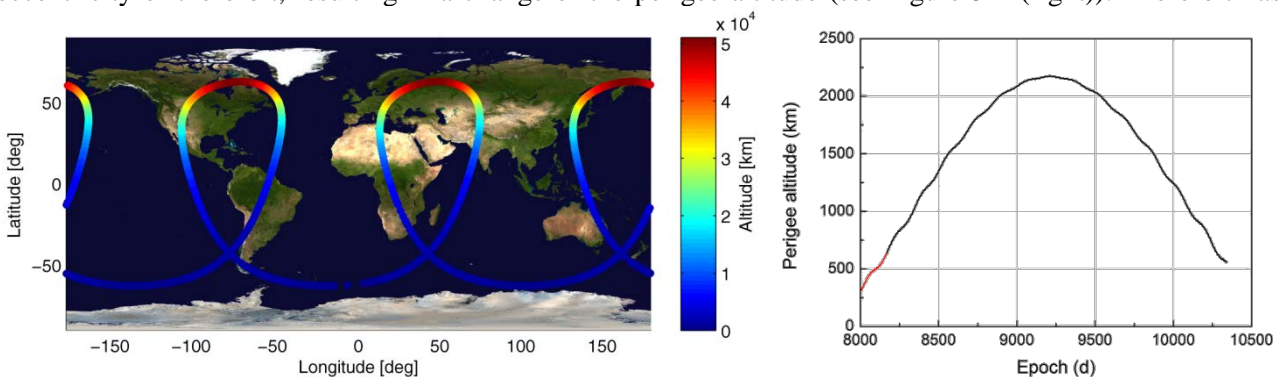


**Figure 5-1:** (Left) Ground track for the STE-QUEST orbit. (Right) Perigee altitude variation over the mission duration. The red segment corresponds to the Commissioning Phase, the black segment covers the Routine Science Phase and an eventual mission extension.

been designed such that the perigee altitude is lowest at the beginning and end of the mission. In this way, the launch mass is maximized and the de-orbiting propellant needs are minimized.

Launch is planned with Soyuz Fregat from Kourou in French-Guyana. After a drift phase, the spacecraft is placed into the final orbit using the Fregat upper stage, which separates and de-orbits after successful insertion. Small corrections are performed on spacecraft resources.

After the 5 years of mission duration, with one year of margin, the spacecraft is de-orbited by its on-board propulsion system to ensure leaving the protected zones in compliance with the space debris policy. The spacecraft would naturally de-orbit, but a safe re-entry cannot be guaranteed without controlled manoeuvres.

### 5.2 Mission Phases

The mission is divided into the following phases (Figure 5-2):

1. Launch and Early Operations;
2. System Commissioning;
3. Science Characterization;
4. Routine Science Operations;
5. Extended Science Operations;
6. De-Orbiting;
7. Post-Operations Phase.

The main activities expected to take place at the STE-QUEST SOC and MOC during the different mission phases are detailed below.

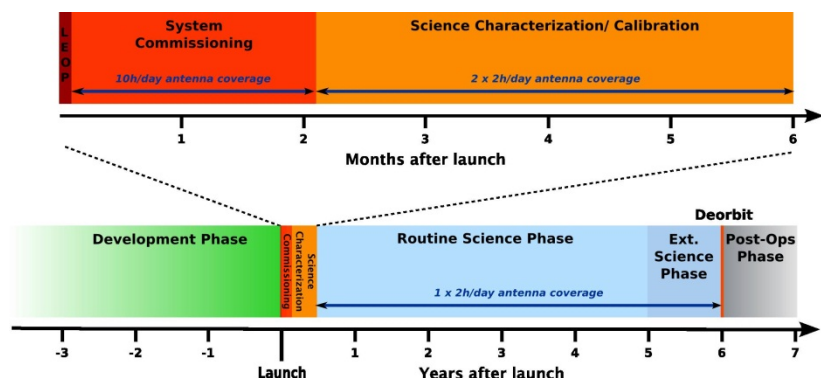


**Figure 5-2:** Overview of STE-QUEST mission phases, excluding the Definition and parts of the Development Phase. The duration of phases is indicative.

### 5.2.1 Launch and Early Orbit Phase

The highly elliptical orbit is reached with a Fregat after a parking orbit and apogee and perigee raising manoeuvres. After separation of STE-QUEST, a de-orbit burn by the Fregat ensures a re-entry. This phase will last up to and including the launcher dispersion correction manoeuvre by the spacecraft propulsion system on day 2 or 3 and it will include the deployment of the solar arrays. Operations will be directly controlled by MOC. Short feedback capability with on-site presence of experts and redundancy of services is needed to enable accelerated reaction in case of problems. During this phase, the following activities are taking place:

**Spacecraft Health Monitoring:** Engineering telemetry is collected during this mission phase, stored on board the spacecraft, and transmitted to ground at the next communication window. The telemetry will include health monitoring of critical parameters at e.g. the propulsion module, AOCS, solar arrays, and payload. During launch and until a safe attitude is acquired, the payload systems shall be switched off with the exception of vacuum pumps and stay-alive heaters. Payload telemetry is limited to the monitoring of the vacuum level at the clock and atom interferometer and of the temperatures at the established reference points.

**Flight Manoeuvres:** Flight manoeuvres for reaching the parking orbit and for tuning perigee and apogee altitudes are designed and executed at MOC under the responsibility of operations teams.

**Communication Needs:** Close to continuous coverage by three ground stations to enable short feedback capability with on-site presence of experts. Two 13 h-shifts of flight operations for 24 h.

### 5.2.2 System Commissioning Phase

During this phase, the functionalities of the different mission elements are established. The System Commissioning Phase ends with a formal in-orbit commissioning review handing the responsibility over from the project manager to the mission manager. SOC will start preparing planning input for the Science Characterization Phase. Feedback capability to enable an accelerated re-planning will be needed for implementing adaptations or in case of problems. This phase is expected to last 2 months. The System Commissioning Phase includes the following activities:

**AOCS Tuning:** AOCS tuning starts once the operational orbit has been reached. During this phase, the STE-QUEST AOCS is commissioned: open loop compensation of non-gravitational accelerations at the instruments location is tested and optimized; pointing performance is measured and fine-tuned.

**Flight Manoeuvres:** Once the operational orbit has been reached, flight manoeuvres for establishing the nominal attitude motion and pointing of the STE-QUEST spacecraft are designed and executed by MOC (see Sec. 5.3.1.3). This attitude motion will be then maintained over the mission duration.

**Payload Functional Verification:** The functionalities of the main instruments and subsystems of the STE-QUEST payload are tested. The instruments will go through the established turn-on and set-up procedures. At this stage, a number of checks at subsystem level is performed: temperature control, laser frequencies tuning and stabilization, laser power tuning and stabilization, magnetic fields characterization and control, characterization of the microvibrations environment. Main instrument functions are exercised and correct telemetry transmission and telecommands reception is checked. Limited performance tests (e.g. short term stability) are also run. Scope of the payload functional verification is to ensure that the environment at the STE-QUEST payload is according to specs (mechanical, thermal, magnetic, etc.) and that on-board instruments and subsystems functionalities, as well as their interfaces (software, data...) with the spacecraft, are fully operational.

**Time and Frequency Link Verification:** The functionalities of the science link are established. The microwave link is turned on. Common-clock tests involving a transportable ground terminal and common-view comparisons between ground clocks connected via an optical fibre can be performed to verify the link stability. In these tests, availability of transportable microwave ground terminals will be crucial. In addition, calibration activities of the science link ground terminals are started.

**GNSS Receiver Verification:** The on-board GNSS receiver is turned on. Orbit data are provided to ODC for testing orbit determination and prediction algorithms and for assessing the receiver performance.

**TM/TC Chain Commissioning:** The full chain of telemetry transmission and telecommands reception, from both the STE-QUEST spacecraft and ground terminals down to the STE-QUEST ESTRACK network and MOC, will be tested and validated.

**Data Processing and Archiving:** The generation of L0 to L4 (see Sec. 6.1) data products is tested. This includes the verification of the involved processes and algorithms as well as of the interfaces between MOC

and SOC, between SOC and the STE-QUEST Archive, between the Archive and IOCs, DPCs, ODC, and the external users (see Figure 6-1).

**Ground Stations Commissioning:** At this stage, designated STE-QUEST ground stations shall have all the interfaces with the science link ground terminal verified. This verification will take place under the responsibility of the institutes operating the ground clocks and it includes performance tests of the delivered clock signal (stability and accuracy), verification of electrical, power, data interfaces, etc.

**Communication Needs:** 2 months of system and payload commissioning with 10 h daily coverage and on site presence of experts and scientists, mainly during working hours, is required in this phase.

### 5.2.3 Science Characterization Phase

During the Science Characterization Phase, the on-board instruments are tuned and verified in terms of performance. Such activities may need to be repeated during the subsequent Routine Science Phase. Indeed, instruments calibration will be continuously improved during the STE-QUEST mission life cycle. This phase is expected to last 4 months, starting from the successful completion of the System Commissioning Phase. SOC will use its science planning system to generate commands to operate the payload according to the procedures also agreed with IOCs. It is expected that instruments tuning and performance evaluation will require a higher level of activity than during the following Routine Science Phase. SOC interactions with IOCs and DPCs will be frequent and fast updates of the software might be required. Non-regular tasks are expected to include the planning of payload configuration changes, updates of configuration and calibration information for data processing, archive data quality checks. During this phase, the following activities are taking place:

**Atom Interferometer Characterization:** The differential atom interferometer is tuned and its performance established. As first, the instrument cycle is optimized: atoms loading and magneto-optical trapping, molasses cooling, magnetic trapping, pre-evaporation in the magnetic potential, dipole trap loading, evaporation and sympathetic cooling. All the different phases need to be optimized in terms of atom number and temperature. Detuning and intensity of the Raman lasers are tuned and the two Rb isotopes are probed on the interferometric sequence. Once detected, atom interference fringes are optimized in terms of S/N ratio and contrast. At this stage, the instrument is ready to be characterized in terms of sensitivity to differential acceleration measurements. Systematic effects induced by gravity gradients, residual rotations, magnetic fields, mean-field energy of the atomic samples, Raman lasers wave front distortions, etc. will be evaluated by launching specific measurement sequences uploaded on the STE-QUEST spacecraft as scheduled commands. At the end of this phase, the performance of the differential atom interferometer is established and validated against the STE-QUEST scientific requirements.

**Atomic Clock Characterization:** The optional STE-QUEST clock would undergo a similar procedure. The instrument cycle is optimized in terms of temperature of the atomic cloud, atom number, launch velocity, and detection parameters. The MOLO microwave frequency reference is used to probe the atoms on the clock transition (detection of Ramsey fringes). Dedicated tests will then follow to evaluate the instrument stability and accuracy. The stability of the instrument can be evaluated via the on-board comparison between MOLO and ATC for integration times up to about 1000 s; for longer integration times, comparisons involving ground clocks with stability better than ATC will be needed. The evaluation of the clock accuracy budget requires a set of measurements for the determination of the systematic offsets of the ATC frequency output. They include the blackbody radiation shift, the cold-collision shift, the second-order Zeeman shift, the shift induced by the distributed phase in the microwave cavity, etc.. Some of them will be evaluated on the basis of the environment seen by the atoms during the clock interrogation cycle (e.g. temperature, magnetic field). The remaining effects will be evaluated by performing differential measurements based on interleaved clock cycles in which the key parameter (e.g. atom density for the collisional shift) is alternated between different values. Such measurements will be planned on the ground and executed following a scheduled sequence of commands that will be uploaded on the STE-QUEST spacecraft. At the end of this phase, the clock performance is established and validated against the STE-QUEST scientific requirements.

**Time and Frequency (T&F) Links Verification:** The ultimate performance of the STE-QUEST time and frequency transfer links are verified and finally established (both stability and accuracy). The first round of calibration activities of the STE-QUEST science link ground terminals are completed. They involve the use of transportable ground terminals to be co-located with the fixed units to perform common-clock tests.

**Data Processing and Archiving:** During this phase, L0 to L2 data products are generated by SOC and IOCs to evaluate the ultimate performance of the on-board instruments. Generation of L3 products will be

exercised to test the involved processes. All data products, including calibration parameters and data processing software, are then uploaded to the STE-QUEST Archive.

**Communication Needs:** 4 months of payload performance characterization with 2 contacts per day of 2 h each during working hours are required in this phase.

### 5.2.4 Routine Science Phase

After successful commissioning, routine science operations start. Science data are collected for a minimum period of 4.5 years, extending to the mission end of life. Activities during this phase are expected to be regular and most interactions between MOC, SOC, IOCs, and DPCs to be at a (semi-)automated level: planning of science operations and their execution, monitoring and calibration of STE-QUEST spacecraft and payload, data acquisition, generation of science data products, archiving of mission products, and interaction with the user community. Non-regular tasks are the planning of payload configuration changes, the update of configuration and calibration information for data processing, archive data quality checks, the maintenance of the publications list. This phase includes the following activities:

**Nominal Payload Operations:** During this phase, the STE-QUEST payload is routinely operated on the basis of a scheduled sequence of commands. The *atom interferometer* will provide differential acceleration measurements between the two Rb isotopes during each perigee passage ( $g > 4.5 \text{ m/s}^2$ ), while the spacecraft is in inertial pointing mode. Instrument calibration will take place during perigee passages or around apogee, where spacecraft rotations can be sensibly reduced. The *science link* enables comparisons between clocks on the ground. The baseline mission architecture foresees 3 ground stations connected to high-performance atomic clocks. The ground terminals might undergo additional calibration during the Routine Science Phase. The optional *Cs clock* is operated in nominal mode, with the MOLO local oscillator steered on the correction signal generated from the frequency detuning measured by the atoms in the ATC physics package. The clock periodically enters the calibration mode, in which specific measurements will be run for checking and continuously improving the clock accuracy.

**Data Processing and Archiving:** Collection of science, telemetry, and housekeeping data (L0) from both the STE-QUEST spacecraft and the ground stations will continue until the end of the mission. The validity of the STE-QUEST data is monitored at MOC, SOC, IOCs and DPCs on the basis of L0 and L1 data as well as of quick-look L2 data. L2 data will indeed provide near real-time information on the payload performance, allowing SOC to plan payload configuration changes in case of anomalies. Invalid data will be flagged. Science data products (L3 and L4) are evaluated as described in Sec. 6.4.2. All data products (L0 to L4), including calibration parameters and data processing software, are continuously archived.

**Communication Needs:** 1 contact per day of a duration of 2 h is foreseen during working hours.

### 5.2.5 Extended Science Phase

This phase covers the possibility of extending the mission duration through the natural prolongation of the activities already described in the Routine Science Phase.

**Decommissioning:** At the end of the Routine Science Phase, decommissioning activities are performed to place the spacecraft in a passive state. All systems will be powered off.

### 5.2.6 Deorbiting

The current STE-QUEST orbit would naturally re-enter the atmosphere after slightly more than 6 years of mission duration, in principle compliant with leaving the LEO/GEO protected zones. At the current level of detail, a safe re-entry, compliant with the space debris mitigation policy and safety measures to avoid casualties on ground, can however not be performed without a controlled manoeuvre. Therefore an active deorbit is required at the end of the mission, with  $\sim 50 \text{ m/s}$  velocity variation.

### 5.2.7 Post-operations Phase

In this phase, the final refinements of the system calibration are achieved in collaboration among the SOC, the IOCs, and the DPCs; at the same time, the data processing system comes to its final status. Extensive support is given to the users' community in the scientific exploitation of the mission data. The final ("legacy") reprocessing of all the mission data is performed towards the end of this phase, using the ultimate version of the data processing tools and calibration, and the explanatory documentation is put into legacy form. Extraction of "Lessons Learned" and look-ahead to future missions is done. This phase is expected to

last about 1 year, depending on the scope of the Legacy Archive. The STE-QUEST Archive will continue to be supported as part of the overall ESAC infrastructure after the end of the Post Operational Phase. Activities, only involving SOC, DPCs, and STE-QUEST Archive, are limited to:

**Data Processing and Archiving:** High-level data products (L3 and L4) are evaluated making full use of the data collected during the mission lifetime. Data products together with the software used for their evaluation are validated and archived.

## 5.3 Spacecraft Design

The main mission drivers and their consequences on the spacecraft design are discussed in this section. These considerations are followed by a summary of the outcome of the two parallel and competitive studies conducted by industry.

### 5.3.1 Mission Drivers and Design Consequences

The main mission drivers are imposed by the payload requirements on the instruments accommodation, the on-board environment (accelerations, rotations, radiation environment), and the operational constraints.

#### 5.3.1.1 Instruments Accommodation Constraints and Spacecraft Attitude

Specific requirements on the orientation of the atom interferometer sensitive axis, of the science link antennas as well as of the optional atomic clock define the STE-QUEST payload, the spacecraft attitude and the configuration options.

The atom interferometer sensitive axis, as identified by the propagation direction of the Raman lasers, shall point towards nadir with an accuracy of better than 3 deg when at perigee. In addition, the position of the dipole trap at the atom interferometry instrument shall be located within 50 cm from the spacecraft centre of mass. This requirement ensures control on the relative displacement of  $^{85}\text{Rb}$  and  $^{87}\text{Rb}$  atomic samples due to the gravitational sag in the optical trap generated by the spacecraft-induced gravity gradients (see Sec. 4.1.1). Gradients produced by the spacecraft self-gravity are specified to be below  $2.5 \cdot 10^{-6} \text{ s}^{-2}$ .

The on-board science link terminals need to be pointed towards nadir to enable clock comparisons over large part of the spacecraft orbit.

In addition, the axis of the optional Cs clock has to be parallel within  $\pm 10$  degree to the spacecraft rotation axis. In conjunction with the nadir-pointing of the link terminals, this requirement defines the propagation direction of the atoms in the caesium tube to be perpendicular to the orbital plane.

Additional accommodation constraints stem from the efforts to reduce cabling and optical fibres length to minimize the payload sensitivity to temperature variations. Special care has to be taken to quantify and limit thermal gradients on cables and fibres.

The operation of the atom interferometer requires tight control on the angular velocity of the STE-QUEST spacecraft with respect to a non-rotating freely falling reference frame. Indeed, rotation rates, averaged over the time between consecutive pulses in the atom interferometer sequence, need to be kept within the interval  $[-10^{-6}, +10^{-6}] \text{ rad/s}$  on the three axes, as a minimum during periods of gravity acceleration higher than  $4.5 \text{ m/s}^2$ . This requirement, together with the constraints on the atom interferometer sensitive axis, imposes the STE-QUEST spacecraft to be inertially pointed when orbiting around perigee, at altitudes below 3000 km (see Figure 5-3).

The operation of the science link requires the on-board antennae to be pointed towards nadir for a large fraction of the STE-QUEST orbit and in particular around apogee. A narrow beam width limits the power necessary to cover the large distance of up to 51000 km. At perigee, lower gain antennae might be used to restrict the

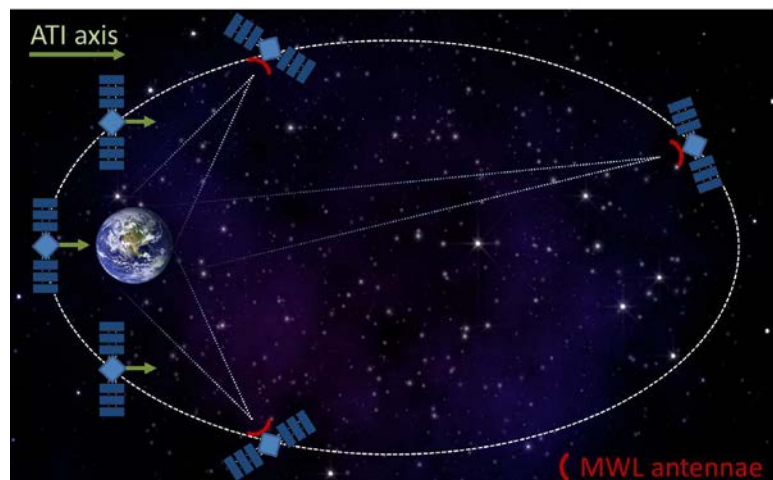


Figure 5-3: The STE-QUEST spacecraft attitude along the orbit.

A narrow beam width limits the power necessary to cover the large distance of up to 51000 km. At perigee, lower gain antennae might be used to restrict the

power flux density on ground and achieve a wide beam width. Also installed on the nadir-pointing panel, the perigee antennae need to close the link with off-pointing between zero and 65 degrees.

The transition between the inertial pointing attitude of perigee passes and the nadir pointing orientation during the remaining orbital arc requires the identification of two transition phases, to take place above 3000 km of altitude, in which dedicated manoeuvres re-orient the spacecraft. Such manoeuvres have been designed and estimated to take no longer than 30 min including the settling time.

**5.3.1.2 Spacecraft Environment**

External forces and torques, mechanical vibrations, and rotations can introduce both noise and systematic shifts on the science measurements performed by the on-board instruments. In addition, the radiation environment shall be carefully taken into account in the payload design to ensure correct operation along the 5 years of mission duration. This imposes a tight control on the environment at the STE-QUEST instruments and subsystems.

**Accelerations, Mechanical Vibrations and Rotations**

Drag forces reach their maximum during perigee passes and for the lowest altitudes (~ 700 km). The corresponding non-gravitational accelerations at the measurement head of the instruments is typically one order of magnitude below the required  $10^{-7} \text{ m/s}^2$  along the sensitive axis of the atom interferometer and  $10^{-6} \text{ m/s}^2$  along the remaining two orthogonal directions. Only in a worst case scenario, when considering high solar activity periods (maxima in the Sun cycle) combined with the maximum spacecraft cross section and the lowest perigee altitude, they get close to requirements. Considering the current launch dates and the natural perigee altitude evolution of the STE-QUEST orbit, the solar activity maxima occur when the perigee is sufficiently high and drag accelerations are expected to be well within the specified values. In addition, the spacecraft cross section can still be minimized for the critical passes, reducing atmospheric drag by about 1 order of magnitude. Drag-free control at the STE-QUEST payload can therefore be avoided. Accelerations induced by solar radiation pressure do not pose problems for the STE-QUEST instruments.

The on-board instruments necessitate a well-controlled microvibration environment. Two requirements define the maximum levels in terms of RMS and spectral density of the acceleration noise in the frequency range of interest for the on-board instruments. Requirements on the accelerations noise at the instruments are shown in Figure 5-4.

External disturbances such as drag, solar radiation pressure, and gravity gradients also result in torques, being responsible for unwanted spacecraft charging, in particular during perigee passes, and subsequent angular momentum accumulation. All these disturbances induce rotation rates that, averaged over the time between consecutive pulses in the atom interferometer sequence, can exceed the specified  $[-10^{-6}, +10^{-6}] \text{ rad/s}$ . The spacecraft cross section is then to be optimized to minimize these effects. At the same time, the on-board AOCS are designed to correctly compensate for non-gravitational accelerations and corresponding torques.

Requirements on spurious accelerations and rotation are violated during the transition phase, when orbital manoeuvres switching the spacecraft attitude from nadir to inertial pointing and vice-versa are executed. Transition phases, required to last less than 30 min, are expected to be concluded in about 900 s. This aspect is already accounted for in the analysis of the scientific performance of STE-QUEST (see Sec. 3.3.2.1).

Assessing the exact environment on the spacecraft requires precise knowledge of the sources of disturbance and the transfer function from source to target. In the early phases of spacecraft design, the transfer function can only be approximated, as can some sources of perturbations. For this reason, a safety margin of one order of magnitude was targeted in assessing compliance to requirements on both rotations and mechanical vibrations.

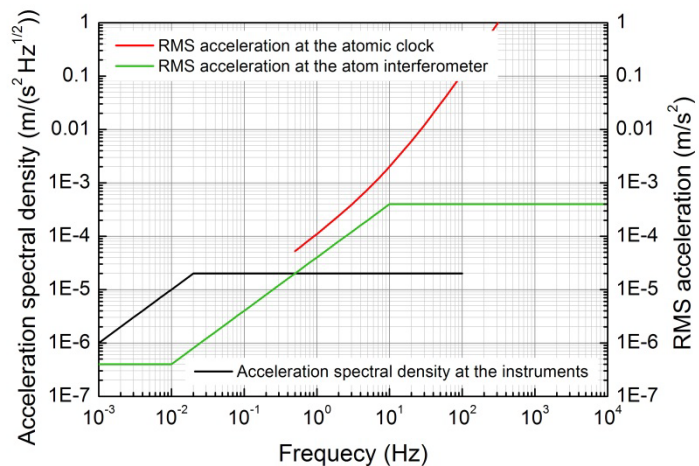


**Figure 5-4:** Requirements on the acceleration spectral density and RMS acceleration at the STE-QUEST instruments.

Following this approach, two different AOCS solutions have been analysed, the first based on reaction wheels, the second making use of the cold gas propulsion technology. Simulations have shown that the perturbation levels expected from reaction wheels are close to the maximum allowed acceleration noise in some frequency bands. On the contrary, requirements can easily be met with a factor of 10 margin by a cold gas propulsion system, as e.g. used for GAIA or GOCE. During the study, the mechanical vibrations introduced by reaction wheels have been analysed and propagated down to the STE-QUEST instruments. Simulation results have shown a good margin with respect to the required spectral density and RMS values for frequencies below 10 Hz. At higher frequencies, peaks violating the specified levels were found. These perturbations can however be strongly reduced by limiting the angular velocity of the wheels and avoiding the excitation of system resonances. As a conclusion, together with the use of dampers and an adequate structural design, the use of wheels appears manageable. A more accurate analysis will certainly be needed during the detailed design phase. Should detailed simulations prove the design based on reaction wheels to be in compliance with STE-QUEST needs, the cold gas system can then be used as a fall-back option. The impact in terms of mass when changing to cold gas from a reaction wheels solution is manageable, but the decision should be taken in the definition phase to avoid costly redesign activities. The two industrial studies presented below are addressing both systems: one design solution uses the cold gas technology as a baseline, the other currently favours an AOCS based on reaction wheels.

Influences of other disturbances are taken into account as far as known, in particular the solar arrays drive mechanisms as well as the influence of the solar arrays orientation and modes on the structural transfer function. Disturbances introduced by the optional optical terminals haven't been characterized, but they can be mitigated as for reaction wheels, by optimizing their operation, using dampers, or fine tuning the structural design.

## Radiation

The STE-QUEST spacecraft crosses the Van Allen radiation belts twice per orbit, accumulating high dose levels in the 5-year mission duration. The expected dose for electrons is comparable to the one experienced by geostationary satellites after 10-15 years. For protons, the levels are similar to those of GNSS satellites. The total flux is comparable for both species in the low energy regimes; for energies above 0.5 MeV, the proton flux is significantly higher.

The total ionizing dose (TID) is dominated by electrons with about 1 Mrad after 3 mm of equivalent aluminium shielding. After 6-7 mm of equivalent shielding, the total dose drops significantly below 100 krad. Sectoring analyses by industry have demonstrated that the equipment inside the spacecraft is subjected to doses below 50 krad at the outside of the unit box. Efficient protection against electrons can be achieved by shielding with high-Z materials, such as tantalum. Sensitive equipment can thus be housed in boxes with a material mix on the box walls and/or spot shielded.

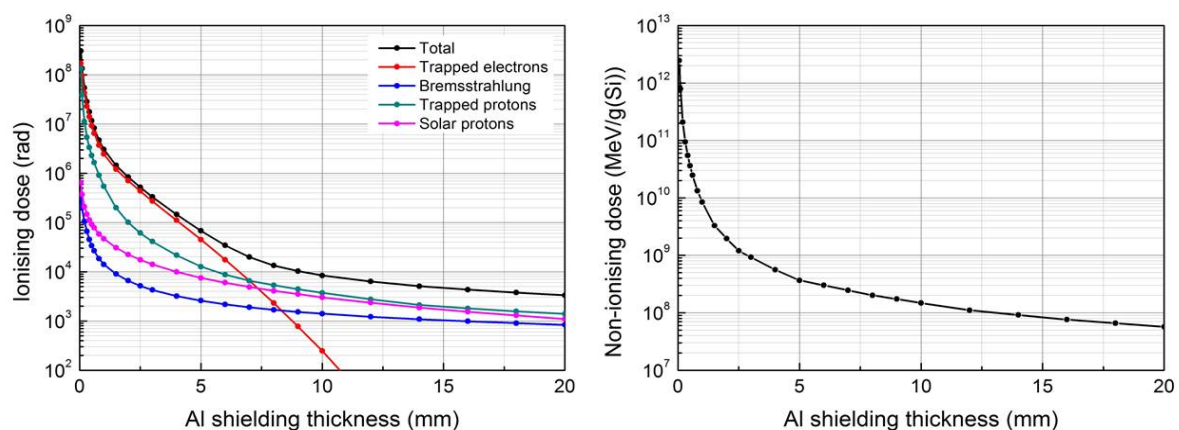


**Figure 5-5:** Total ionizing dose (left) and non-ionizing dose (right) as a function of shielding depth for the STE-QUEST mission duration.

Protons with high energies penetrate standard Al shielding more easily and influence mostly optical components. Shielding against protons is more efficient using low Z-materials. Special care has to be taken for the fibres connecting the laser sources with the physics packages and the mirrors and optical components, especially of MOLO. Dedicated radiation tests have been performed on the MOLO critical elements, the mode-locked laser driving the frequency comb generator [LECOMTE (2013)] and the high-finesse mirrors of

the MOLO cavity [CHEN (2013)], showing no degradation of performance under the doses and the energy spectra expected for STE-QUEST after 10 mm of equivalent Al shield.

**5.3.1.3 Payload Operational Scenarios**

The operational scenario presented below has been derived to ensure optimal conditions for both instruments, taking into account the different constraints.

	Perigee Science Phase	Perigee-Apogee Transition	Apogee Science Phase	Apogee-Perigee Transition
<i>Duration (h)</i>	0.56	0.25	14.9	0.25
<i>Altitude (km)</i>	700 – 3000	3000 – 7000	7000 - 51000	7000 - 3000
Payload Element	Operational Mode			
<i>Atom Interferometer</i>	ON	STDBY	STDBY/CAL	STDBY
<i>MWL</i>	ON	OFF	ON	ON
<i>GNSS Receiver</i>	ON	ON	ON	ON
<i>NGRM</i>	ON	ON	ON	ON
<i>Atomic Clock (Optional)</i>	ON	ON	ON	ON
<i>Optical Link (Optional)</i>	OFF	OFF	ON	OFF

**Table 5-1:** Operational scenario of STE-QUEST. STDBY: Stand-by; CAL: Calibration.

During the perigee pass, for altitudes below 3000 km, the spacecraft mode is optimized for the atom interferometer operation. The spacecraft has an inertial pointing with the instrument sensitive axis aligned along nadir to within 3 deg when at perigee. The atomic clock and microwave link are available and operating during this phase. For the remaining part of the orbit and particularly around apogee, operations are optimized for clock comparison measurements. The spacecraft is nadir pointing, with the antennae beams covering the Earth. During this phase of the orbit, the interferometer performs calibration activities. Both inertial and nadir pointing phases are connected by a transition phase, during which the spacecraft does not fulfil the requirements on accelerations and rotations. Nonetheless, the clock comparison measurements continue without interruption. Data generated during this phase can be analysed and corrected or discarded if negatively affected by the environment. Orbital maintenance, solar arrays pointing, and possibly wheel offloading (where necessary) also take place during the transition phase.

Due to the specific pointing strategy in combination with the chosen orbit, the Sun is encountered from almost all angles during the mission. This requires solar arrays able to point to all directions during the mission or to be sufficiently oversized to cope with illumination at different angles.

**5.3.2 Spacecraft Design: Solution A**

**5.3.2.1 Configuration**

Characteristic for this solution is the octagonal structure and the integration of payload module and service module. Service module and propellant tanks take the lower part of the structure, based on a standard central cylinder architecture. The payload module is integrated on the upper part of the structure, with the atom interferometer protruding into the central cylinder of the service module. The outer structure serves as the first radiation shield for the components. Figure 5-6 shows the solution in flight and launch configuration.

Due to the modular approach, only structural and electrical harness interfaces are required between the service and payload module, with the propulsion system designed to be integrated onto the service module. The passive thermal control is independent on each module.

The solar arrays ( $2 \times 8.8 \text{ m}^2$ ) are attached to the  $-y$  and  $+y$  panels and canted at 45 deg to ensure sufficient illumination angle during all mission phases. Rotation of the arrays is possible with a one-axis solar array drive around the  $y$ -axis. The spacecraft body measures  $2.5 \text{ m} \times 2.5 \text{ m} \times 2.7 \text{ m}$ , with the optional optical link terminals extending the width to 3.6 m on one axis. With the solar arrays deployed, the spacecraft envelope is  $12.6 \text{ m} \times 2.5 \text{ m} \times 9.7 \text{ m}$ .

The de-orbiting thrusters for the controlled de-orbiting manoeuvre, 6 orbit control thrusters at 22 N, are integrated at the launcher interface.

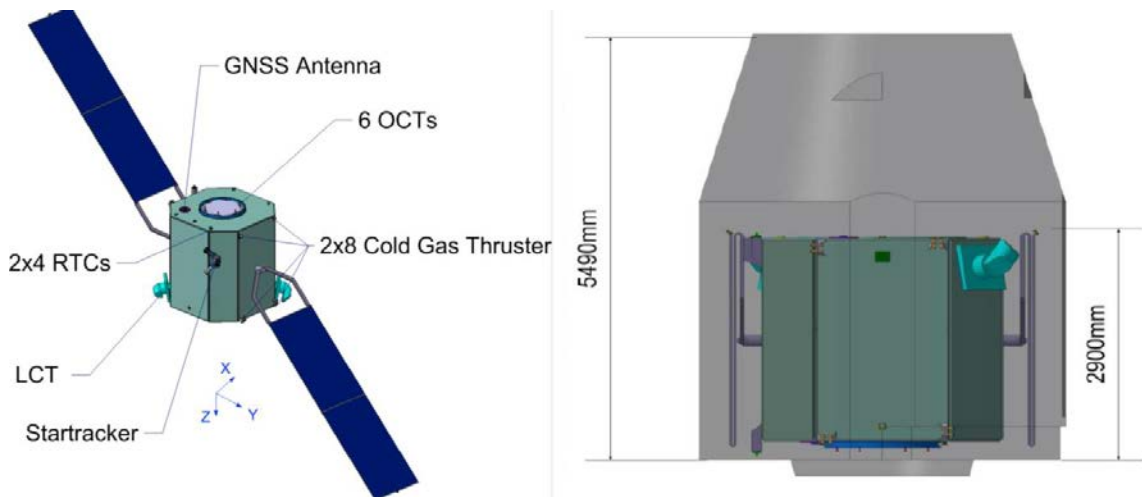


**Figure 5-6:** Proposed configuration for Solution A. (Left) Flight configuration, with the nadir panel facing downwards in z-direction and the launcher interface panel facing upwards. Radiators are located on the x panels (payload module panels). (Right) Stowed configuration for launch in Soyuz-Fregat envelope (reduced volume for demonstration of compatibility with the dual launch adapter ASAP-S).

**5.3.2.2 Payload Accommodation**

All payload subsystems are accommodated within the payload module, shown in Figure 5-7.

On the interface panel to the service module, extending into the central cylinder, is the physics package of the atom interferometer with its magnetic shielding. The measurement volume of the physics package is within 30 cm along z and 5 cm along x and y of the spacecraft centre of mass. All other atom interferometer units, the three laser system boxes, instrument control unit, and supporting units are placed on the +z face of the interface panel. Solution A chose to accommodate the laser system into three separate boxes from the total allocated volume. Fibres and harness are routed through the panel at the centre to the physics package.

The hexagonal structure is closed on the +x side by the nadir panel, onto which the microwave link systems and antennae are mounted. No spacecraft appendices extend further than the +x panel, providing an obstruction free accommodation for the antennae, with no significant multipath contributors. The microwave link control electronics are placed close to the centre of the inner face of the +x panel, in close proximity to the antennae and the optional atomic clock.

The upper part houses all units related to the atomic clock instrument. The caesium tube, together with the laser source, the microwave synthesis chain, and supporting equipment, is located in the central hexagonal inner structure, with blue colour code in the figure. The axis of the caesium tube, identified by the propagation direction of the atoms, is collinear with the designed rotation axis of the spacecraft during nadir pointing, i.e. perpendicular to the orbital plane.

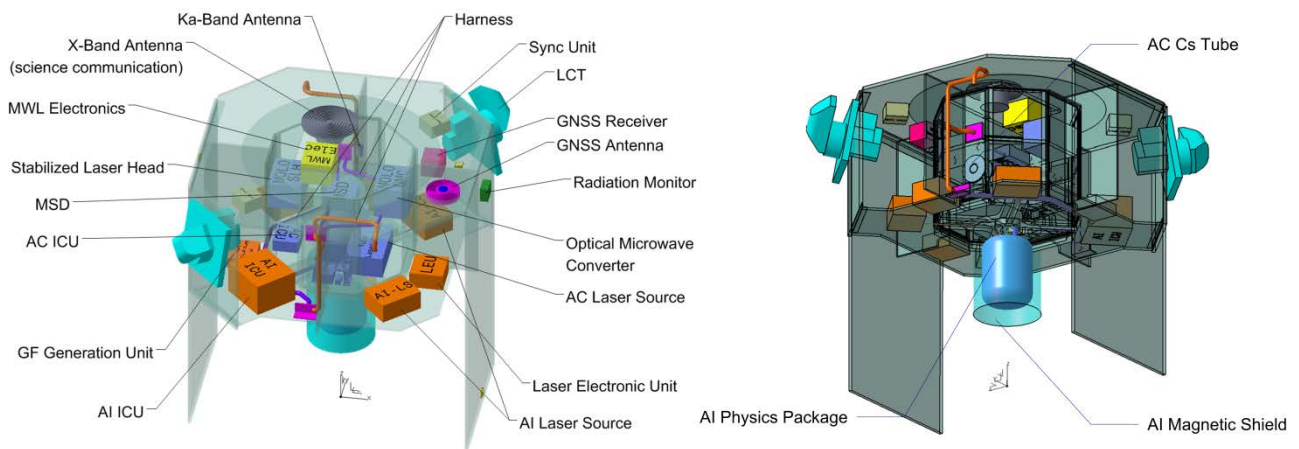


**Figure 5-7:** Location of the payload units. The atom interferometer (AI) is located on the interface plate to the service module with the physics package. Units are colour coded in orange and its magnetic shielding in turquoise. The atomic clock (AC) resides within the hexagonal inner structure.

The optional laser communication terminals are placed on separate side-panels, close to the clock location. This shortens the required fibre lengths. The optical terminal electronics are integrated into the backplane of the terminal itself, protruding into the structure.

The GNSS receiver for the precise orbit determination, as well as the Next Generation Radiation Monitor (NGRM), are located in the payload module. GNSS antennae share the nadir panel with the microwave link antennae.

Two other side panels are available as radiator surface for payload thermal control. Heat from the units is transferred via heat-pipes onto these panels.

#### **5.3.2.3 Attitude and Orbit Control System**

Solution A opted for a combined cold gas and hydrazine architecture for attitude and orbit control. Measurements of the spacecraft attitude are provided by three star trackers, one inertial measurement unit, and coarse Sun sensors.

The hydrazine system supports the major orbital manoeuvres required, the safe mode, and it is also performing the attitude slews to change from inertial to nadir-pointing twice per orbit. With 2 sets of 4 canted 1 N thrusters, the system achieves full torque authority. In addition, six 22 N orbital control thrusters, with 2 units providing the required redundancy, perform the de-orbiting. All these tasks require a propellant mass of about 230 kg.

The cold gas system compensates drag and torque from atmosphere, magnetic moment, and solar pressure and assists the settling after the fast slews. It is based on the GAIA cold gas system with no significant modifications. In a nominal and a redundant branch, it employs two sets of 8 proportional micro-thrusters, providing a thrust range from 1 to 3000  $\mu\text{N}$ . The cold gas system consumes a propellant mass of 35 kg over the mission duration, including margins.

#### **5.3.2.4 Power Subsystem**

The power system relies on solar arrays and batteries for providing the necessary power to the spacecraft. The power architecture is sized for 2.3 kW, providing a 28 V regulated bus for platform systems and payload elements with low power consumption, as well as a 50 V battery regulated bus for the instruments.

Canted 45 deg solar arrays, oversized to accommodate non-perpendicular incident angles, provide power to the power control and distribution unit via Maximum Power Point Tracking (MPPT) conversion. The array consists of 2 wings of 8.8 m<sup>2</sup>, with 2 panels each, for a full mechanical surface of 17.6 m<sup>2</sup>. The panels are made from triple junction 3G30 cells with 30% efficiency, covered by 76  $\mu\text{m}$  cover glass to protect the cells from the radiation environment.

During eclipse phases, as well as in safe mode and LEOP, batteries provide power in case illumination is not sufficient. The battery capacity is sized for the longest eclipse with full payload operation at ~2300 Wh.

#### **5.3.2.5 Thermal Design**

The spacecraft is thermally shielded from the environment using external multi-layer insulation. Heaters and radiators control the temperature. Heaters are used for electrical components and propellant tanks, with a power dimensioned to 150 W. No dedicated radiators are installed on the service module.

The payload instruments are controlled to within  $\pm 3$  °C per orbit around 20 °C in all cases. In order to remove the high power dissipated from the instruments, heat pipes connect the instruments to the radiator panels on the  $\pm x$  faces. The available radiator area is sized at 3.2 m<sup>2</sup> and 1.6 m<sup>2</sup> per panel. In the coldest case, radiators reach -40 °C. The optical communication terminals have their own radiator on the mounting face.

A seasonal yaw flip reduces the fluctuations of the heat flux on the radiators and might lead to elimination of the +x radiator area.

#### **5.3.2.6 Command and Data Handling, Communications**

The spacecraft is controlled by a standard Leon 2 based Command and Data Management Unit (CDMU). While the interferometer generates a significant data rate at 110 kb/s when measuring, this data is only collected during perigee passes. The optional atomic clock has a much lower data rate, but continuous operations along the whole orbit make it dominate the data volume per orbit. Still, the CDMU-integrated memory of 12 Gb end-of-life (with upgrade option to 32 Gb) is sufficient. No additional memory module is foreseen.

Telemetry and telecommands can be handled within 2-hour contacts with ESA ground stations using a medium gain X-band antenna, with two low gain X-band antennae available for contingency.

### 5.3.3 Spacecraft Design: Solution B

#### 5.3.3.1 Configuration

Solution B is characterized through a distinct separation between service module and payload module, as shown in Figure 5-8. The service module is based on a heritage platform with central cylinder structure, only adjusted for height. The payload module is constructed as a box with internal shear panels and accommodates all payload items. The two modules are connected via structural and electrical interfaces only, with both modules having their own passive thermal control system. Struts connect the box-shaped payload module to the main cylinder in the service module. The main part of the atom interferometer resides in this interface structure between the two modules.

The solar arrays are controlled by two-degree of freedom drive mechanisms, allowing them to face the Sun with good illumination angles at all times. The arrays consist of 2 panels per wing, with each wing providing a surface of  $4.9 \text{ m}^2$ , for a total of  $9.8 \text{ m}^2$ . The flight configuration has an envelope of  $2 \text{ m} \times 4.2 \text{ m} \times 10.7 \text{ m}$ ,  $2 \text{ m} \times 3.3 \text{ m} \times 4.2 \text{ m}$  when stowed.

Active de-orbiting is performed on reaction control thrusters, 4 + 4 at 1 N, integrated within the launcher interface ring on the  $-y$  panel.

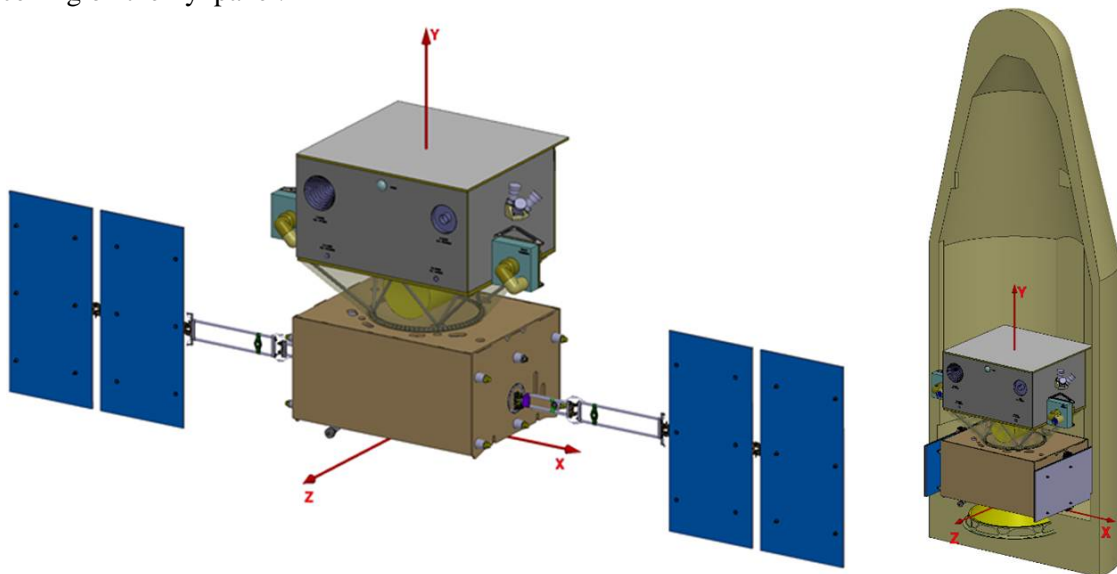


**Figure 5-8:** Proposed configuration for Solution B. (Left) Spacecraft in flight configuration. The nadir panel is facing forward along the  $+z$  direction. Launcher interface is on the  $-y$  panel. (Right) stowed configuration in Soyuz-Fregat fairing.

#### 5.3.3.2 Payload Accommodation

The separate payload compartment in Figure 5-8 houses all payload units.

The atom interferometer units are mainly mounted on the inside of the lower  $y$ -panel of the payload module, connected by heat-pipes to the external radiators Figure 5-9. Mounted on the outside of the same panel, inside the interconnection area between payload module and service module, the physics package with its magnetic shield is connected to the other atom interferometer units through a harness throughput in the panel. The physics package measurement volume is within 50 cm from the spacecraft centre of mass. In Solution B, the laser system of the atom interferometer has not been split in separate boxes. Instead, the full volume is accommodated in a single box, located on the right of Figure 5-9. Enough room on the panels is available to support splitting the volume into separate boxes.

All units of the optional atomic clock are placed on an internal vertical panel in the  $x$ - $y$  plane. The caesium tube and the propagation direction of the atoms are therefore collinear to the spacecraft rotation axis for nadir pointing by design.

Placed close to the clock units, on the  $+z$  outer panel, are the microwave link units. Internally mounted on this panel is the MWL electronics box. The antennae are located externally, on the nadir pointing  $+z$  panel. The  $+z$  panel is the nadir-most part of the spacecraft in flight configuration, limiting detrimental influences on the antennae phase patterns.

Also internally, but on the atomic clock panel, are the electronics of the optional laser communication terminals, connected to the actual terminals via dedicated mounts on the outer  $\pm x$  panels (see Figure 5-8).

In addition to the payload units, the star tracker has been located on the payload module.

NGRM is located internally on the  $-y$  panel. Two GNSS antennae are placed on the nadir and anti-nadir faces of the payload module, with the GNSS receiver electronics in-between them.

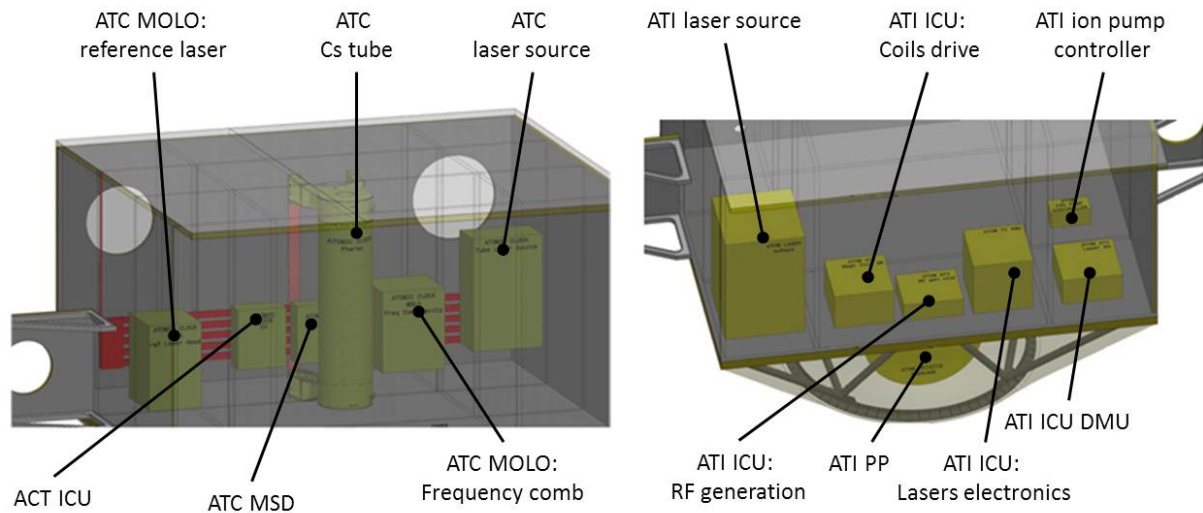


**Figure 5-9:** Payload accommodation in Solution B. (Left) Atomic clock accommodation vertical to launcher direction. (Right) Atom interferometer accommodation: the physics package is within the volume of the interface

### 5.3.3.3 Attitude and Orbit Control System

Solution B has opted for a hydrazine and reaction wheel architecture to perform attitude and orbit control tasks. Measurements for AOCS functions are provided by a three-head star tracker, coarse rate sensors, and coarse sun sensors. As this solution does not implement an Inertial Measurement Unit (IMU), the system needs to pre-compensate for predictable disturbances, mostly during perigee pass, e.g. gravity torque. These forces will thus have to be estimated and compensated by properly commanding the AOCS.

The hydrazine propulsion system is sized mainly for the de-orbit, requiring a  $\Delta v$  of about 50 m/s, and attitude as well as safe mode manoeuvres. This requires a propellant mass of 95 kg. Two sets of four 1 N thrusters in redundant configuration provide full control authority and are used for the de-orbit burn.

For fine attitude control, four reaction wheels, specified at 12 Nm-s, of which one is redundant, have full torque capability. The use range of the wheels has been limited to avoid operational regimes producing microvibrations exceeding the specified levels (Sec. 5.3.1.2). In addition, the wheels are mounted on dampers with 7 Hz cut-off frequency. After 15-20 orbits, the wheels are offloaded by the hydrazine system.

### 5.3.3.4 Power Subsystem

The power architecture is based on solar arrays and batteries to provide a design power of 1900 W to the spacecraft. A solar array with 2 wings of two panels with total surface area of 9.8 m<sup>2</sup> supplies around 2300 W of power. Being built from 3G28 cells, the design can move to 3G30 cells for additional margin. Wings are actuated in two degrees of freedom to allow all angles of Sun-incidence during the mission.

A lithium-ion battery supports eclipses and safe mode with a capacity of 120 Ah (~ 6000 Wh). More stringent bus voltage control can be implemented, utilizing the battery at the expense of increased design size. Battery sizing is aligned with the longest eclipse as worst case.

The power control and distribution unit utilizes MPPTs and supplies a 50 V unregulated bus for instruments and most platform equipment. A 28 V regulated bus is used for additional payload items and some platform equipment.

### 5.3.3.5 Thermal Design

Wrapped in Kapton MLI, the payload module is protected from the external environment. The top  $+y$  panel serves as a radiator for the payload with an active surface area of 4.5 m<sup>2</sup>. Additional dedicated radiators for the optical link terminals are located on the  $\pm x$  panels, directly next to the units. The instrument units are regulated by heat-pipes, integrated into the mounting interface. Precise control to meet the required  $\pm 3$  K of temperature variations per orbit is assisted by heater lines with a total power of 45 W.

Like the payload module, the platform is covered in MLI with the exception of the optical solar reflector radiators distributed on the  $-z$  panel where highly dissipating units are located. The radiators provide a combined area of  $1.9 \text{ m}^2$ . No heat-pipes are foreseen in the service module. Heaters are integrated for propulsion, external components, and safe mode, delivering 85 W, as calculated for the worst case scenario.

**5.3.3.6 Command and Data Handling, Communications**

The spacecraft is controlled using a Leonardo-3G based system management unit. Again, the low data volume allows for using the integrated mass memory of 32 Gb, beginning of life ( $2 \times 16 \text{ Gb}$ ) embedded in the unit to store all telemetry data for at least 4 orbits (11 Gb). Connections to instruments are based on Spacewire bus, with a 1553 bus architecture provided to connect payload and platform units.

Communications with ground are established on a standard X-band system using GAIA heritage. Two low gain antennae provide full hemispherical coverage and transmit the required data volume within 2 h contact time with ground.

**5.4 Mass and Power Budget**

The mass budgets for the two design solution are presented below. The optical link as well as the atomic clock instrument have been treated separately as optional add-ons. However, additional mass reduction can be expected if the options are not integrated in the spacecraft due to second-order effects on system sizing. These were not taken into account here to give a more credible figure, should options be baselined as part of the payload configuration.

A significant mass difference exists between the two solutions, resulting from the two very different concepts and design choices. On the service module, the choices of power subsystem and AOCS architecture as well as structural design are the main contributors. Due to the choice of AOCS actuation, the propellant mass is disparate. For the payload module, the thermal subsystem represents the largest difference. The differences in the instrument masses between the two solutions stem from differing designs of the supporting payload elements as well as a slightly higher internal contingency – on top of the required one – in Solution A.

The mass is calculated with a subsystem/unit level margin based on the unit’s current Technology Readiness Level (TRL), with an additional 20% system level margin applied on the total mass, according to the applicable margin philosophy [SRE-PA (2011)]. Both designs show comfortable mass margin towards the launcher capacity, with additional launch margin available through optimization of the ascent trajectory.

<b>Mass Budget</b>	<b>Solution A</b>	<b>Solution B</b>
	Mass (kg)	Mass (kg)
<b>Service Module Total</b>	<b>780.4</b>	<b>498.8</b>
<b>Payload Module Total</b>	<b>603.5</b>	<b>515.9</b>
PLM Structure	168.0	153.0
PLM Instruments	316.5	279.0
<b>Total Dry Mass</b>	<b>1383.9</b>	<b>1014.5</b>
<b>Margin [SRE-PA (2011)]</b>	<b>277</b>	<b>203</b>
Propellant	258.8	95
<b>S/C TOTAL MASS (Core Payload)</b>	<b>2005</b>	<b>1428</b>
Target Launch Capacity	2350	2350
<b>Launch Margin (Target)</b>	<b>345</b>	<b>922</b>
Optical Link (optional)	122.96	117.20
Atomic Clock (optional)	146.6	136.5
<b>S/C TOTAL MASS (with options)</b>	<b>2327</b>	<b>1732</b>

The STE-QUEST power budget is dominated by the power demands of the instruments. The table below details the average power figures in the most demanding mode of operation, occurring during the perigee science phase in the baseline payload configuration. If the optical link (OL) is also present, the apogee science phase drives the STE-QUEST power demand. The total power figures of the different options are also reported below. No significant deviations exist here between the two proposed solutions.

<b>Power Budget (nominal)</b>	<b>Solution A</b>	<b>Solution B</b>
	Power (W)	Power (W)
Service Module Total	247	229
Payload Module Total	744	817
PLM Other	124	197
PLM Instruments	620	620
<b>Total Power (Core Payload)</b>	<b>1082</b>	<b>1046</b>
<b>Margin</b>	<b>217</b>	<b>209</b>
<b>S/C TOTAL POWER</b>		
Core Payload Instruments	1299	1255
Including Optical Link (optional)	1394	1472
Including Atomic Clock (optional)	1820	1904

## 5.5 Technical Risk Mitigation

Most of the spacecraft design stayed close to existing components and design practices. Nonetheless, some areas required focussed attention and a more novel approach. Risk mitigation has thus been addressed, especially in the area of the microvibration environment and the use of mechanisms as well as in the use of subsystems new on the market and proposed for use.

The microvibration environment at the instrument interface is challenging to predict in detail in early phases. Analyses have been conducted to assess the effects and in all areas. Where the results are at least one order of magnitude on the safe side, the risk has been considered as mitigated. Where this margin could not be established, mitigation measures have been proposed in case detailed calculations revealed violations. These include the use of dampers, structural stiffening or softening, as well as limiting the operating range of mechanisms, especially rotary equipment.

A special case arose for Solution B, where wheels are used for attitude control. With the same procedure as above, mitigation measures are identified, up to a switch from wheels back to cold gas actuation for the AOCS system, resulting in a higher total mass for Solution B.

For mechanisms without microvibration characterization, such tests will be integrated into the development.

Solution A uses 3G30 cells in the design. This cell is not yet qualified, although qualification is expected within the next few years. A fall-back exists in the use of 3G28 cells, which are fully qualified.

Radiation environment in Total Ionising Dose (TID) is commensurate with existing GEO qualified equipment. Instruments are well shielded inside the spacecraft. Critical components, not available in radiation hardened version, can be spot-shielded if required.

For the core payload configuration, not including the optional atomic clock and optical link, launch mass margins are highly comfortable at 345 kg in the lowest case, in addition to the 20% system level margins. The margins are expected to increase even further after optimizing the design on the basis of the core payload configuration. Likewise, several design simplifications – and thus risks reduction – are also expected. They will mainly affect the power generation and thermal systems.

## 5.6 Conclusion

A compliant orbit to the science objectives has been found, maximizing the measurement time at apogee, the duration of common-view contacts, and the measurement time along the orbit between apogee and perigee. The orbit had undergone multiple optimizations during the study leading to this solution, easing requirements on de-orbiting and increasing launch-able mass.

The assessment studies yielded technically feasible design solutions for the baseline including all options. Major area for detailed study remains the choice of AOCS systems between cold-gas and reaction wheels, with cold-gas representing the safest approach with more than sufficient margin towards the requirements. The instruments and payload items have been accommodated with respect to all their requirements. Both solutions maintain a positive launch margin to both target and maximum launch mass. For the core payload configuration, without the optional elements, the mission design is well below the launch margins; design simplifications will further enhance margins and reduce design complexity and risks.

No critical technologies nor a necessity to use new, unproven, technologies have been identified on platform side, employing to a large extent existing components. For any component without direct heritage, backup solutions are identified and available.



### 6.1.1 Level 0 (L0): Raw Data

The STE-QUEST L0 data are the spacecraft and payload raw data, the ground segment raw data as well as the required ancillary data after the following processes: format synchronisation, decoding, de-multiplexing, time tagging in various time scales (STE-QUEST on-board time, science link time, UTC, TAI, etc.), and sequence reconstruction. The information contained in these products shall permit to rebuild the general context in which the products have been generated and to fully re-process the data, if needed. In particular, each instrument data shall be linked to the STE-QUEST environment. L0 data consist of:

- Telecommands and configuration parameters sent to spacecraft and ground terminals;
- Raw spacecraft, payload, ground terminals, and ground clock telemetry data;
- Spacecraft and payload ancillary data (status, scheduled operations, orbit information data - velocity, position, attitude, etc.) and ground terminals ancillary data (meteorological data, solar activity, etc.);
- Operations data: operations plans, both for the payload and ground segment, operations requests, operations reports, mission timeline, etc.;
- STE-QUEST database.

### 6.1.2 Level 1 (L1): Engineering Data

L1 data products are Level 0 products converted into physical/engineering values and dated according to the same time scale (UTC, GPS, TAI, STE-QUEST on-board time, etc.) and reference frame (ITRF, BCRS, GCRS, etc.). They also include the offsets among the different ground and on-board time scales used for the L0 products time tagging. UTC or its best local realization UTC(k) is the preferred time scale; ITRF is the preferred reference frame for the STE-QUEST data.

### 6.1.3 Level 2 (L2): Quick-look Performance Data

L2 data products are L1 data processed in near real-time, with a delay only depending on link availability and low-level processing needed to generate the data product. They are mainly used to evaluate the status of the on-board instruments, of the science links as well as of the clocks on the ground. Clock comparisons will be here evaluated to a reduced performance level ( $< 1 \cdot 10^{-15}$ ) on the basis of quick-look orbit determination or even orbit prediction products. L2 data can be further classified as follows:

#### Level 2A (L2A): Instruments Performance Data

- Near real-time data generated from the on-board comparison of clocks and oscillators;
- Clocks frequency offset and uncertainty budget continuously updated: cold collisions, magnetic fields, blackbody radiation, distributed cavity phase shift, etc.;
- Link calibration measurements performed at the space and ground terminals;
- Differential acceleration measurements performed by the atom interferometer;
- Atom interferometer systematic effects continuously updated: magnetic field, residual non-gravitational accelerations, rotations and Coriolis effect, atomic trajectories, etc.

#### Level 2B (L2B): Quick-look Orbitography Products

L2B data are near real-time orbit determination, possibly orbit prediction products, necessary for evaluating the comparison of clocks on the ground with the on-board clock to a frequency uncertainty level of  $1 \cdot 10^{-15}$ .

#### Level 2C (L2C): Quick-look Clock Comparison Results

L2C data are near real-time clock comparisons during each passage over any ground terminal (see Sec. 6.4.2.1). This is a quick-look product based on L2B orbitography data and used to monitor the correct functioning of the clocks and the science links involved in the comparison.

### 6.1.4 Level 3 (L3): Full Performance Clock Comparisons Results

L3 data are the full performance results of the clock comparisons, evaluated on the basis of Precise Orbit Determination (POD) products. L3 data can be further classified as follows:

#### Level 3A (L3A): POD Data Products

L3A data are the POD products needed for evaluating clock comparison measurements to full performance.

#### Level 3B (L3B): Clock Comparisons Results

L3B data products are the full performance comparisons of clocks, based on the L3A orbitography product and the science link data (see Sec. 6.4.2.1).

### 6.1.5 Level 4 (L4): High-level Data

L4 data products are provided by the scientific community. They include:

- Regular reports on the continuous comparison between the reference clock providing the signal to the link ground terminal and additional clocks eventually available at the ground station: they include all the information needed to identify type, status, mode and performance of the available ground clocks;
- Ground clocks characterization measurements;
- Comparisons of the reference ground clocks via GPS and TWSTFT for UTC(k) generation;
- Results of the analysis performed on L2 and L3 data to achieve the STE-QUEST mission objectives: clock red-shift tests, Eötvös parameter measurements (see Sec. 6.4.2.2), comparisons of clocks on the ground, geopotential measurements, etc.;
- Scientific papers.

## 6.2 Mission Operations Elements

Mission operations elements are labelled in blue in Figure 6-1. They include:

- The ESA tracking station network ESTRACK, representing the direct interface through which the STE-QUEST spacecraft downloads telemetry (TM) and receives telecommands (TC);
- The Mission Operations Centre (MOC), coordinating all mission operations activities and implementing them within the mission boundaries and constraints;
- A distributed network of ground terminals (both in the microwave and optical domain), linked through the STE-QUEST time and frequency transfer system.

### 6.2.1 ESTRACK Network

The ESA tracking station network ESTRACK is a worldwide system of ground stations providing the necessary link between the orbiting spacecraft and the STE-QUEST Mission Operations Centre (MOC) at ESOC. ESTRACK stations are remotely controlled from the ESTRACK Control Centre at ESOC. Each of them hosts one or more terminals comprising an antenna and the associated signal processing system. Command uplink, telemetry downloading, and navigation services will be provided to STE-QUEST via ESA. Specific services that are provided to STE-QUEST include:

- Supporting the design and development of the STE-QUEST TM/TC communication units;
- Supporting the verification of the space-to-ground communications for telemetry and telecommands;
- Receiving spacecraft telemetry and ancillary data (L0) and routing them to the STE-QUEST MOC;
- Transmitting the telecommands received from the MOC to the STE-QUEST spacecraft;
- Delivering tracking, navigation data, event logs, and related ancillary STE-QUEST data to the MOC.

### 6.2.2 Mission Operations Centre

The Mission Operations Centre is responsible for the planning, the implementation and the correct execution of all spacecraft and ground network operations, for ensuring that the hardware is operated according to the established procedures, for providing the STE-QUEST Science Operations Centre (SOC) with all the mission telemetry and raw data. The main functions of the STE-QUEST MOC are described below.

#### 6.2.2.1 Monitoring and Control

MOC is responsible for monitoring and controlling the STE-QUEST spacecraft as well as the network of ground terminal interfacing STE-QUEST to ground clocks via the science link. Its functions include:

- Monitoring the spacecraft and the ground terminals telemetry;
- Monitoring status, health, and safety of both the spacecraft and the network of ground terminals;
- Conducting off-line performance analysis;
- Supporting the definition of telecommands and scheduled sequences for operating the spacecraft and the network of ground terminals;
- Implementing telecommands and scheduled sequences for operating the STE-QUEST spacecraft and the STE-QUEST ground terminals;

- Identifying anomalies, contributing to troubleshooting, and finally correcting them;
- Promptly intervening in case of anomaly with procedures to safeguard the STE-QUEST hardware;
- Coordinating activities related to spacecraft manoeuvres;
- Operating simulators for the validation of commands and procedures, for troubleshooting, and resolution of anomalies.

#### 6.2.2.2 Orbit and Attitude Control

Orbit and attitude control functions include the definition and implementation of all the operations needed to deliver the STE-QUEST spacecraft from launch into its final orbit and for manoeuvring it as required and according to the mission constraints. Navigation operations include:

- Performing trajectory and attitude analysis;
- Performing orbit prediction and determination based on available navigation data;
- Defining and implementing manoeuvres during the cruise and orbit injection phase;
- Defining and implementing orbit and attitude adjustment manoeuvres according to the mission plans during the STE-QUEST lifetime.

#### 6.2.2.3 Planning

Specific planning activities include:

- Generating the master schedule for the operation of spacecraft, payload and ground terminals; the master schedule is based on the inputs of the STE-QUEST Science Operations Centre (SOC);
- Integrating telecommands and scheduled sequences in the master schedule;
- Validating the master schedule against mission resources (power, data storage, link availability, etc.).

### 6.2.3 Distributed Network of Ground Stations

One of the strengths of the STE-QUEST mission resides in its networking potential. STE-QUEST is a distributed system able to connect clocks on the ground in a global network enabling cross comparisons of clocks on a worldwide scale. In this respect, the network of ground station is as important as the STE-QUEST satellite and its scientific payload. By the time of the mission, the three ground stations (Turin (I), Tokyo (JP), and Boulder (US)) will distributed time and frequency (by optical fibre or other) to many other users and laboratories world-wide. For example, an optical fibre network interconnecting about a dozen laboratories and metrology institutes in Europe, including the ground stations selected for STE-QUEST is already being established to date. As experienced for the ACES mission, it is likely that when nearing launch additional institutes will become interested in hosting ground stations and will find funding to do so. That will increase the networking potential of STE-QUEST to the mutual benefit of all partners.

The STE-QUEST ground terminals are microwave stations interfacing the local clocks on the ground to the STE-QUEST frequency reference. Microwave and optical (optional) ground terminals will be remotely controlled by the MOC according to the STE-QUEST master schedule. In each terminal, a computer drives the steering unit based on the STE-QUEST orbit prediction files, it collects telemetry and science data both from the local clocks and the terminal electronics, and interfaces directly with the STE-QUEST MOC where telemetry and housekeeping data are downloaded.

## 6.3 Science Operations Elements

Science operations elements are labelled in green in Figure 6-1. They include:

- The Science Operations Centre (SOC), coordinating all science operations activities, responsible for optimizing the scientific return of the mission and for its exploitation;
- The Archive, a complete repository of all the raw and processed data, maintained by SOC;
- The Data Processing Centres (DPCs), responsible for processing mission data and for generating higher level data products;
- The Instrument Operations Centres (IOCs), responsible for near real-time monitoring and control of the STE-QUEST instruments as well as for analysing and processing instrument data;
- The Orbitography Data Centre (ODC), responsible for orbit determination and prediction products.

### 6.3.1 Science Operations Centre

The Science Operations Centre is developed and operated by ESA. It defines the STE-QUEST science operations at spacecraft, instruments, and ground segment level; it coordinates the analysis and processing of the science data as well as the archiving of raw data and mission data products (L0 to L4). It is directly interfaced to the STE-QUEST Archive, the central hub to which all involved entities and data processing centres are also connected. SOC main functions are described below.

#### 6.3.1.1 Science Operations

The STE-QUEST SOC is the unique point of contact with the MOC on matters relevant for science planning, science operations, and related telecommands requests, involving both the space hardware and the network of ground terminals. Specific activities include:

- Performing the scientific mission planning for spacecraft and instrument operations;
- Planning spacecraft operation requests as needed during the commissioning, calibration, and routine science phases;
- Planning instruments operation requests as needed during the commissioning, calibration and routine science phases;
- Defining the clock comparisons sessions and scheduling ground terminals operations;
- Monitoring, in collaboration with the IOCs, the scientific performance of the STE-QUEST payload and the ground network and timely notifying the MOC in case of anomaly;
- Supporting the IOCs in their tasks and interactions via dedicated Instrument Operations Scientists;
- Supporting troubleshooting activities in case of anomaly and malfunction;
- Maintaining a copy of the full STE-QUEST simulator used by the MOC for procedures validation;
- Maintaining an electronic archive of project documentation, e.g. instrument performance documents, operation manuals, telemetry parameters, list of ground clocks, etc..

#### 6.3.1.2 Data Processing

It is SOC responsibility to coordinate the data analysis effort and supervise the correct archiving of the STE-QUEST data and data products. Specific activities include:

- Processing raw payload and ground segment data and generating engineering data products (L1);
- Based on the algorithms developed by DPCs, providing quick-look analysis (L2) of the STE-QUEST data for near real-time monitoring of the STE-QUEST scientific performance.

#### 6.3.1.3 Archiving

Data archiving activities include:

- Supporting the definition of guidelines and standards (architecture, standards, configuration control, etc.) for data analysis and archiving;
- Taking responsibility for validating the STE-QUEST data and data products by applying all the necessary quality controls before their archiving;
- Archiving raw data, telemetry and higher level data products;
- Taking responsibility for the operation and maintenance of the STE-QUEST Archive.

#### 6.3.1.4 Users Support

The STE-QUEST SOC is responsible for the definition, the operation, and the maintenance of the interface between the STE-QUEST Archive and the community of external users. Specific activities include:

- Providing helpdesk support and documentation for users, in collaboration with the IOCs and DPCs;
- Providing and maintaining the mission web portal;
- Providing data analysis tools developed by the DPCs;
- Organising, in collaboration with the DPCs and IOCs, user support and data analysis workshops;
- Supporting the organisation of mission-related scientific meetings and conferences;
- Provide a catalogue of the STE-QUEST publications, possibly linked to the relevant Archive data.

### 6.3.2 Instrument Operations Centre

The on-board instruments will be monitored by the STE-QUEST Instrument Operations Centres. IOCs are assumed to be developed and operated under national funds. ESA will support these activities through the

Instrument Operations Scientists, who will provide full visibility on instrument monitoring and characterization aspects. IOC activities include:

- Supporting the STE-QUEST SOC in the definition of the instrument operations and generating requests for telecommands and scheduled sequences;
- Requesting changes in the instrument configuration to the STE-QUEST SOC when needed;
- Analysing instrument data (L1), generating higher level data products directly related to the instrument, and uploading them in the STE-QUEST Archive after all the necessary quality controls;
- Supporting the SOC in the near real-time monitoring of the on-board instruments;
- Monitoring the instrument performance and interacting with the SOC for scheduling periodic measurement campaigns to regularly check and improve it along the mission lifecycle;
- Supporting the maintenance of the instrument on-board software;
- Supporting troubleshooting activities in case of anomalies in the instrument operations.

### **6.3.3 Orbitography Data Centre**

Orbit information is important both for quick-look performance analysis and for evaluating the science data products of the mission. ODC will be responsible for providing the orbitography products required by STE-QUEST for scientific purposes. This specific function could also be integrated either in the DPCs or at the MOC. ODC activities include:

- Supporting the STE-QUEST SOC in the definition of the orbitography products;
- Defining the algorithms for the processing of available navigation data (GNSS and science link data);
- Developing and maintaining the orbitography processing software;
- Providing L2B and L3C data products;
- Validating L2B and L3C data by applying the necessary quality controls before archiving.

### **6.3.4 Data Processing Centre**

The analysis of the clock comparisons and the processing of the differential acceleration measurements are the key DPCs activities (see Sec. 6.4.2).

The importance of data analysis for the mission success, the precision and confidence that needs to be reached in the evaluation of an eventual EEP violation, the correct evaluation of instruments accuracy budgets, and the level of processing required for the generation of the final data products requires at least two DPCs analysing independently the two main science data products of STE-QUEST, the differential acceleration measurements and the clock comparison measurements. The DPCs are expected to work in parallel on the same science data, perform cross-checks and compare the final results. DPCs are assumed to be developed and operated under national funds. Their activities include:

- Defining the scientific algorithms for the processing of clock comparisons;
- Developing and maintaining the data processing software;
- Developing and operating simulation tools to validate and cross check the data processing software;
- Supporting SOC in the implementation of data analysis algorithms for operational purposes (L2C and eventually L3B);
- Providing L3B and L4 data products;
- Taking responsibility for validating L3B and L4 data products by applying all the necessary quality controls before their archiving;
- Interfacing with the twin DPC for cross-checks and comparisons of the results.

### **6.3.5 Data Archive**

The STE-QUEST Archive is a central repository with a unique interface for all the information that is relevant to the STE-QUEST mission. It is located at ESAC, under SOC responsibility.

#### **6.3.5.1 Archive Content**

The content of the Archive falls into the following general categories, according to the nature of the data:

- STE-QUEST data and data products (L0 to L4) and mission database;
- Downloadable software: Data analysis algorithms and toolsets developed by the STE-QUEST DPCs will be stored and made available in case of later re-processing needs;

- Non-downloadable software: Software, mainly related to operations, not intended to be retrieved or run by an end user, stored for configuration control and traceability (e.g. on-board software).
- Simulator: The full STE-QUEST simulator used by the MOC for running procedures validation.
- Project documentation: All documents (filed in electronic form) relevant to the STE-QUEST scientific data and instruments performance, operations manuals, STE-QUEST catalogues (e.g. list of telemetry parameters, list of available products), accessible through proper interfaces.
- Scientific papers: A catalogue of refereed papers, which publish STE-QUEST results will be, as far as possible, assembled and maintained; publications will be linked to the relevant STE-QUEST data.

#### 6.3.5.2 General Capabilities of the Archive Interface

The main features of the STE-QUEST Archive are the content and the speed, as well as the flexibility and friendliness of the access to those contents. In general, the Archive is required to be friendly for the novice user, flexible for the expert user, and reasonably fast for all users. The Archive must protect the proprietary status of data that has not yet become public.

The search interface for the general user consists of standard pre-defined, yet flexible, queries, with the majority of search parameters indexed for rapid access. The interface for expert users shall permit searches against all queryable contents of the STE-QUEST Archive. It is necessary that the expert user has great flexibility at hand, including the possibility of using high-level languages (e.g. SQL) to write queries. The search interface shall provide quick (i.e. a few seconds) feedback on the expected results of a query in terms of number of matching items. The results shall be sortable according to customisable parameters (e.g. time, length of data taking, ground clock type, ground clock position, experiment type, etc.). Users shall be able to specify which data products for which runs they want to retrieve and they shall be given options on the mode of retrieval. It shall be possible to save search results in different formats: ASCII, Matlab Binary (TBC), XML, HTML (TBC).

## 6.4 Data Handling

### 6.4.1 Data Flows

STE-QUEST data flows are shown in Figure 6-2. Raw data generated by the STE-QUEST spacecraft and ground terminals (L0) are routed to the MOC, where they are used for basic monitoring and health status checks. MOC provides SOC with both near real-time raw data and a consolidated version of them, obtained at the MOC after gaps removal and integrity checks. Near real-time data are used for quick look analysis. SOC is responsible for the generation of L1 data products as well as L2 data products other than the instrument-related ones. Raw data (L0) and processed L1 and L2 data are ingested in the STE-QUEST Archive in near real-time. From there and in near real-time, they are made available to IOCs and DPCs. IOCs retrieve instrument-related L1 data from the Archive and process them to generate instrument L2A products. Orbitography products, both quick look (L2B) and full performance ones (L3A), are generated by the STE-QUEST ODC. Orbit determination and prediction services can eventually be provided by ESA/ESOC or DPCs. DPCs are responsible for the generation of L3B and L4 data products. Data received from each centre will be archived and tagged with information on their provenance and on the software used for their generation. DPCs are assumed to be provided by the Payload Consortium(a), although one centre might be located at the SOC, supported by the Payload Consortium(a).

### 6.4.2 Data Processing

In this section we describe the data analysis steps leading to the final scientific products of the mission:

- Differential acceleration measurements by atom interferometry and evaluation of the Eötvös parameter;
- Clock comparison measurements.

The data processes outlined here will be implemented and run by the STE-QUEST DPCs for the generation of L3b and L4 data products as well as by SOC for the generation of L2 quick-look data.

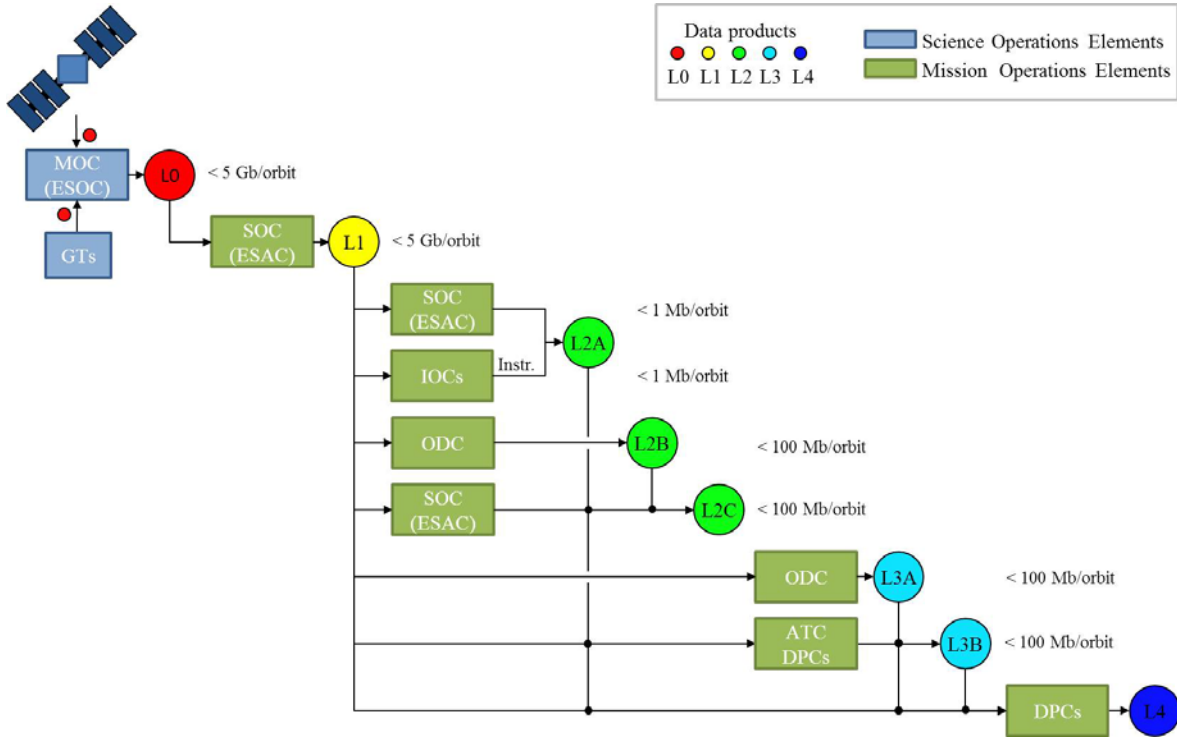


**Figure 6-2:** Data flows and generation of the STE-QUEST data products. The schematic also provides a rough order of magnitude of the expected data volumes per orbit

**6.4.2.1 Clock Comparison Measurements**

As discussed in Sec. 4.1.2.1, the comparison of two ground clocks in common-view is obtained from the difference of simultaneous space-to-ground comparisons with the on-board frequency reference (USO or optional atomic clock). Therefore, following the data analysis approach proposed in DUCHAYNE (2008) and DUCHAYNE (2009), we will discuss how to process the data resulting from individual space-to-ground comparisons. MWL operation is shown in Figure 6-3. The uplink signal with frequency  $f_1$  is coherently generated from the ground clock at coordinate time  $t_1^0$  and emitted at  $t_1$  from the terminal antenna. After propagation through the atmosphere, it reaches the flight segment antenna at coordinate time  $t_2$  and its time of arrival is measured with respect to the space clock at coordinate time  $t_2^0$ . Similarly, the two downlink signals with frequency  $f_2$  and  $f_3$  are coherently generated from the space clock and emitted towards the ground station. Each end of the link measures the delay between the incoming code sequence (carrier cycle) and the same sequence of code (carrier cycle) generated at the terminal, in the local clock timescale ( $\tau^s$  or  $\tau^g$ ):

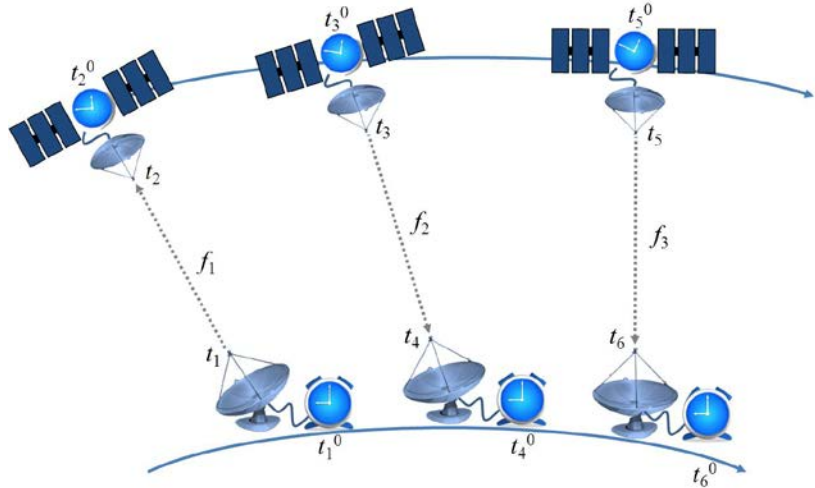


**Figure 6-3:** Architecture of the STE-QUEST microwave link. Both code and carrier phase delay measurement are provided for each of the three frequencies in the link ( $f_1$ ,  $f_2$ , and  $f_3$ ), corresponding to a total of 6 observables.

$$\begin{aligned}
 \Delta\tau^s(\tau^s(t_2^0)) &= \tau^g(t_1^0) - \tau^s(t_2^0) = \text{Desynch}(t_2^0) - \left[ [\Delta_{T_{X_1}}^g]^t + T_{12} + [\Delta_{R_{X_1}}^s]^t \right]^g \\
 \Delta\tau^g(\tau^g(t_4^0)) &= \tau^s(t_3^0) - \tau^g(t_4^0) = -\text{Desynch}(t_4^0) - \left[ [\Delta_{T_2}^s]^t + T_{34} + [\Delta_{R_{X_2}}^g]^t \right]^s \\
 \Delta\tau^g(\tau^g(t_6^0)) &= \tau^s(t_5^0) - \tau^g(t_6^0) = \text{Desynch}(t_6^0) - \left[ [\Delta_{T_{X_3}}^s]^t + T_{56} + [\Delta_{R_{X_3}}^g]^t \right]^s
 \end{aligned}
 \tag{6-1}$$

Both a code and a carrier phase delay measurement is performed for each of the three link frequencies  $f_1, f_2,$  and  $f_3$ , providing a total of 6 observables. As shown in Equations (6-1), the link observables are expressed in terms of the desynchronization,  $\text{Desynch}(t^0) = \tau^g(t^0) - \tau^s(t^0)$ , between the space clock and the ground clock, the instrumental delays  $\Delta_{\text{Tx,Rx}}^{s,g}$  in transmission (Tx) and reception (Rx) at the space (s) and ground (g) terminal for the three link frequencies, and the propagation delays  $T_{ij} = t_j - t_i$ , expressed in coordinate time.  $T_{ij}$  accounts for the free travel time of the link signal between space and ground as well as for the atmospheric propagation delays (troposphere, ionosphere). [...]  $^{s,g}$  represents the transformation of a coordinate time interval into a proper time interval of the local clock in space or on the ground:

$$[T_{12}]^s = \int_{t_1}^{t_2} \left( 1 - \frac{U(t, \mathbf{x}^s)}{c^2} - \frac{\mathbf{v}^s(t)^2}{2c^2} \right) dt, \tag{6-2}$$

where  $U(t, \mathbf{x}^s)$  is the gravitational potential at the clock position;  $\mathbf{v}(t)$  and  $\mathbf{x}^s(t)$  are the clock position and velocity in the selected reference system. In a similar way, [...]  $^t$  defines the transformation of the proper time interval  $\tau_{12}^s = \tau_2^s - \tau_1^s$  into the corresponding coordinate time interval:

$$[\tau_{12}^s]^t = \int_{\tau_1^s}^{\tau_2^s} \left( 1 + \frac{U(t, \mathbf{x}^s)}{c^2} + \frac{\mathbf{v}^s(t)^2}{2c^2} \right) d\tau^s. \tag{6-3}$$

These terms embed the relativistic effects of interest for STE-QUEST: gravitational red-shift and second-order Doppler effect. The goal of the data analysis software is therefore to provide:

- A TEC measurement along the line of sight. This data product is obtained from the combination  $\Delta\tau^g(\tau^g(t_4^0)) - \Delta\tau^g(\tau^g(t_6^0))$  and it is used for the evaluation of the ionospheric delay.
- The desynchronization between the space and the ground clock to the required stability and accuracy levels (see Sec. 3.3.2.1). This is the main data product of the STE-QUEST link and it can be obtained from  $\Delta\tau^s(\tau^s(t_2^0)) - \Delta\tau^g(\tau^g(t_4^0))$ .
- The total propagation delay, including the contribution of both the range and the troposphere. The round trip time of the link signal is obtained from  $\Delta\tau^s(\tau^s(t_2^0)) + \Delta\tau^g(\tau^g(t_4^0))$ . This data product will allow to estimate the range on the basis of available tropospheric models or to measure the tropospheric propagation delays through an independent range determination (e.g. GNSS).

Figure 6-4 shows input data and scientific products of the STE-QUEST link processing software. Orbit

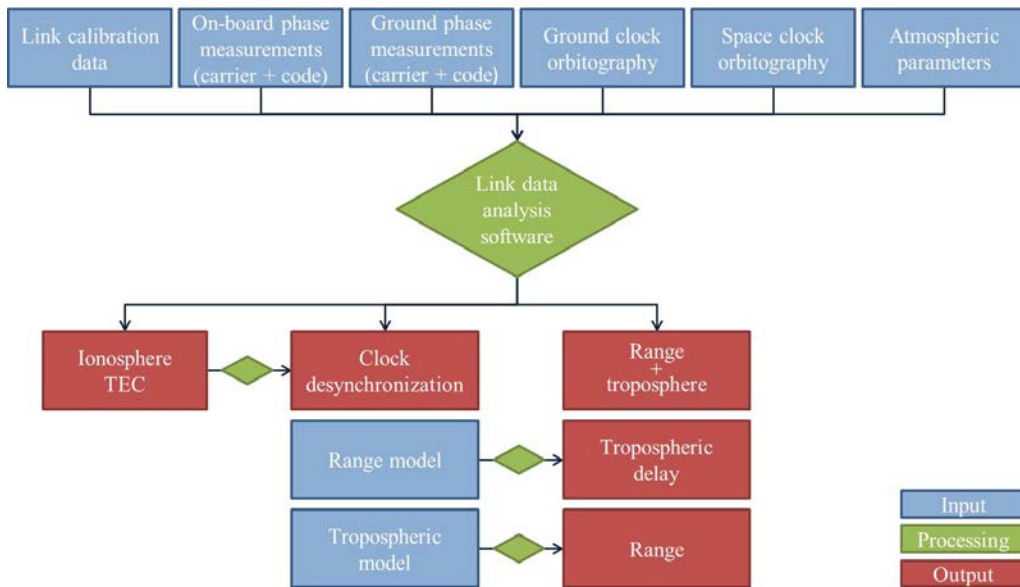


Figure 6-4: Input data and scientific products of the science link processing software.

determination of the space clock and positioning of the clocks on the ground are essential to correctly evaluate the measurement results (see Sec. 3.3.2.1). As shown in DUCHAYNE (2008) and DUCHAYNE (2009), the effect of inaccuracies in the orbit determination of the space clock can be drastically reduced by operating the asynchronous link in the so called  $\Lambda$ -configuration, with  $t_2 = t_3$ . Matching the  $\Lambda$ -configuration requires the calibration of absolute instrumental delays, both in transmission and reception, at the flight and ground terminal electronics. A set of additional calibration data needed for the link operation (including for

instance the calibration of the flight segment antennae phase patterns) as well as ancillary information (e.g. temperature, pressure, humidity at the ground stations) enter the data analysis software for the generation of the final products.

The analysis of the STE-QUEST space-to-ground clock comparisons will benefit from the software already developed for the ACES mission. The ACES data analysis software is described in MEYNADIER (2011). The code includes algorithms for measuring and controlling the instabilities introduced by atmospheric propagation delays (ionosphere and troposphere), for the correct identification of phase ambiguities and cycle slips and for the evaluation of relativistic effects. The software has already been tested on simulated data having the same noise behaviour measured during the engineering model tests of the ACES MWL.

#### 6.4.2.2 Determination of the Eötvös Parameter

Testing the Universality of Free Fall at the level of one part in  $10^{15}$  implies a measurement of the differential acceleration between the two atomic species at the same level of relative uncertainty. The measurement uncertainty is constantly evaluated during the mission lifetime by performing dedicated measurements to characterize the instrument systematic shifts Sec. 4.1.1. As gravity acceleration  $g$  decreases with the distance from Earth, the signal measuring an eventual WEP violation is maximized when the differential atom interferometry instrument is operated close to Earth. This naturally defines two distinct operational phases of the atom interferometry instrument: differential acceleration measurements around the perigee of the STE-QUEST orbit are used for WEP tests; instrument calibration measurements are then performed during the remaining fraction of the orbit and in particular around apogee where spacecraft rotations and residual accelerations are minimized.

The data processing of the atom interferometry measurements can therefore be summarized as in Figure 6-5. Atom interferometry measurements are corrected for systematic effects and combined with the local acceleration of gravity to provide a measurement of the Eötvös parameter. The gravitational acceleration is obtained from Earth gravity models on the basis of orbit information data. The ultimate measurement sensitivity is reached by averaging over the mission lifetime (see Sec. 3.3.1.3).

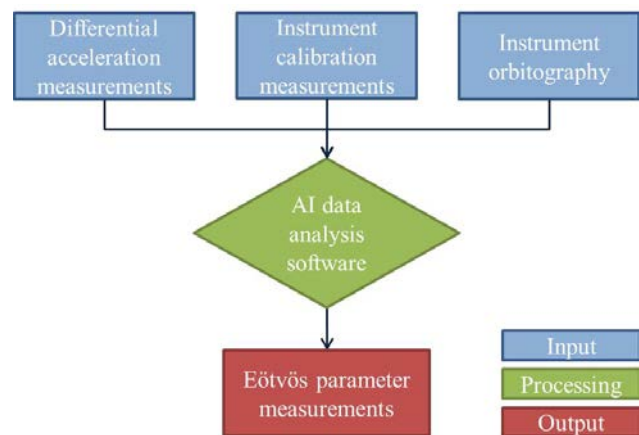


**Figure 6-5:** Input data and scientific products of the software processing the atom interferometry measurements performed by STE-QUEST.

#### 6.4.2.3 STE-QUEST Data Analysis Challenge

Maximizing the scientific return of the mission requires the development of a data analysis infrastructure commensurate with the challenges imposed by STE-QUEST in the comparison of distant clocks and in the measurement of differential accelerations. STE-QUEST will allow comparisons of clocks on the ground down to  $1 \cdot 10^{-18}$ . Reaching such frequency uncertainty levels requires correct modelling of the relativistic effects, control of the noise sources and correct calibration of instrumental effects, control of atmospheric propagation delays, modelling of the link measurement process. To some extent, the analysis of clock comparison data is similar to the activity of the International GNSS Service (IGS) analysis centres. At the same time, the atom interferometer will provide differential acceleration measurements down to the  $1 \cdot 10^{-15}$  level, where control of systematic effects becomes challenging.

Therefore, the robustness of the final result will strongly rely on the availability of several data centres (see Figure 6-1) able to work in parallel on the basis of independent data analysis software and constantly running cross checks and comparisons. During the development and debugging phase, the STE-QUEST data centres will work on independent codes both for measurements simulation and for their analysis. This would allow to run data analysis challenges between centres in which data simulation activities are completely decoupled from their processing. After their validation, the availability of independent data centres becomes essential in the operational phase to correctly interpret the measurements and to ensure confidence in the final result, particularly in case a violation of the Einstein Equivalence Principle is found.

# 7 Management

## 7.1 Project Management

ESA, through its Directorate of Science and Robotic Exploration will lead the development, launch, and operations of STE-QUEST. ESA is responsible for the development, integration, test, verification, and timely delivery of the spacecraft, as well as development and delivery of STE-QUEST MOC and SOC. Management and control of spacecraft bus and payload interfaces will be led by ESA.

For these activities, ESA appoints a Project Manager, who implements and manages ESA's responsibilities during the development and implementation phases, until launch and system commissioning.

The ESA Project Manager will be directly supported in the execution of the programme by the engineering, administrative, and project control staff of the ESA Project Office. The Project Office will hand over responsibility of the mission to the ESA Mission Manager after system commissioning.

The Mission Manager takes responsibility for spacecraft operations, the payload, and the ground segment, excluding the nationally funded IOCs and DPCs.

A Science Team will be appointed by ESA and, chaired by the Project Scientist, will develop the science strategy and guide science operations planning and execution.

## 7.2 Procurement Philosophy

### 7.2.1 System Procurement

On system level, the Definition Phase (B1) is conducted in parallel competitive contracts. A single system prime will be chosen through open competition after Mission Adoption for the Implementation Phase (B2/C/D). The industrial structure will take into account the geographical distribution requirements. The industrial prime will deliver the fully integrated system to ESA and be responsible for design, manufacturing, integrations, testing, and verification of the spacecraft. ESA will control and monitor the activities.

### 7.2.2 Payload Procurement

The STE-QUEST payload suite is divided into ESA provided elements and instruments under the responsibility of the PI-led consortia. ESA provided elements are the microwave time & frequency link and the GNSS receiver, which follow the system procurement philosophy and are contracted under prime responsibility. PI-provided instruments are the differential atom interferometer and eventually the atomic clock (optional payload element). The optional optical link will follow the instrument procurement scheme.

All instrument components and support equipment will be provided by instrument consortia, led by a Principal Investigator and funded through National Funding Agencies. The Lead Funding Agencies (LFAs) assume full responsibility for instruments development and their delivery to ESA as well as the necessary operations support, data processing, and archiving. The instruments will be delivered functional and performance tested and will, upon receipt by ESA, be supplied to the prime as Customer Furnished Items (CFI) for integration. The commitments, roles, and responsibilities between ESA and the LFA(s) will be formalized via multi-lateral-agreements.

## 7.3 Schedule

A tentative schedule has been developed and is shown in Figure 7-1, assuming a mission selection in the first quarter of 2014. Following the selection, the Definition Phase (B1) system studies are expected to be started in mid-2014 for about 16 months. Together with the System Requirements Review in the fourth quarter of 2015, this enables the final Mission Adoption in the first quarter of 2016. The planned launch date has been set to 2024, while requiring compatibility with a 2022 launch date, pending the decision on the L1 (JUICE) launch date. For the schedule, a 2022 launch date has been assumed with a requirement to be compatible with an additional two years of storage, to fulfil the requirements on the earlier launch date.

The first Definition Phase (B1) is concluded by the System Requirements Review. Technology activities will run in parallel to increase the TRL of any unit to at least TRL 5, if necessary. Upon successful completion of the SRR and the final Mission Adoption, the mission goes into Implementation Phase (B2/C/D). The start of phase B2/C/D is foreseen for the third quarter of 2016. Within this phase, the Preliminary Design Review

(PDR), Critical Design Review (CDR), and Flight Acceptance Review (FAR) constitute the major milestones. The implementation phase is scheduled for < 6.5 years, including a schedule contingency of 6 months, considered adequate for a relatively standard platform design, and given the non-critical launch date from a mission analysis point of view.

Instrument development follows a parallel, similar schedule. Upon Mission Selection, the instrument consortia will commence the instrument definition phase and enter implementation after Mission Adoption. Before Mission Adoption, instrument maturity has to approach TRL 5. Instrument reviews are aligned with the system level reviews and key delivery dates are indicated in Figure 7-1.

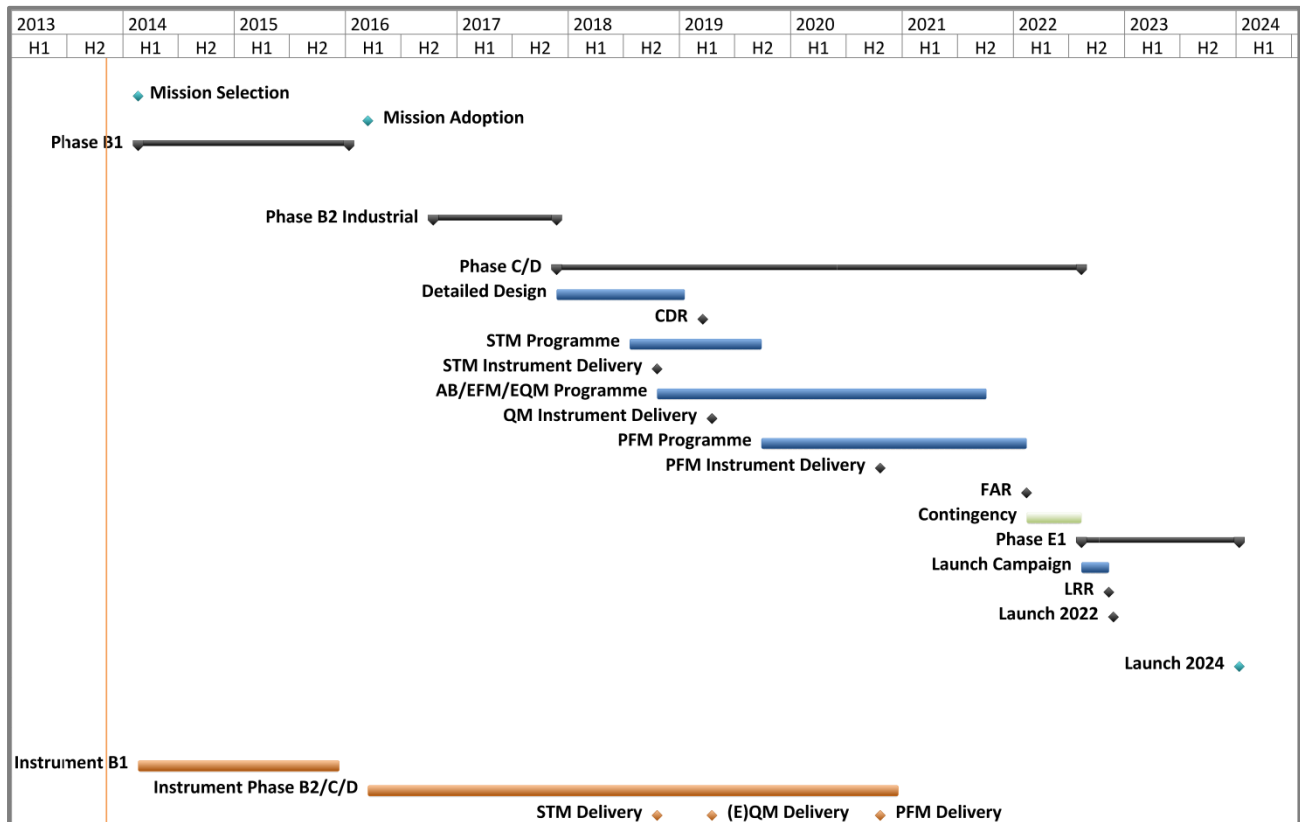


Figure 7-1: Tentative schedule for the STE-QUEST mission starting from phase B1.

## 7.4 Science Management

The success of STE-QUEST is directly related to the proper definition of mission objectives and scientific requirements, their translation in terms of instruments performance, the delivery of instruments and subsystems satisfying such performances, their correct integration in the payload, the definition and implementation of an adequate mission plan, the preparation of the scientific algorithms for data analysis, the generation and the exploitation of the STE-QUEST mission products. From this point of view, the STE-QUEST Science Team has a key role in:

- Defining and maintaining the STE-QUEST mission objectives and scientific requirements; STE-QUEST mission objectives and scientific requirements are reviewed and approved by ESA;
- Supporting the development and the implementation of the STE-QUEST mission during all its phases to ensure fulfilment of the STE-QUEST mission objectives and scientific requirements;
- Supporting the definition of verification procedures and criteria of the STE-QUEST scientific performances and for the implementation of the verification tests;
- Supervising the development of the STE-QUEST instruments in line with the established performance requirements;
- Defining the scientific algorithms for data analysis and mission products exploitation;
- Supporting the definition of an optimized utilization and exploitation plan of the STE-QUEST mission;

- Analysing and exploiting the STE-QUEST data and data products;
- Validating the scientific products of the STE-QUEST mission before their release to the scientific community;
- Within the data established right policy, overseeing publications of results by proprietary data holders and ensuring that they meet adequate scientific standards;
- Supporting promotion, communication, and outreach activities.

#### 7.4.1 The ESA Project Scientist and the STE-QUEST Science Team

The STE-QUEST Science Team monitors and advises the ACES Project/Operations Team on all aspects affecting STE-QUEST scientific performance. The following key roles have been identified in the Science Team:

- The **ESA Project Scientist (PS)**, representing the link between the Science Team and the STE-QUEST Project/Mission Operations Management in ESA;
- The **Instrument Consortium Coordinator/s (ICC)**, focal point for the science-related aspects as well as the scientific performance of the STE-QUEST instrument/s;
- The **Data Analysis Coordinator/s (DAC)**, responsible for the definition of scientific algorithms for data analysis, data analysis, mission products generation, and exploitation;
- The **Ground Clocks Coordinator (GCC)**, acting as focal point for the coordination activities and the monitoring of the ground network of atomic clocks participating to STE-QUEST;
- The on-site **Ground Clock Responsible/s (GCR)**, in charge of on-site verification, operation, and maintenance of the ground clocks contributing to STE-QUEST network.

The PS is the ESA interface with the Science Team. Within ESA, he liaises with the STE-QUEST Project Manager and the STE-QUEST Project Team until completion of in-orbit commissioning and afterwards with the STE-QUEST Mission Operations Management. He chairs the Science Team and coordinates its activities. The ESA PS keeps the Science Team informed about the STE-QUEST mission activities managed by ESA. During all the mission phases, the ESA PS supports the STE-QUEST project team to ensure the correct implementation of established scientific requirements. During the operational and post operational phase, the ESA PS will participate to the generation of the scientific products, their archival, and distribution to the scientific community.

The Science Team members meet regularly. When needed, ad-hoc experts can also be invited to attend the meetings. In addition to regular meetings, there will be, when needed, splinter meetings to address and solve specific problems. The Science Team members are appointed for the full duration of the program.

#### 7.4.2 STE-QUEST Data Policy

Data directly resulting from the STE-QUEST spacecraft and ground segment (raw and calibrated data) are owned by ESA and are provided by ESA to the STE-QUEST Science Team for analysis and publication of the scientific results.

The STE-QUEST Instrument Consortia and Science Team will coordinate an optimal utilization and exploitation plan of the STE-QUEST data and data products. External users interested in participating to the STE-QUEST data analysis shall apply to ESA. Upon positive evaluation of the data analysis proposal by the STE-QUEST Science Team and after ESA approval, the responsible scientists are entitled to access the complete STE-QUEST data or part of it for analysis and publication of the results.

ESA will grant a right of prior access to the STE-QUEST data for scientific analysis and first publications for a period of one year, beginning on the date of receipt of the data in a form suitable for analysis and after their validation by the STE-QUEST Science Team. During this period, access to the data will be limited to:

- Members of the Science Team, and their support teams;
- Members of the Science Operation Centre;
- Members of the Data Processing Centres;
- Members of the Instrument Operations Centres;
- Members of the Instrument Consortia;
- Accredited external users.

During the proprietary period, all scientific publications require validation and approval by the STE-QUEST Science Team. However, such a review shall not unduly withhold the publication and shall be carried out within a reasonable time.

All data shall be protected, distributed, stored and handled by ESA in accordance with the applicable data policy. Arrangements shall be made with the STE-QUEST users so that they are committed to:

- Expeditiously provide to ESA an analysis of the results obtained from the planned scientific investigations;
- Take all reasonable steps to make these results available to the scientific community, or alternatively, authorize ESA to do so, through publication in appropriate journals or other established channels as soon as possible and consistent with good scientific practice.

## 8 Communications and Outreach

The STE-QUEST mission will be given proper importance and visibility within the framework of the communication activities of the ESA Science Programme.

ESA, the STE-QUEST Instrument Consortia, and the Science Team have the duty to exploit the outreach and educational potential of the mission. They develop plans and secure the necessary resources to inform the general public, to produce education and outreach material such as high quality website, booklets, school material, press releases, popular science-level material, simulations, audio-visual, etc.

During the development phase of the mission, ESA will set up web pages on the STE-QUEST mission as an information tool for the general public and the media. With the progress of the mission the web pages will be enriched with more material and features.

Press releases and public events will be organized by ESA to inform the public about major events during the mission lifecycle, e.g. STE-QUEST launch, first results, completion of the data analysis and release of the mission data and data products to the public.

ESA is responsible for planning and coordinating education and outreach activities related to STE-QUEST.

A Communications and Outreach Plan will be developed and jointly executed by ESA, the Instrument Consortia, and the Science Team. The following guidelines are applicable:

- ESA has the lead on the execution of all education and outreach activities of STE-QUEST within the data rights framework outlined in Sec. 7.4.2;
- Members of the STE-QUEST Instrument Consortia and Science Team have the duty to support ESA with respect to communications, education, and outreach activities;
- ESA gives credit to members of the STE-QUEST Instrument Consortia and Science Team regarding scientific and technical results when applicable;
- ESA reserves the right to use any data-set for education and outreach purposes.

The Project Scientist will initiate and publish project-related progress reports and reviews of scientific results from the mission. Scientific articles suitable for public release will be provided by the members of the STE-QUEST Science Team, upon their own initiative or upon request from the Project Scientist, at any time during the development, operational, and post-operational phases of the mission.

## Acronyms

<b>ACES</b>	Atomic Clock Ensemble in Space	<b>GEOSS</b>	Global Earth Observation System of Systems
<b>A/D</b>	Analogue/Digital	<b>GGOS</b>	Global Geodetic Observing System
<b>AIV</b>	Assembly, Integration, and Test	<b>GLONASS</b>	GLObalnaya NAVigatsionnaya Sputnikovaya Sistema
<b>AOCS</b>	Attitude and Orbit Control System	<b>GNSS</b>	Global Navigation Satellite System
<b>ASAP</b>	Arianespace System for Auxiliary Payloads	<b>GR</b>	General Relativity
<b>ATC</b>	ATomic Clock	<b>GRACE</b>	Gravity Recovery And Climate Experiment
<b>ATI</b>	ATom Interferometer	<b>GRASP</b>	Geodetic Reference Antenna in Space
<b>BBN</b>	Big Bang Nucleosynthesis	<b>GOCE</b>	Gravity Field and Steady-State Ocean Circulation Explorer
<b>BEC</b>	Bose-Einstein Condensate	<b>GRACE</b>	Gravity Recovery And Climate Experiment
<b>BEH</b>	Brout-Englers-Higgs	<b>GT</b>	Ground Terminal
<b>CCD</b>	Charge-Coupled Device	<b>ICC</b>	Instrument Consortium Coordinator
<b>CDF</b>	Concurrent Design Facility	<b>ICE</b>	Interferometrie Coherente pour l'Espace
<b>CDMU</b>	Command and Data Management Unit	<b>ICRF</b>	International Celestial Reference Frame
<b>CFI</b>	Customer Furnished Item	<b>ICU</b>	Instrument Control Unit
<b>CHAMP</b>	CHALLENGING Minisatellite Payload	<b>IF</b>	Intermediate Frequency
<b>COTS</b>	Commercial Off-The-Shelf	<b>IGS</b>	International GNSS Service
<b>CPT</b>	Charge conjugation, Parity, Time reversal	<b>IMU</b>	Inertial Measurement Unit
<b>CST</b>	CaeSium Tube	<b>IOC</b>	Instruments Operations Centre
<b>DAC</b>	Data Analysis Coordinator	<b>IPTA</b>	International Pulsar Timing Array
<b>DE</b>	Dark Energy	<b>ISS</b>	International Space Station
<b>Delta-DOR</b>	Delta-Differential One-way Range	<b>JASON</b>	Joint Altimetry Satellite Oceanography Network
<b>DKC</b>	Delta Kick Cooling	<b><math>\Lambda</math>-CDM</b>	Lambda, Cold Dark Matter
<b>DLL</b>	Delay Locked Loop	<b>LAS</b>	LASer Source
<b>DM</b>	Dark Matter	<b>LCT</b>	Laser Communication Terminal
<b>DMU</b>	Data Management Unit	<b>LEO</b>	Low Earth Orbit
<b>DORIS</b>	Doppler Orbitography and Radio positioning Integrated by Satellite	<b>LFA</b>	Lead Funding Agency
<b>DPC</b>	Data Processing Centre	<b>LHC</b>	Large Hadron Collider
<b>EAL</b>	Echelle Atomique Libre	<b>LISA PF</b>	Laser Interferometer Space Antenna PathFinder
<b>EEP</b>	Einstein Equivalence Principle	<b>LLI</b>	Local Lorentz Invariance
<b>EOM</b>	Electro-Optic Modulator	<b>LPI</b>	Local Position Invariance
<b>EP</b>	Electronics Package	<b>LS</b>	Laser System
<b>ESA</b>	European Space Agency	<b>LMT</b>	Large Momentum Transfer
<b>ESAC</b>	European Space Astronomy Centre	<b>MLI</b>	Multi-Layer Insulator
<b>ESOC</b>	European Space Operations Centre	<b>MOC</b>	Mission Operations Centre
<b>ESTEC</b>	European Space Research and Technology Centre	<b>MOLO</b>	Microwave to Optical Local Oscillator
<b>FPR-AT</b>	Fundamental Physics Roadmap - Advisory Team	<b>MOT</b>	Magneto-Optical Trap
<b>GAIA</b>	Global Astrometric Interferometer for Astrophysics		
<b>GCC</b>	Ground Clocks Coordinator		
<b>GCR</b>	Ground Clock Responsible		
<b>GEO</b>	Group on Earth Observations		

<b>MSD</b>	Microwave Synthesis and Distribution	<b>SAI</b>	Space Atom Interferometer
<b>MWL</b>	MicroWave Link	<b>SAW</b>	Surface Acoustic Wave Filter
<b>MWO</b>	MicroWave Oscillator	<b>SciRD</b>	Science Requirements Document
<b>MPPT</b>	Maximum Power Point Tracking	<b>SEP</b>	Strong Equivalence Principle
<b>NASA</b>	National Aeronautics and Space Administration	<b>SI</b>	Système International
<b>NEO</b>	Near Earth Orbit	<b>SLH</b>	Stabilized Laser Head
<b>NGRM</b>	Next Generation Radiation Monitor	<b>SLR</b>	Satellite Laser Ranging
<b>NMI</b>	National Metrology Institute	<b>SME</b>	Standard Model Extension
<b>ODC</b>	Orbitography Data Centre	<b>SOC</b>	Science Operations Centre
<b>ODT</b>	Optical Dipole Trap	<b>SSO</b>	Secondary Scientific Objective
<b>OGS</b>	Optical ground Station	<b>SST</b>	Science Study Team
<b>OL</b>	Optical Link	<b>STE</b>	Space-Time Explorer
<b>OMC</b>	Optical Microwave Converter	<b>STE-QUEST</b>	Space-Time Explorer and Quantum Equivalence principle
<b>PAT</b>	Pointing, Aquisition, and Tracking		Space Test
<b>PHARAO</b>	Projet d'Horloge Atomique par Refroidissement d'Atomes en Orbite	<b>SUGRA</b>	SUper GRAvity
<b>PI</b>	Principal Investigator	<b>S/N</b>	Signal to Noise ratio
<b>POD</b>	Precise Orbit Determination	<b>TAI</b>	Temps Atomique International
<b>PN</b>	Pseudo-Noise	<b>TBC</b>	To Be Confirmed
<b>PP</b>	Physics Package	<b>TBD</b>	To Be Defined
<b>PPN</b>	Parametrized Post Newtonian	<b>TC</b>	TeleCommand
<b>PPS</b>	Pulse Per Second	<b>TEC</b>	Total Electron Content
<b>PRR</b>	Preliminary Requirements Review	<b>TID</b>	Total Ionising Dose
<b>PS</b>	Project Scientist	<b>TNID</b>	Total Non-Ionising Dose
<b>PSO</b>	Primary Scientific Objective	<b>TM</b>	TeleMetry
<b>QFT</b>	Quantum Field Theory	<b>TRL</b>	Technology Readiness Level
<b>QM</b>	Quantum Mechanics	<b>T&amp;F</b>	Time and Frequency
<b>QUANTUS</b>	QUANTengase Unter Schwerelosigkeit	<b>UFF</b>	Universality of Free Fall
<b>Q-WEP</b>	Quantum Weak Equivalence Principle test	<b>USO</b>	Ultra-Stable Oscillator
		<b>UTC</b>	Universal Time Coordinated
		<b>UT</b>	Universal Time
		<b>VLBI</b>	Very Long Baseline Interferometry
		<b>WEP</b>	Weak Equivalence Principle

## References

- Ade P. et al. (The Planck Collaboration), arXiv: 1303.5076 (2013)
- Adelberger E.G. et al., *Ann. Rev. Nucl. Part. Sci.* **53**, 77 (2009)
- Alfaro J. et al., *Phys. Rev. D* **65**, 103509 (2002)
- Altin P.A. et al., *Rev. Sci. Instrum.* **81**, 063103 (2010)
- Altschul B. and Kostelecký V.A., *Phys. Lett. B* **628**, 106 (2005)
- Altschul B., *Phys. Rev. D* **79**, 061702 (2009)
- Altschul B. et al., *Phys. Rev. D* **81**, 065028 (2010)
- Antoniadis I. et al., *Nucl. Phys. B* **516**, 70 (1998)
- Antoniadis I. et al., *C. R. Physique* **12**, 755 (2011)
- Armendariz-Picon C. et al., *Phys. Rev. Lett.* **85**, 4438 (2000)
- Armendariz-Picon C. et al., *Phys. Rev. D* **63**, 103510 (2001)
- Ascarrunz F.G. et al., *Proceedings of the 30<sup>th</sup> Precise Time and Time Interval (PTTI) Conference*, 1998
- Audoin C. and Guinot B., *The Measurement of Time*, Cambridge University Press, 2001
- Bailey Q.G. and Kostelecký V. A., *Phys. Rev. D* **74**, 045001 (2006)
- Bailey Q.G., *Phys. Rev. D* **80**, 044004 (2009)
- Bar-Sever Y. et al., *Proceedings for 2<sup>nd</sup> International Colloquium - Scientific and Fundamental Aspects of the Galileo Programme*, 2009
- Bean R., *Phys. Rev. D* **78**, 023009 (2008)
- Bento M.C. et al., *Phys. Rev. D* **66**, 043507 (2002)
- Bertolami O. and Paramos J., *Phys. Rev. D* **71**, 023521 (2005)
- Bezrukov F.L. and Shaposhnikov M., *Phys. Lett. B* **659**, 703 (2008)
- Bezrukov et al., *JHEP* **1101**, 016 (2011)
- Bilic N. et al., *Phys. Lett. B* **535**, 17 (2002)
- Binétruy P. et al., *A Roadmap for Fundamental Physics in Space*, <http://sci.esa.int/fprat>, 26 July 2010
- Bjerhammar A., *Journal of Geodesy* **59(3)**, 207 (1985)
- Bluhm R. et al., *Phys. Rev. D* **68**, 125008 (2003)
- Bondaescu R. et al., *Geophys. J. Int.* **191**, 78 (2012)
- Bourdel Th., *Comptes Rendus Physique* **12**, 779 (2011)
- Brax P. et al., *Phys. Rev. D* **70**, 123518 (2004)
- Cacciapuoti L. et al., *STE-QUEST Science Requirements Document*, **FPM-SA-Dc-00001**, Issue 1, Rev. 5, 22 April 2013
- Caldwell R.R., *Phys. Lett. B* **545**, 23 (2002)
- Capozziello S. and De Laurentis M., *Phys. Repts.* **509**, 167 (2011)
- Carroll S. M., *Phys. Rev. Lett.* **81**, 3067 (1998)
- Carroll S.M. et al., *Phys. Rev. Lett.* **87**, 141601 (2001)
- Carroll S.M. et al., *Phys. Rev. Lett.* **103**, 011301 (2009)
- Carroll S.M. et al., *Phys. Rev. D* **81**, 063507 (2010)
- Chen Q-F et al., arXiv:1308.6383 (2013)
- Chiba T. et al., *Phys. Rev. D* **62**, 023511 (2000)
- Cladé P. et al., *Eur. Phys. J. D* **59**, 349 (2010)
- Clowe D. et al., *Astrophys. J.* **648**, L109 (2006)
- Colella, R. et al., *Phys. Rev. Lett.* **34**, 1472 (1975)
- Colladay D. and Kostelecký V.A., *Phys. Rev. D* **55**, 6760 (1997)
- Colladay D. and Kostelecký V.A., *Phys. Rev. D* **58**, 116002 (1998)
- Damour T. et al., *Phys. Rev. Lett.* **64**, 123 (1990)
- Damour T. and Polyakov A.M., *Nucl. Phys. B* **423**, 532 (1994)
- Damour T., *Class. Quantum Grav.* **13**, A33 (1996)
- Damour T., in C. Amsler et al. (Particle Data Group), *Phys. Lett.* **B667**, 1 (2008), 2010 update
- Damour T. and Donoghue J.F., *Phys. Rev. D* **82**, 084033 (2010)
- Damour T., arXiv:1202.6311 (2012)
- Davies P.C.W., *Class. Quantum Grav.* **21**, 2761 (2004)
- Debs J.E. et al., *Phys. Rev. A* **84**, 033610 (2011)
- Delva P. et al., *IAU Joint Discussion 7: Space-Time Reference Systems for Future Research*, IAU General Assembly, 2012
- Dicke R.H., *The Theoretical Significance of Experimental Relativity*, Gordon and Breach, New York, 1964
- Dickerson S.M. et al., *Phys. Rev. Lett.* **111**, 083001 (2013)
- Dimopoulos S. and Giudice G., *Phys. Lett. B* **379**, 105 (1996)
- Dimopoulos S. et al., *Phys. Rev. D* **78**, 042003 (2008)
- Doser M., *J. Phys.: Conf. Ser.* **199**, 012009 (2010)
- Duchayne L. et al., *A&A* **504**, 653661 (2009)
- Duchayne L., PhD thesis, <http://tel.archives-ouvertes.fr/tel-00349882/fr/>, Observatoire de Paris (France) 2008
- Dvali G. R. et al., *Phys. Lett. B* **485**, 208 (2000)
- Eisenstein D. J. and Hu W., *Astrophys. J.* **496**, 605 (1998)

- Eisenstein D. J. et al. (SDSS), *Astrophys. J.* **633**, 560 (2005)
- Faber S.M. and Gallagher J.S., *Annu. Rev. Astron. & Astrophys.* **17**, 135 (1979)
- Fayet P., *Phys Lett B* **171**, 261 (1986)
- Fayet P., *Nucl Phys B*, **347**, 743 (1990)
- Ferrero A. and Altschul B., *Phys. Rev. D* **80**, 125010 (2009)
- Fonville B. et al., *Proceedings of the 36th Annual Precise Time and Time Interval (PTTI) Conference*, 2004
- Foster G.T. et al., *Opt. Lett.* **27**, 951 (2002)
- Fray S. et al., *Phys. Rev. Lett.* **93**, 240404 (2004)
- Garnavich P. M. et al. (Supernova Search Team), *Astrophys. J.* **509**, 74 (1998)
- Gambini R. and Pullin J., *Phys. Rev. D* **59**, 124021 (1999)
- Geiger R. et al., *Nat. Comm.* **2**, 474 (2011)
- Geisel I. et al., *Appl. Phys. Lett.* **102**, 214105 (2013)
- GEO, The Global Earth Observing System of Systems (GEOSS) - 10-Year Implementation Plan, <http://earthobservations.org/> (2005)
- Giulini D., in *Quantum Field Theory and Gravity*, p. 345, F. Finster et al. Eds., Springer, 2012
- Greenberg O.W., *Phys. Rev. Lett.* **89**, 231602 (2002)
- Gross R. et al. in *Global Geodetic Observing System*, p. 209, Plag H-P. and Pearlman M. Eds. Springer, 2009
- Guena J. et al., *Phys. Rev. Lett.* **109**, 080801 (2012)
- Gubser S.S. and Peebles P.J.E., *Phys. Rev. D* **70**, 123510 (2004)
- Haugan M., *Ann. Phys. (N.Y.)* **118**, 156 (1979)
- Hejc G. et al., *Proceeding of the 41<sup>st</sup> Precise Time and Time Interval (PTTI) Conference*, 2009
- Hobbs G., *Proceedings of Int. Astron. Union* **8**, S291 (2012)
- Hobinger T. et al., *Radio Science*, **48**, 1 (2013)
- Hoedl S.A. et al., *Phys. Rev. Lett.* **106**, 041801 (2011)
- Hoffman B., *Phys. Rev. Lett.* **121**, 337 (1961)
- Hogan J.M. et al., *arXiv.org* 0806.3261 (2008)
- Hu W. and Sugiyama N., *Phys. Rev. D* **51**, 2599 (1995)
- Jungman G. et al., *Phys. Rev. D* **54**, 1332 (1996)
- Kajari E. et al., *Appl. Phys. B* **100**, 43 (2010)
- Kamenshchik A. Y. et al., *Phys. Lett. B* **511**, 265 (2001)
- Kaplan E., *Understanding GPS: Principles and Applications*, ArtechHouse, 1996
- Kasevich M. and Chu S. *Phys. Rev. Lett* **67**, 181 (1991)
- Kesden M. and Kamionkowski M., *Phys. Rev. Lett.* **97**, 131303 (2006)a
- Kesden M. and Kamionkowski M., *Phys. Rev. D* **74**, 083007 (2006)b
- Khoury J. et al., *Phys. Rev. Lett.* **93**, 171104 (2004)
- Khoury J. and Veltman A., *Phys. Rev. D* **69**, 044026 (2004)
- Klinkhamer F.R. and Rupp C., *Phys. Rev. D* **70**, 045020 (2004)
- Knop R. A. et al. (Supernova Cosmology Project), *Astrophys. J.* **598**, 102 (2003)
- Kostelecký V.A. and Samuel S., *Phys. Rev. D* **39**, 683 (1989)
- Kostelecký V.A. and Potting R., *Nucl. Phys. B* **359**, 545 (1991)
- Kostelecký V.A. and Lane C.D., *Phys. Rev. D* **60**, 116010 (1999)a
- Kostelecký V.A. and Lane C.D., *J. Math. Phys.* **40**, 6245 (1999)b
- Kostelecký V.A. et al., *Phys. Rev. D* **68**, 123511 (2003)
- Kostelecký V.A., *Phys. Rev. D* **69**, 105009 (2004)
- Kostelecký V.A. et al., *Phys. Rev. Lett.* **100**, 111102 (2008)
- Kostelecký V.A. and Tasson J.D., *Phys. Rev. Lett.* **102**, 010402 (2009)a
- Kostelecký V.A. and Mewes M., *Phys. Rev. D* **80**, 015020 (2009)b
- Kostelecký V.A. and Russell N., *Rev. Mod. Phys.* **83**, 11 (2011)a; update on arXiv: 0801.0287
- Kostelecký V.A. and Tasson J. D., *Phys. Rev. D* **83**, 016013 (2011)b
- Kostelecký V.A. and Mewes M., *Phys. Rev. D* **85**, 096005 (2012)
- Krisher T.P. et al., *Phys. Rev. Lett.* **70**, 2213 (1993)
- Lämmerzahl C., *General Relativity & Gravitation* **28**, 1043 (1996)
- Lecomte S. et al., in preparation
- Leefer N. et al., *Phys. Rev. Lett.* **111**, 060801 (2013)
- Lévêque T. et al., *Phys. Rev. Lett.* **103**, 080405 (2009)
- Littrell K.C. et al., *Phys. Rev. A* **56**, 1767 (1997)
- Lopez O. et al., *Appl. Phys. B* **110**, 3 (2013)
- LoPresto J.C. et al., *Astrophys. J.* **376**, 757 (1991)
- Maartens R. and Koyama K., *Living Rev. Relativity* **13**, (2010), 5
- Merlet S. et al., *Metrologia* **47**, L9 (2010)
- Meynadier F. et al., *ACES Microwave Link Data Analysis Software - User Requirements Document*, ACES-URD-SYRTE-FM-001-D, Iss. D, Rev.1, 5 April 2011
- Mocioiu I. at al., *Phys. Lett. B* **489**, 390 (2000)

- Müller H. et al., *Nature* **463**, 926 (2010)
- Müntinga H. et al., *Phys. Rev. Lett.* **110**, 093602 (2013)
- Murphy M.T. et al., *Lecture Notes Phys.* **648**, 131 (2004)
- Murphy M. T. et al., *Science* **320**, 1611 (2008)
- Nojiri S. and Odintsov S.D., *Int. J. Geom. Meth. Mod. Phys.* **4**, 115 (2007)
- Nordtvedt K., *Phys. Rev. D* **11**, 245 (1975)
- Nyman R.A. et al., *Appl. Phys. B* **84**, 673 (2006)
- OPERA Collaboration, *J. High Energy Phys.* **153**, 1 (2013)
- Osłowski S. et al., *Mon. Not. R. Astron. Soc.* **418**, 1258 (2011)
- Pavlis N.K. and Weiss M.A., *Metrologia* **40**, 66 (2003)
- Peik E. and Tamm C., *Europhys. Lett.* **61**, 181 (2003)
- Perez P. and Sacquin Y., *Classical & Quantum Gravity* **29**, 184008 (2012)
- Perlmutter S. et al., *Astrophys. J.* **517**, 565 (1999)
- Peters A. et al., *Nature* **400**, 849 (1999)
- Piester D. et al., *IEEE Trans. Ultrason. Ferroelectr. Freq. Control* **55**, 1906 (2008)
- Pound R. and Rebka G., *Phys. Rev. Lett.* **4**, 337 (1960)
- Predehl K. et al., *Science* **336**, 441 (2012)
- Ratra B. and Peebles J., *Phys. Rev. D* **37**, 321 (1988)
- Riess A.G. et al., *Astron. J.* **116**, 1009 (1998)
- Rosenband T. et al., *Science* **319**, 1808 (2008)
- Rost M. et al., *Metrologia* **49**, 772 (2012)
- Rothacher M. et al. in *Global Geodetic Observing System*, p. 209, Plag H-P. and Pearlman M. Eds. Springer, 2009
- Rubakov V.A., *Phys. Usp.* **44**, 871 (2001)
- Rudolph J. et al., *Microgravity Sci. Technol.* **23**, 287 (2011)
- Rummel R. et al., *Towards an Integrated Global Geodetic Observing System (Iggos)*, Illustrated edition, Springer-Verlag Berlin and Heidelberg GmbH & Co. K., 2000
- Schiff L., *Am. J. Phys.* **28**, 340 (1960)
- Schiller S. et al., *Experimental Astronomy* **23**, 573 (2009)
- Schlamming S. et al., *Phys. Rev. Lett.* **100**, 041101 (2008)
- Sorrentino F. et al., *Microgravity Sci. Technol.* **22**, 551 (2010)
- SRE-PA/2011.097, Issue 1- Revision 3, (15/06/2012)
- Storey P. and Cohen-Tannoudji C., *J. Phys. II France* **4**, 1999 (1994)
- Taylor T.R. and Veneziano G., *Phys. Lett. B* **213**, 450 (1988)
- Thorne K.S. et al., *Phys. Rev. D* **7**, 3563 (1973)
- Tino G.M. et al., *Nuclear Physics B (Proc. Suppl)* **143**, 203 (2013)
- Touboul P. and Rodrigues M., *Class. Quantum Grav.* **18**, 2487 (2001)
- Unnikrishnan C.S. and Gillies G.T., *Physics Letters A* **377**, 60 (2012)
- Van Dierendonck A.J. et al., *Navigation* **39**, 265 (1992)
- Van Zoest T., et al., *Science* **328**, 1540 (2010)
- Varoquaux G. et al., *New J. Phys.* **11**, 113010 (2009).
- Viola L. and Onofrio R., *Phys. Rev. D* **55**, 455 (1997)
- Vessot R. and Levine M., *Gen. Rel. and Grav.* **10**, 181 (1979)
- Vessot R.F.C. et al., *Phys. Rev. Lett.* **45**, 2081 (1980)
- Wald R., *General Relativity*, University of Chicago Press, 1984
- Wang B. et al., *Sci. Rep.* **2**, 556 (2012)
- Weinberg S., *Gravitation and Cosmology*, Wiley, 1972
- Weinberg S., *Rev. Mod. Phys.* **61**, 1 (1989)
- Wetterich C., *Nucl. Phys. B* **302**, 668 (1988)
- Williams J.G. et al., *Phys. Rev. Lett.* **93**, 261101 (2004)
- Will C.M., *Theory and Experiment in Gravitational Physics*, Cambridge University Press, 1993
- Will C.M., *Living Rev. Relativity* **9**, 3 (2006)
- Wolf P. and Petit G., *A&A* **304**, 653 (1995)
- Wolf P. et al., *Phys. Rev. Lett.* **96**, 060801 (2006)
- Wolf P. et al., *Classical & Quantum Gravity* **28**, 145017 (2011) doi:10.1088/0264-9381/28/14/145017
- Zaldarriaga M. et al., *Astrophys. J.* **488**, 1 (1997)
- Zhang P. et al., *Phys. Rev. Lett.* **99**, 141302 (2007)

# Acknowledgments

The STE-QUEST Assessment Study was led by the Science Study Team and the ESA Study Team. Significant support was provided by numerous scientists strongly involved in the elaboration of the science case, in the simulation activities, in the payload and instruments studies.

## Differential Atom Interferometer Consortium

**Principal Investigator:** Ernst Rasel (LUH, Germany).

**Co-Principal Investigators:** Kai Bongs (Birmingham University, United Kingdom), Philippe Bouyer (Bordeaux University, France), Steve Lecomte (CSEM, Switzerland), Achim Peters (HUB, Germany), Carlos Sopena (ICE, Spain), Guglielmo Tino (Firenze University, Italy), Wolf von Klitzing (FORTH, Greece), Martin Zelan (SP, Sweden).

**Project Manager:** Claus Braxmaier (ZARM, Germany); **System Engineer:** Thilo Schuldt (ZARM, Germany); **Product Assurance:** TAS (Italy); **Risk Management:** TAS (Italy); **Launch Services:** TAS (Italy); **Laser Package:** Didier Massonnet (CNES, France); **Physics Package:** Naceur Gaaloul (LUH, Germany); **Electronics Package:** Chris Chaloner (SEA, United Kingdom); **Software:** Carlos Sopena (ICE, Spain); **Payload Operations:** Arnaud Landragin (LNE-SYRTE, France); **Science Ground Segment and Data Processing:** Arnaud Landragin (LNE-SYRTE, France); **Simulations:** Wolfgang Schleich (Ulm University, Germany).

**Co-investigators:** (**France**) Arnaud Landragin (LNE-SYRTE), Didier Massonnet (CNES), Nassim Zahzam (ONERA); (**Germany**) Claus Braxmaier (ZARM), W. Ertmer (LUH), Naceur Gaaloul (LUH), N. Gürlebeck (ZARM), Ulrich Johann (Astrium), Claus Lämmerzahl, (ZARM), Wolfgang Schleich (Ulm University), Thilo Schuldt (DLR), Klaus Sengstock (UHH), Reinhold Walser (TUDA), Peter Weßels (LZH), A. Wicht (FBH); (**Italy**) Fiodor Sorrentino (Firenze University); (**Greece**) Nikolaos Uzunoglu (NTUA); (**Switzerland**) Philippe Jetzer (Zurich University), G. Mileti (Neuchatel University); (**Sweden**) J. Nilsson (RUAG), (**United Kingdom**) Chris Chaloner (SEA), Michael Williams (Astrium).

**Collaborators:** (**France**) Brynle Barrett (Bordeaux University), Baptiste Battelier (Bordeaux University), Andrea Bertoldi (Bordeaux University), Thomas Lévêque (CNES); (**Germany**) Deborah Aguilera (DLR), Michael Chwalla (Astrium), Domenico Gerardi (Astrium), Cristina Gherasim (TUDA), Martin Gohlke (DLR), Jens Grosse (DLR), Jonas Hartwig (LUH), Matthias Hauth (HUB), Ortwin Hellmig (UHH), Sven Hermann (ZARM), Markus Krutzik (HUB), Roman Nolte (TUDA), Benny Rievers (ZARM), Albert Roura (Ulm University), Christian Schubert (LUH), André Wenzlawski (UHH), Patrick Windpassinger (UHH); (**Greece**) Vasiliki Bolpasi (FORTH); (**Italy**) Nicola Poli (Firenze University); (**Spain**) Ivan Lloro Boada (ICE), Lluís Gesa Boté (ICE), Ignacio Mateos (ICE), Miguel Nofrarias Serra (ICE), (**Switzerland**) Christophe Affolderbach (Neuchatel University), Ruxandra Bodaescu (Zurich University), Thomas Südmeyer (Neuchatel University); (**United Kingdom**) Chris Chaloner (SEA), Philip Ireland (SEA), Emanuele Rocco (Birmingham University), David Summers (SEA), Christian Trenkel (Astrium), Tristan Valenzuela (Birmingham University), Michael Williams (Astrium).

## Atomic Clock Consortium

**Principal Investigator:** Philip Tuckey (LNE-SYRTE, France).

**Co-Principal Investigators:** Patrick Gill (NPL, United Kingdom), Philippe Laurent (LNE-SYRTE, France), Steve Lecomte (CSEM, Switzerland), Stephan Schiller (HHUD, Germany), Martin Zelan (SP, Sweden).

**Project Manager:** Didier Massonnet (CNES, France); **System Engineer:** Christophe Delaroche (CNES, France); **Product Assurance:** Sabine Julien (CNES, France); **AIV:** Olivier Grosjean (CNES, France); **MOLO Subsystem:** Uwe Sterr (PTB, Germany); **MSD Subsystem:** Gilles Cibiël (CNES, France); **LAS Subsystem:** Benoit Faure (CNES, France); **CST Subsystem:** Olivier Grosjean (CNES, France); **ICU Subsystem:** Per-Olof Lindqvist (RUAG Space AB, Sweden); **Payload Operations:** Philippe Laurent (LNE-SYRTE, France), Uwe Sterr (PTB, Germany); **Science Ground Segment and Data Processing:** Peter Wolf (LNE-SYRTE, France); **Clock Science Studies and Simulations:** Stephan Schiller (HHUD, Germany).

**Co-Investigators:** (**France**) Vincent Giordano (FEMTO-ST), Didier Massonnet (CNES); (**Germany**) Uwe Sterr (PTB); (**Switzerland**) André Stefanov (Bern University); (**United Kingdom**) Kai Bongs (Birmingham University); (**United States**) Kurt Gible (Penn State University).

**Collaborators:** (**France**) Christine Guerlin (LKB-ENS), Serge Reynaud (Jussieu University), Enrico Rubbiola (FEMTO-ST); (**Germany**) Ingo Ernsting (HHUD), Ronald Holtzwarth (MENLO), Alexander

Nevsky (HHUD); **(Spain)** Miguel Nofrarias Serra (ICE); **(Sweden)** Kenneth Jaldehag (SP); **(Switzerland)** Erwin Portuondo-Campa (CSEM); **(United Kingdom)** Setnam Shemar (NPL).

#### **Time & Frequency Comparisons Science Ground Segment**

**Co-Investigators:** **(France)** Vincent Giordano (FEMTO-ST), Philippe Laurent (LNE-SYRTE), Christophe Salomon (ENS-LKB), Etienne Samain (GéoAzur), François Vernotte (UTINAM) ; **(Germany)** Ernst Rasel (LUH), Stephan Schiller (HHUD), Ulrich Schreiber (FESG), Uwe Sterr (PTB); **(Italy)** Salvatore Capozziello (Napoli University), Luciano Iess (La Sapienza University), Filippo Levi (INRIM), Marco Prevedelli (Bologna University), Guglielmo Tino (Firenze University); **(Netherlands)** Eberhard Gill (TU Delft); **(Spain)** Carlos Sopena (ICE); **(Switzerland)** Philippe Jetzer (Zurich University), Steve Lecomte (CSEM), André Stefanov (Bern University); **(United Kingdom)** Patrick Gill (NPL), Kai Bongs (Birmingham University); **(Australia)** Mike Tobar (UWA); **(Canada)** John Bernard (NRC); **(China)** Xuzong Chen (Beijing University), Zhanjun Fang (NIM), Liang Liu (SIOM), Shougang Zhang (NTSC); **(Japan)** Yuko Hanado (NICT), Feng-Lei Hong (NMIL), Hidetoshi Katori (Tokyo University); **(United States)** Brett Altshul (South-Carolina University), Quentin Bailey (Embry-Riddle University), Kurt Gibble (Penn State University), Leo Hollberg (Stanford University), Chris Oates (NIST), Jay Tasson (Carleton College), Nan Yu (JPL).

#### **Science Working Group**

**Coordinators:** Philippe Jetzer (Zurich University, Switzerland), Peter Wolf (LNE-SYRTE, France).

**Members:** Luc Blanchet (IAP-Paris, France), Luigi Cacciapuoti (ESA, The Netherlands), Salvatore Capozziello (Naples University, Italy), Domenico Giulini (ITP-Hannover, Germany), Serge Reynaud (LKB, France).

#### **Reference Frames and Geodesy Working Group**

**Coordinator:** Drazen Svehla (Germany).

**Members:** Jozsef Adam, (Budapest University, Hungary), Graham Appleby (NERC, United Kingdom), Richard Biancale (CNES, France), Luigi Cacciapuoti (ESA, The Netherlands), Urs Hugentobler (TU München, Germany), Luciano Iess (Università La Sapienza University, Italy), Axel Nothnagel (Bonn University, Germany), Markus Rothacher (ETH Zurich, Switzerland), Harald Schuh (GFZ, Germany), Pascal Willis (Institute Physique du Globe de Paris, France), Marek Ziebart (UCL London, United Kingdom).